POLITECNICO
MILANO 1863

SCUOLA DI INGEGNERIA INDUSTRIALE
E DELL'INFORMAZIONE

Executive Summary of the Thesis

Studio relativo ai rientri di calore in serbatoi criogenici ad alta pressione per l'azoto

Laurea Magistrale in Chemical Engineering - Ingegneria Chimica

Author: Linda Tommasi

Advisor: Prof. Valentina Busini

Co-advisor: David Manzoni, Giulia Tomellini

Academic year: 2023-2024

1. Introduzione

Nel settore industriale, l'azoto liquido (LN_2) è ampiamente utilizzato in vari ambiti, come quello alimentare, elettronico, aerospaziale. Nonostante il mercato in crescita, la produzione e la distribuzione di LN_2 sono soggette ad ingenti costi.

I serbatoi criogenici conservano LN_2 a basse temperature, riscontrando problematiche come i rientri termici e il fenomeno di autopressurizzazione. Per motivi di sicurezza, questi serbatoi non vengono riempiti completamente, bensì al 50/60%, lasciando uno spazio chiamato "cuscinetto di gas". Tuttavia, questa pratica porta a perdite economiche dovute all'evaporazione e a un aumento dei costi logistici dovuti ai maggiori viaggi di rifornimento.

Questa ricerca, in collaborazione con Air Liquide, mira a comprendere l'influenza del fenomeno dei rientri termici in modo tale da implementare una configurazione ottimale in termini di sicurezza e design.

2. Stato dell'arte

2.1. Serbatoi criogenici

I serbatoi criogenici industriali vengono utilizzati per conservare sostanze come azoto, ossigeno, elio, argon e idrogeno a temperature estremamente basse, tipicamente al di sotto dei -150°C. Questi serbatoi sono progettati per gestire prodotti con punto di ebollizione al di sotto della temperatura ambiente, garantendo conservazione e trasporto in sicurezza ed efficienza.

Un aspetto fondamentale nel design del serbatoio è l'isolamento termico, mirato a minimizzare lo scambio di calore con l'ambiente circostante. Un design tipico prevede serbatoi a doppia parete con una cavità isolata sottovuoto tra il serbatoio interno in acciaio inossidabile e il serbatoio esterno in acciaio al carbonio. Vari materiali isolanti, come perlite, aerogel di silice e riempitivi in schiuma, vengono impiegati in base all'applicazione e alle condizioni ambientali.

Il monitoraggio del livello di vuoto e l'esecuzione di ristrutturazioni sono cruciali per prevenire i rientri di calore. Dispositivi di sicurezza, inclusi valvole di sicurezza e dischi di rottura, sono integrati per prevenire sovrapressioni e garantire l'operatività in sicurezza. Inoltre, meccanismi di recupero del calore e vaporizzatori giocano un ruolo significativo nel minimizzare le perdite di

prodotto e mantenere una pressione stabile nel serbatoio [3].

2.2. Revisione della letteratura

La revisione della letteratura è divisa in due categorie principali: l'analisi della conducibilità termica dei serbatoi criogenici e lo studio dei fenomeni legati ai rientri termici.
La misurazione accurata della conducibilità termica spesso ha presentato sfide dovute alle tecniche e metodologie associate. I progressi nella modellizzazione della conducibilità termica hanno utilizzato approcci sia teorici sia sperimentali, con un focus particolare sui materiali isolanti a base di perlite e le loro variazioni riguardanti parametri come temperatura e vuoto.
Negli ultimi decenni, l'interesse per l'autopressurizzazione, la stratificazione termica e l'evaporazione criogenica è cresciuto insieme agli avanzamenti nelle tecnologie aerospaziali e all'uso industriale di gas come azoto, ossigeno e LNG.
Le analisi numeriche hanno esplorato modelli di flusso e stratificazione termica all'interno di serbatoi cilindrici criogenici, investigando gli effetti di vari parametri su velocità e temperature del liquido. Studi recenti hanno approfondito la convezione naturale e la stratificazione termica all'interno dei serbatoi, rivelando che l'evaporazione del liquido contribuisce ad aumenti di pressione nella zona di vapore.
I modelli attuali si basano sul flusso di calore in ingresso e sugli studi empirici. Tuttavia, sono emersi modelli più sofisticati, che considerano l'equilibrio termico tra le fasi liquida e gassosa, nonché l'impatto del riscaldamento su ciascuna fase.

3. Materiale e metodi

Lo studio si è focalizzato in primo luogo sull'analisi delle modalità di rientro termico. Ciò ha richiesto un'attenta esaminazione della conducibilità termica del materiale del serbatoio e dei flussi di calore che si verificano all'interno del sistema. Comprendere come il calore viene trasferito all'interno del serbatoio risulta cruciale per prevedere accuratamente la quantità di prodotto di evaporazione. Questa valutazione consente di identificare i parametri che influenzano maggiormente il fenomeno di scambio termico, così da individuare i punti critici che riducono le performance in termini di isolamento.
Successivamente, è stata descritta la variazione delle variabili coinvolte nel processo utilizzando bilanci di massa ed energia. Ciò ha permesso di sviluppare un modello matematico che tiene conto di fattori cruciali come la temperatura del liquido criogenico, la pressione all'interno del serbatoio e il tasso di evaporazione del prodotto. Questo modello è progettato per adattarsi a una vasta gamma di condizioni ambientali e tipi di serbatoi criogenici, fornendo una stima accurata del comportamento del sistema in diversi scenari operativi.
Riguardo ai principali fattori coinvolti nei rientri termici, è stato valutato il contributo della conduzione solida, della radiazione e della conduzione attraverso il gas interstiziale all'interno della cavità, assumendo il fenomeno di convezione trascurabile.
E' stato utilizzato un modello fisico per prevedere le conducibilità termiche dei materiali isolanti in base a vari fattori.
Le equazioni 1 e 2 sono utilizzate per calcolare la conducibilità termica [4].

$$k_e = k_{s.e} + k_g \tag{1}$$

$$k_e = 0.00252T + 7.98 \times 10^{-8} T^3 + \frac{1.243 T^{0.587} P}{0.895T + P} \tag{2}$$

Dove $k_{s.e}$ e k_g rappresentano la conducibilità termica effettiva di un materiale isolante, T è la temperatura assoluta in K e P è la pressione dell'intercapedine in Pa.
La conducibilità termica effettiva di un materiale isolante può essere stimata sommando tre contributi principali: il contributo solido, rappresentato come una legge lineare o di potenza della temperatura, il contributo radiativo, rappresentato come una potenza cubica della temperatura, e il contributo del gas interstiziale, rappresentato come una funzione polinomiale razionale della pressione e della temperatura.
Per il calcolo del flusso di calore, viene impiegata l'equazione di Fourier, tenendo conto della dipendenza della conducibilità dalla temperatura e dell'area media di scambio.
Durante lo sviluppo del modello, sono state considerate alcune ipotesi ed assunzioni.

Per semplificare il calcolo, è stato assunto che il liquido criogenico in equilibrio sia stratificato nella parte superiore, risultando in condizioni di saturazione, mentre il liquido freddo, sul fondo del serbatoio, rimanga in stato di sottoraffreddamento anche nelle nuove condizioni di pressione. Con l'aumentare del tempo, il liquido sottoraffreddato si restringe, poiché, a causa del rientro termico, una parte evolve in liquido caldo in condizioni di saturazione, mentre una parte del liquido caldo in equilibrio evapora, incrementando la fase gassosa [2] [1].
Le ipotesi utilizzate per il modello sono le seguenti:

1. Condizione non operativa del serbatoio;
2. Condizioni di vuoto perfetto, distribuzione omogenea della perlite;
3. Serbatoio chiuso, incapace di scambiare massa con l'esterno, condizioni non isobariche;
4. Flusso di calore costante;
5. Il calore in ingresso viene considerato interamente come calore latente per vaporizzare il liquido;
6. Fasi vapore-liquido in equilibrio termico durante l'intero processo;
7. Stratificazione delle fasi: liquido sottoraffreddato sul fondo, liquido saturo al di sopra e vapore in cima al serbatoio;
8. Flussi circolanti, convezione locale e vortici trascurabili.

A partire dalle equazioni derivate dai bilanci di massa ed energia, modellati secondo le ipotesi applicate, l'equazione riguardante il tasso di evaporazione e la massa satura sono date rispettivamente dalle equazioni 3 e 4.

$$\epsilon_v = \exp\left(\frac{C_{PC,i}(T_{C,0} - T_{C,i})}{\Delta H_{\text{vap,i}}}\right) \tag{3}$$

$$m_{C,i} = \frac{Q \cdot \Delta t}{H_{C,i} - H_{F,i}} \tag{4}$$

Conoscendo le condizioni iniziali di pressione e temperatura del liquido criogenico e utilizzando i dati termodinamici disponibili per la fase sottoraffreddata e satura alla pressione iniziale, è possibile determinare la massa satura nel momento desiderato, così come il tasso di evaporazione.
Pertanto, è possibile ottenere il valore della massa evaporata a ciascun intervallo di tempo e aggiornare le masse e i volumi del liquido sottoraffreddato, del liquido saturo e del vapore.
In questo modo, essendo in grado di determinare la variazione di masse e volumi ad ogni istante, e quindi anche delle densità molari, utilizzando la relazione di Peng-Robinson, è stato possibile calcolare l'aumento di pressione dovuto al fenomeno di evaporazione.
Basandosi su queste equazioni, è stato implementato uno strumento di calcolo per fornire una descrizione del processo di evaporazione e dell'andamento della pressione nel tempo, fino al raggiungimento della massima pressione consentita.
Per i serbatoi con un MAWP, maximum allowable working pressure, più alto della pressione supercritica della sostanza criogenica, è stato sviluppato un modello di calcolo valido dal raggiungimento della regione supercritica, con l'assunzione di trasformazione isocora. L'equazione di riferimento per l'entalpia relativa alla massa nella fase supercritica ad ogni istante considerato è data dall'equazione 5.

$$H_i = \frac{Q \cdot \Delta t - m_{\text{tot}} \cdot H_{i-1}}{m_{\text{tot}}} \tag{5}$$

In questo modo, conoscendo le condizioni iniziali della massa supercritica e utilizzando i dati termodinamici relativi alle trasformazioni isocore della sostanza in esame nello stato supercritico, è possibile risalire alla pressione e alla temperatura ad ogni istante, associate all'entalpia calcolata.
Una volta raggiunta la massima pressione ammissibile del serbatoio, il ciclo iterativo viene interrotto, poiché intervengono misure di sicurezza per impedire un ulteriore aumento della pressione.
Il modello di calcolo delineato segue un approccio sistematico, partendo dall'immissione delle informazioni necessarie per calcolare il flusso di calore in ingresso e procedendo in modo iterativo per determinare i tassi di evaporazione e le masse delle fasi nel tempo. Questo processo iterativo prevede l'aggiornamento delle quantità di liquido sottoraffreddato, liquido saturo e vapore in base ai fenomeni di evaporazione, considerando le variazioni di massa, volume e densità. Il modello impiega l'equazione di Peng-Robinson per calcolare gli incrementi di pressione risultanti dall'evaporazione.
Le variabili di output includono il tasso di evaporazione, le masse di liquido e vapore, la pressione, la temperatura, la densità e l'entalpia ad

ogni intervallo di tempo. Questi output offrono spunti sull'autopressurizzazione e sui fenomeni di evaporazione in diverse condizioni di stoccaggio. Inoltre, il modello è cruciale per stimare il tempo necessario per raggiungere la MAWP durante l'inattività del serbatoio, migliorando il processo decisionale e la sicurezza industriale, stimando anche il comportamento della pressione nella regione supercritica.

4. Risultati

Inizialmente, lo strumento di calcolo è stato applicato a un serbatoio di ossigeno a media pressione per convalidare il modello con i dati sperimentali disponibili. I dati sperimentali sono conformi allo standard internazionale ISO21014, relativo alle prestazioni di isolamento dei contenitori criogenici. Questi dati forniscono il tasso di evaporazione giornaliero misurando il flusso di gas come flusso massivo utilizzando un misuratore di flusso massico. Nello specifico, per un serbatoio di ossigeno criogenico con una configurazione verticale e isolamento in perlite sottovuoto, con una capacità compresa tra 60 e 70 mila litri, con temperatura esterna di 15°C e una pressione operativa di 17 Barg, lo standard prevede una perdita volumetrica giornaliera prevista del 0,13% del prodotto inizialmente immagazzinato. Attraverso il modello proposto si ottiene un valore del 0,21%, considerato coerente con il risultato atteso.
Inoltre, è stata condotta un'analisi di sensitività variando parametri come la conducibilità dello strato di isolamento, il grado di vuoto nello spazio interstiziale e la temperatura esterna. Il parametro che si è rivelato essere più impattante è la variazione del grado di vuoto, che comporta un cambiamento significativo sia nell'oscillazione della pressione che nel tasso di evaporazione giornaliero.
Il modello è stato successivamente applicato al caso di maggiore interesse: un serbatoio di azoto ad alta pressione con capacità di 20 m^3 e una pressione di 31 Barg. La Figura 1 mostra l'evoluzione del volume del liquido criogenico e della pressione su base giornaliera nella regione subcritica, mentre la Figura 2 descrive l'oscillazione della pressione nella regione supercritica fino al MAWP. Nella regione supercritica, la tendenza della pressione presenta un'inclinazione più ripida rispetto alla regione subcritica, indicando un aumento più pronunciato della pressione nel tempo. Ciò suggerisce che spingere i serbatoi a tali pressioni potrebbe comportare fluttuazioni di pressione significative e incontrollabili.
In particolare, nella regione subcritica, la variazione di pressione è di circa 0,1 bar al giorno. Tuttavia, nella regione supercritica, la pressione aumenta di 3 bar in circa 22 ore, raggiungendo il MAWP.

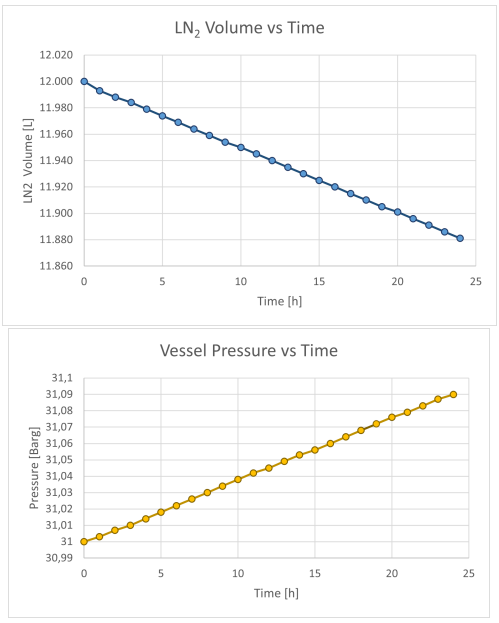

Figure 1: Trend del volume liquido [L] e della pressione [Barg] rispetto al tempo [h]. Stato subcritico.

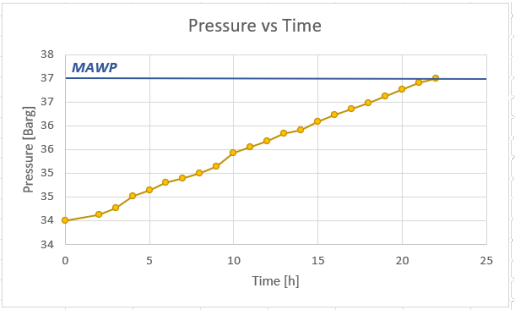

Figure 2: Trend della pressione rispetto al tempo. Stato supercritico.

La ricerca di una configurazione ottimale è stata quindi condotta sulla capacità più comunemente utilizzata per i serbatoi di azoto ad alta pressione, 3 m^3 a 31 Barg. La tabella e i grafici riassumono i risultati ottenuti dal modello di calcolo basato su diversi livelli di riempimento e

testando due diversi gradi di vuoto nello spazio interstiziale: uno relativo ai serbatoi standard (0,26 mBar) e uno dei serbatoi di ultima generazione (0,04 mBar). La tabella 1 e la figura 3 consentono di evidenziare il tasso di evaporazione (NER) e il trend della pressione per diversi % di riempimento.

Tasso di evaporazione - diverse % di riempimento

% di riempimento	NER
50	2,4
60	2
65	1,9
70	1,8
75	1,64
80	1,6
85	1,45

Table 1: Tasso di evaporazione- % di riempimento. Sostanza: Azoto. Capacità: 3 000 L.

Figure 3: Trend della pressione e rispetto al tempo- 50, 60, 65, 70, 75, 80, 85 % di riempimento. Sostanza: Azoto. Capacità: 3000 L.

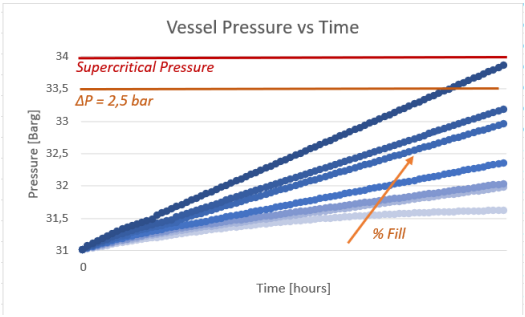

L'approccio utilizzato mira a conservare il più possibile il prodotto, evitando così rilasci diretti nell'atmosfera per abbassare la pressione del serbatoio. Questa strategia privilegia l'efficienza.
Di conseguenza, il serbatoio non viene spinto alle condizioni di pressione massima consentite. Invece, è consigliabile rimanere al di sotto delle condizioni supercritiche e impostare un limite massimo di 2,5 bar nel corso di una settimana. In base al design del serbatoio e delle condizioni operative considerate, il limite potenziale di riempimento risulta essere circa l'80%.

Poiché i serbatoi sono tipicamente riempiti al 50 /60%, l'adozione del nuovo livello ottenuto tramite il modello di calcolo proposto, comporta una differenza significativa nei chilogrammi di azoto criogenico stoccabili e nel numero di viaggi di rifornimento necessari.
Inoltre, combinando la nuova configurazione ottimizzata con l'ultizzo di serbatoi di nuova generazione (intercapedine con grado di vuoto 0,04 mBar) è possibile ridurre notevolmente la perdita di azoto annuale, come rappresentato in tabella 2.

Azoto perso in evaporazione - diverse condizioni di vuoto

Vuoto [mBar]	Azoto [Kg]
0,26	16 065
0,04	6 318

Table 2: Azoto perso in evaporazione [Kg]- diverse condizioni di vuoto. Sostanza: Azoto criogenico. Capacità: 3 000 L.

Infine, con l'obiettivo di descrivere l'impatto economico sui costi di trasporto della nuova configurazione ottimizzata, è stato realizzato un confronto tra le prestazioni di un serbatoio standard esistente e la nuova configurazione.
Per i calcoli, si considera un cliente situato a 50 km dal sito, caratterizzato da 2 consegne mensili con un riempimento del serbatoio del 50%. Ogni consegna consiste in 1 148 kg.
Annualmente, vengono effettuate un totale di 24 consegne, con uno scarico di 27 552 kg. Tuttavia, essendo un serbatoio standard, 16 065 kg di questo verranno persi in evaporazione. Solo 11 487 kg dei totali consegnati sono effettivamente utilizzati annualmente. Questo dato rappresenta il consumo netto annuale.
Assumendo che il serbatoio venga sostituito con un design identico ma con l'intercapedine di ultima generazione, il cliente dispone di ulteriori 9 747 kg di azoto criogenico, non soggetti all'evaporazione.
Con la nuova configurazione ottimizzata, poiché il serbatoio raggiunge l'80 % di capacità, ad ogni rifornimento è possibile scaricare 1 836 kg. Tenendo conto del consumo annuale netto del cliente, dei chilogrammi risparmiati in termini

di evaporazione con la nuova configurazione e dell'aumento del livello di riempimento, è possibile ridurre le consegne annuali da 24 a 6. È possibile determinare i risparmi annuali in termini di costi sia per l'azienda che per il consumatore legati al numero di consegne e ai costi di trasporto. Le seguenti equazioni considerano una tariffa fissa per consegna per il cliente, 150 €, e un costo per consegna per il produttore relativo ai chilometri percorsi, 106 €.

$$\text{Risparmio produttore} = 106\,[€] \times 18 = 1908\,[€] \tag{6}$$

$$\text{Risparmio cliente} = 150\,[€] \times 18 = 2700\,[€] \tag{7}$$

E' possibile infine calcolare la differenza in termini di kg/CO2 emessi nel caso della configurazione iniziale del serbatoio e della configurazione ottimizzata, utilizzando un fattore moltiplicativo che tiene conto delle emissioni associate sia al trasporto che alla produzione.
La tabella 6 evidenzia le emissioni basate sugli scenari considerati:

Emissioni di CO_2 in un anno- diverse condizioni del serbatoio.

	Emissioni [t]
Standard	10 249
Ottimizzato	4 097

Table 3: Emissioni annuali di CO_2- diverse condizioni del serbatoio.

5. Conclusioni

L'azoto liquido è ampiamente utilizzato in vari settori industriali, con un mercato globale in costante crescita. Tuttavia, i costi di produzione e distribuzione ostacolano tale crescita. I serbatoi di azoto criogenico, affrontano sfide nella gestione del calore e nella regolazione della pressione.
Queste sfide portano alla perdita di prodotto a causa dell'evaporazione e ai limiti sul riempimento del serbatoio, aumentando i costi di rifornimento e trasporto. Comprendere il fenomeno dei rientri termici è fondamentale per ottimizzare il design e il funzionamento del serbatoio, al fine di mitigare le perdite economiche e garantire la sicurezza.
Lo studio si è concentrato sui meccanismi di scambio termico e sullo sviluppo di un modello matematico per prevedere le tendenze della pressione del serbatoio e del tasso di evaporazione. Sono state derivate relazioni semplificate dai bilanci di massa ed energia, consentendo la modellazione predittiva.
L'analisi di sensitività ha rivelato il grado di vuoto come parametro critico di progettazione del serbatoio. Ottimizzare le configurazioni del serbatoio basate sui risultati del modello può aumentare i livelli di riempimento garantendo al contempo la sicurezza.
Dal modello di calcolo è stato possibile determinare per un serbatoio alta pressione di azoto, un nuovo livello di riempimento ottimale, garantendo la sicurezza in termini di innalzamento di pressione. Inoltre èstato possibile calcolare la differenza in kg di massa evaporata tra il design standard e il design ottimale, con intercapedine a vuoto maggiore.
La stima dei risparmi economici, in termini logistici, e le riduzioni delle emissioni di biossido di carbonio ottimizzando la configurazione del serbatoio, ha evidenziato benefici significativi rispetto alle configurazioni standard.
Il modello matematico riproducibile fornisce uno strumento prezioso per lo studio delle variabili coinvolte nello scambio termico, offrendo una stima rapida senza costose procedure sperimentali.
La crescente richiesta di sostanze criogeniche e il potenziale di esse per future applicazioni sottolinea l'importanza di ulteriori indagini sulla modellazione computazionale e sull'ingegneria dei materiali e della progettazione dei serbatoi criogenici.

References

[1] Velisa Vesovic Calogero Migliore, Cristina Tubilleja. Weathering prediction model for stored liquefied natural gas (lng). *Journal of natural gas science and engineering*, 2015.

[2] Velisa Vesovic Felipe Huerta. Cfd modelling of the isobaric evaporation of cryogenic liq-

uids in storage tanks. *International Journal of Heat and Mass Transfer*, 2021.

[3] Thomas M. Flynn. *Cryogenic Engineering*. Marcel Dekker, USA, 2005.

[4] Ram R. Ratnakar, Zhe Sun, and Vemuri Balakotaiah. Effective thermal conductivity of insulation materials for cryogenic lh2 storage tanks: A review. *International Journal of Hydrogen Energy*, pages 7770–7793, 2023.

POLITECNICO
MILANO 1863

SCUOLA DI INGEGNERIA INDUSTRIALE
E DELL'INFORMAZIONE

Executive Summary of the Thesis

Study of heat losses in cryogenic high-pressure nitrogen tanks

Laurea Magistrale in Chemical Engineering - Ingegneria Chimica

Author: Linda Tommasi

Advisor: Prof. Valentina Busini

Co-advisor: David Manzoni, Giulia Tomellini

Academic year: 2023-2024

1. Introduction

In the industrial sector, liquid nitrogen (LN_2) is widely used in various fields, such as food, electronics, aerospace, and recently even in medicine. Despite the growing market, the production and distribution of LN_2 entail significant costs.
Cryogenic tanks store LN_2 at low temperatures, encountering issues such as thermal reentries and the phenomenon of autopressurization. For safety reasons, these tanks are not filled completely but rather at 50/60%, leaving a space called a "gas cushion." However, this practice leads to economic losses due to evaporation and substantial additional logistics costs due to increased refilling trips.
This research, conducted in collaboration with Air Liquide, aims to understand the influence of thermal reentry phenomena in order to implement an optimal configuration in terms of safety and design.

2. State of art

2.1. Cryogenic tanks

Industrial cryogenic tanks are utilized for storing substances like nitrogen, oxygen, helium, argon, and hydrogen at extremely low temperatures, typically below -150°C. These tanks are engineered to handle materials with boiling points below room temperature, ensuring both efficient and safe storage and transportation.
A pivotal aspect in tank design is thermal insulation, aimed at minimizing heat exchange with the surroundings. A prevalent design entails double-walled tanks with a vacuum-insulated cavity between the inner stainless steel tank and the outer carbon steel tank. Various insulation materials, such as perlite, silica aerogel, and foam fillings, are employed based on the application and environmental conditions.
Monitoring the vacuum level and undertaking revamping are crucial to prevent refrigerant loss and uphold product integrity. Safety devices, including pressure relief valves and rupture discs, are integrated to prevent overpressure and ensure safe operation. Furthermore, heat recovery mechanisms and vaporizers play a significant role in minimizing product loss and maintaining stable tank pressure [3].

2.2. Literature review

The literature review is divided into two main categories: the analysis of thermal conductivity and the study of thermal reentry phenomena.
Accurately measuring thermal conductivity has

often posed challenges due to associated techniques and methodologies. Advances in modeling thermal conductivity have utilized both theoretical and experimental approaches, with a particular focus on perlite-based insulation materials and their variations concerning parameters such as temperature and vacuum.
In recent decades, interest in the autopressurization, thermal stratification, and cryogenic evaporation has grown alongside advancements in aerospace technologies and the industrial use of gases like nitrogen, oxygen, and LNG.
Numerical analyses have explored flow and thermal stratification models within cylindrical cryogenic tanks, investigating the effects of various parameters on liquid velocities and temperatures. Recent studies have delved into natural convection and thermal stratification within tanks, revealing that liquid evaporation contributes to pressure increases in the vapor zone. Current models rely on incoming heat flow and empirical studies. However, more sophisticated models have emerged, considering thermal equilibrium between liquid and vapor phases, as well as the impact of heating on each phase.

3. Materials and Methods

The study focused initially on the analysis of thermal reentry modes. This required a careful examination of the thermal conductivity of the tank material and the heat flows that occur within the system. Understanding how heat is transferred inside the tank is crucial for accurately predicting the amount of evaporated product. This evaluation allows identifying the parameters that most influence the heat exchange phenomenon, thus identifying the critical points that reduce insulation performance.
Subsequently, the variation of the variables involved in the process was described using mass and energy balances. This allowed the development of a mathematical model that takes into account crucial factors such as the temperature of the cryogenic liquid, the pressure inside the tank, and the product's evaporation rate. This model is designed to adapt to a wide range of environmental conditions and types of cryogenic tanks, providing an accurate estimate of the system's behavior in different operational scenarios.
Regarding the main factors involved in thermal reentries, the contribution of solid conduction, radiation, and conduction through the interstitial gas inside the cavity was evaluated, assuming negligible convection phenomena.
A physical model was used to predict the thermal conductivities of insulating materials based on various factors.
The equations 1 and 2 are used to calculate thermal conductivity [4].

$$k_e = k_{s.e} + k_g \tag{1}$$

$$k_e = 0.00252T + 7.98 \times 10^{-8} T^3 + \frac{1.243 T^{0.587} P}{0.895T + P} \tag{2}$$

Where $k_{s.e}$ and k_g represent the effective thermal conductivity of an insulating material, T is the absolute temperature in K, and P is the pressure of the vacuum layer in Pa. The effective thermal conductivity of an insulating material can be estimated by adding three main contributions: the solid contribution, represented as a linear or power law of temperature, the radiative contribution, represented as a cubic power of temperature, and the contribution of the interstitial gas, represented as a rational polynomial function of pressure and temperature.
For the calculation of heat flow, Fourier's equation is used, taking into account the dependence of conductivity on temperature and the average exchange area.
During the model development, some assumptions considered.
To simplify the calculation, it was assumed that the cryogenic liquid in equilibrium is stratified at the top, resulting in saturation conditions, while the cold liquid at the bottom of the tank remains in a subcooled state even under the new pressure conditions.
As time progresses, the subcooled liquid shrinks, due to the thermal reentry, a part evolves into warm liquid under saturation conditions, while a part of the warm liquid in equilibrium evaporates, increasing the gaseous phase [2] [1].
The assumptions used for the model are as follows:

1. Non-operational condition of the tank;
2. Perfect vacuum conditions, homogeneous distribution of perlite;
3. Closed tank, incapable of exchanging mass with the outside, non-isobaric conditions;

4. Constant heat flow;
5. Incoming heat is considered entirely as latent heat to vaporize the liquid;
6. Vapor-liquid phases in thermal equilibrium during the entire process;
7. Phases stratification: subcooled liquid at the bottom, saturated liquid above, and vapor at the top of the tank;
8. Circulating flows, local convection, and negligible vortices.

Starting from the equations derived from mass and energy balances, modeled according to the applied assumptions, the equation regarding the evaporation rate and the saturated mass are given respectively by equations 3 and 4.

$$\epsilon_v = \exp\left(\frac{C_{PC,i}(T_{C,0} - T_{C,i})}{\Delta H_{\text{vap,i}}}\right) \tag{3}$$

$$m_{C,i} = \frac{Q \cdot \Delta t}{H_{C,i} - H_{F,i}} \tag{4}$$

Knowing the initial conditions of pressure and temperature of the cryogenic liquid and using the available thermodynamic data for the subcooled and saturated phases at the initial pressure, it is possible to determine the saturated mass at the desired time, as well as the evaporation rate.

Therefore, it is possible to obtain the value of the evaporated mass at each time interval and update the masses and volumes of the subcooled liquid, saturated liquid, and vapor.

In this way, being able to determine the variation of masses and volumes at each instant, and therefore also of molar densities, using the Peng-Robinson relation, it was possible to calculate the pressure increase due to the evaporation phenomenon.

Based on these equations, a calculation tool has been implemented to provide a description of the evaporation process and pressure trend over time, until the maximum allowable pressure is reached.

For tanks with a MAWP, maximum allowable working pressure, higher than the supercritical pressure of the cryogenic substance, a calculation model has been developed valid from the reaching of the supercritical region, with the assumption of isochoric transformation. The reference equation for the enthalpy relative to the mass in the supercritical phase at each considered instant is given by equation 5.

$$H_i = \frac{Q \cdot \Delta t - m_{\text{tot}} \cdot H_{i-1}}{m_{\text{tot}}} \tag{5}$$

In this way, knowing the initial conditions of the supercritical mass and using the thermodynamic data related to the isochoric transformations of the substance under examination in the supercritical state, it is possible to determine the pressure and temperature at each instant, associated with the calculated enthalpy.

Once the maximum allowable pressure of the tank is reached, the iterative cycle is interrupted, as safety measures intervene to prevent further pressure increase.

The outlined calculation model follows a systematic approach, starting from the input of the necessary information to calculate the incoming heat flow and proceeding iteratively to determine the evaporation rates and phase masses over time. This iterative process involves updating the quantities of subcooled liquid, saturated liquid, and vapor based on evaporation phenomena, considering variations in mass, volume, and density. The model employs the Peng-Robinson equation to calculate pressure increments resulting from evaporation.

The output variables include the evaporation rate, liquid and vapor masses, pressure, temperature, density, and enthalpy at each time interval. These outputs provide insights into autopressurization and evaporation phenomena under different storage conditions. Furthermore, the model is crucial for estimating the time required to reach the MAWP during tank inactivity, improving decision-making and industrial safety, also estimating pressure behavior in the supercritical region.

4. Results

Initially, the computational tool was applied to a medium-pressure oxygen tank to validate the model with available experimental data. The experimental data conforms to the international standard ISO21014, relating to the insulation performance of cryogenic taks. These data provide the daily evaporation rate by measuring the gas flow as mass flow using a mass flow meter. Specifically, for a cryogenic oxygen tank with a vertical configuration and vacuum perlite insulation, with a capacity ranging from 60 to 70 thousand liters, with an external temperature

of 15°C and an operating pressure of 17 Barg, the standard predicts an expected daily volumetric loss of 0.13% of the initially stored product. Through the proposed model, a value of 0.21% is obtained, considered coherent with the expected result.
Furthermore, a sensitivity analysis was conducted by varying parameters such as insulation layer conductivity, vacuum level in the interstitial space, and external temperature. The parameter that proved to be most impactful is the variation in the vacuum level, which results in a significant change in both pressure oscillation and daily evaporation rate.
The model was subsequently applied to the case of greater interest: a high-pressure nitrogen tank with a capacity of 20 m^3 and a pressure of 31 Barg. Figure 1 shows the evolution of liquid cryogenic volume and pressure on a daily basis in the subcritical region, while Figure 2 describes the pressure oscillation in the supercritical region up to the MAWP. In the supercritical region, the pressure trend has a steeper inclination compared to the subcritical region, indicating a more pronounced increase in pressure over time. This suggests that pushing tanks to such pressures could result in significant and uncontrollable pressure fluctuations.
In the subcritical region, the pressure variation is approximately 0.1 bar per day. However, in the supercritical region, the pressure increases by 3 bar in about 22 hours, reaching the MAWP.

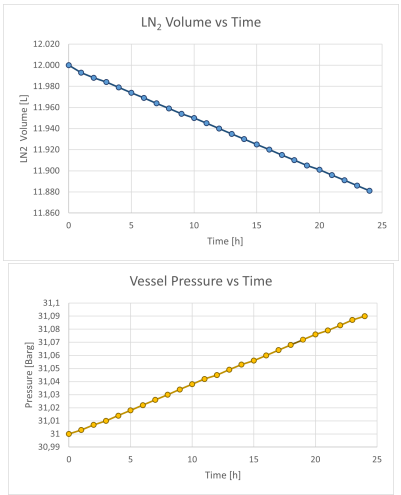

Figure 1: Trend of liquid volume [L] and pressure [Barg] with respect to time [h]. Subcritical state.

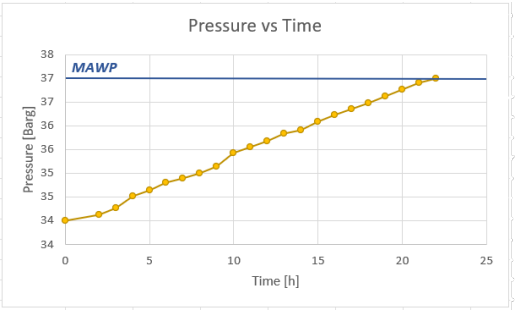

Figure 2: Trend of pressure with respect to time. Supercritical state.

The search for an optimal configuration was then conducted on the most commonly used capacity for high-pressure nitrogen tanks, 3 m^3 at 31 Barg. Table 1 and the graphs summarize the results obtained from the calculation model based on different filling levels and testing two different vacuum levels in the interstitial space: one relative to standard tanks (0.26 mBar) and one of the latest generation tanks (0.04 mBar).
Table 1 and Figure 3 highlight the evaporation rate (NER) and pressure trend for different % filling levels.

Evaporation rate - different % filling levels

% Filling	NER
50	2.4
60	2
65	1.9
70	1.8
75	1.64
80	1.6
85	1.45

Table 1: Evaporation rate - % Filling. Substance: Nitrogen. Capacity: 3 000 L.

Figure 3: Pressure trend with respect to time - 50, 60, 65, 70, 75, 80, 85 % filling levels. Substance: Nitrogen. Capacity: 3 000 L.

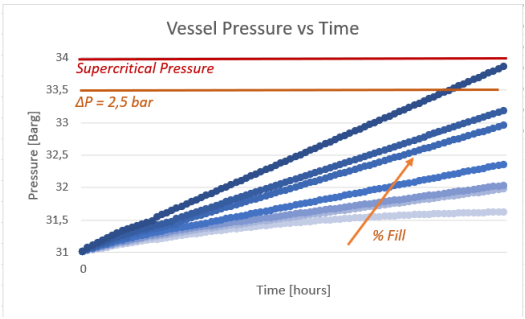

The approach used aims to conserve the product as much as possible, thus avoiding direct releases into the atmosphere to lower tank pressure. This strategy favors efficiency.
Consequently, the tank is not pushed to the maximum allowed pressure conditions. Instead, it is advisable to stay below the supercritical conditions and set the safety valve, with a limit of 2.5 bar over the course of a week. Based on the tank design and considered operating conditions, the potential filling limit is approximately 80%.
Since tanks are typically filled to 50/60%, adopting the new level obtained through the proposed calculation model results in a significant difference in kilograms of cryogenic nitrogen stored and the number of refueling trips required.
Furthermore, by combining the new optimized configuration with the use of latest-generation tanks (pressure of vacuum layer at 0.04 mBar), it is possible to significantly reduce annual nitrogen loss, as represented in Table 2.

Nitrogen wasted in evaporation - different vacuum conditions

Vacuum [mBar]	LN_2 [Kg]
0.26	16 065
0.04	6 318

Table 2: Nitrogen wasted in evaporation [Kg] - different vacuum conditions. Substance: Cryogenic Nitrogen. Capacity: 3 000 L.

Finally, with the aim of describing the economic impact on transportation costs of the new optimized configuration, a comparison was made between the performance of an existing standard tank and the new configuration.
For the calculations, a customer located 50 km from the site is considered, characterized by 2 monthly deliveries with a tank filling of 50%. Each delivery consists of 1 148 kg. Annually, a total of 24 deliveries are made, with a discharge of 27 552 kg. However, being a standard tank, 16 065 kg of this are lost in evaporation. Only 11 487 kg of the total delivered are actually used annually. This data represents the annual net consumption.
Assuming the tank is replaced with an identical design but with the latest generation vacuum pressure, the customer has an additional 9 747 kg of cryogenic nitrogen, not subject to evaporation.
With the new optimized configuration, since the tank reaches 80% capacity, it is possible to discharge 1 836 kg at each refueling. Taking into account the customer's annual net consumption, kilograms saved in terms of evaporation with the new configuration, and the increased filling level, it is possible to reduce annual deliveries from 24 to 6. Annual savings in terms of costs for both the company and the consumer related to the number of deliveries and transportation costs can be determined. The following equations consider a fixed delivery fee for the customer, €150, and a delivery cost for the producer related to kilometers traveled, €106.

$$\text{Producer Savings} = 106\,[€] \times 18 = 1908\,[€] \tag{6}$$

$$\text{Customer Savings} = 150\,[€] \times 18 = 2700\,[€] \tag{7}$$

Finally, it is possible to calculate the difference in terms of kg/CO_2 emitted in the case of the initial tank configuration and the optimized configuration, using a multiplicative factor that takes into account emissions associated with both transportation and production.
Table 6 highlights emissions based on the scenarios considered:

CO_2 emissions in one year - different tank conditions.

	Emissions [tonne]
Standard	10 249
Optimized	4 097

Table 3: Annual CO_2 emissions - different tank conditions.

5. Conclusions

Liquid nitrogen is widely used in various industrial sectors, with a growing global market. However, production and distribution costs hinder this growth. Cryogenic nitrogen tanks face challenges in heat management and pressure regulation.
These challenges lead to product loss due to evaporation and limits on tank filling, increasing refueling and transportation costs. Understanding the phenomenon of thermal returns is essential to optimize tank design and operation, in order to mitigate economic losses and ensure safety.
The study focused on heat exchange mechanisms and the development of a mathematical model to predict tank pressure trends and evaporation rates. Simplified relationships were derived from mass and energy balances, allowing predictive modeling.
Sensitivity analysis revealed vacuum level as a critical tank design parameter. Optimizing tank configurations based on model results can increase filling levels while ensuring safety.
From the calculation model, it was possible to determine for a high-pressure nitrogen tank, a new optimal filling level, ensuring safety in terms of pressure rise. It was also possible to calculate the difference in kilograms of evaporated mass between standard and optimal designs, with higher vacuum.
Estimating economic savings in logistical terms, and reductions in carbon dioxide emissions by optimizing tank configuration, highlighted significant benefits compared to standard configurations.
The reproducible mathematical model provides a valuable tool for studying variables involved in heat exchange, offering rapid estimation without costly experimental procedures.
The increasing demand for cryogenic substances and their potential for future applications underscores the importance of further investigations into computational modeling and the engineering of materials and cryogenic tank design.

References

[1] Velisa Vesovic Calogero Migliore, Cristina Tubilleja. Weathering prediction model for stored liquefied natural gas (lng). *Journal of natural gas science and engineering*, 2015.

[2] Velisa Vesovic Felipe Huerta. Cfd modelling of the isobaric evaporation of cryogenic liquids in storage tanks. *International Journal of Heat and Mass Transfer*, 2021.

[3] Thomas M. Flynn. *Cryogenic Engineering*. Marcel Dekker, USA, 2005.

[4] Ram R. Ratnakar, Zhe Sun, and Vemuri Balakotaiah. Effective thermal conductivity of insulation materials for cryogenic lh2 storage tanks: A review. *International Journal of Hydrogen Energy*, pages 7770–7793, 2023.

POLITECNICO
MILANO 1863

SCUOLA DI INGEGNERIA INDUSTRIALE
E DELL'INFORMAZIONE

Study of heat losses in cryogenic high-pressure nitrogen tanks

Tesi di Laurea Magistrale in
Chemical Engineering - Ingegneria Chimica

Author: **Linda Tommasi**

Student ID: 994873
Advisor: Prof. Valentina Busini
Co-advisors: David Manzoni, Giulia Tomellini
Academic Year: 2023-24

Ringraziamenti

In primo luogo, ringrazio la mia relatrice Valentina Busini, per avermi costantemente seguita in questo percorso di tesi. I suoi spunti, le sue analisi critiche e le sue proposte sono state fondamentali per lo sviluppo e l'implementazione della ricerca.

Ringrazio inoltre David Manzoni, per aver creduto e avrmi dato la possibilità di svolgere la ricerca con il team Air Liquide. Il suo tempo e la sua esperienza sono state preziosi per la ricerca. La fiducia che ha riposto in me dal primo giorno mi ha permesso di svolgere in serenità e curiosità l'esperienza di tesi in azienda, in modo da mettermi in gioco e poter cogliere al massimo questa opportunità.

Ringrazio Giulia Tomellini per avermi aiutata e affiancata per lo sviluppo del modello di calcolo, la sua professionalità e supporto sono state cruciali nel supermanento degli ostacoli riscontrati durante lo sviluppo della tesi.

Ringrazio infine mia sorella e i miei genitori, senza i quali questo lungo e gratificante viaggio non sarebbe stato possibile.

Abstract

Liquid nitrogen (LN_2) is widely employed across various industries, encompassing food, pharmaceuticals, and electronics. Despite the expanding global market for liquid nitrogen, production and distribution costs present significant challenges. Cryogenic tanks are specifically engineered to sustain the liquid at low temperatures but encounter issues related to heat and autopressurization. These challenges are particularly pronounced in high-pressure tanks, which, for safety reasons, are typically filled to only 50-60% capacity, leaving empty space to accommodate evaporation and volume fluctuations. Such design decisions lead to economic disadvantages, including additional logistics costs due to increased refilling trips.

The study aims to comprehend the primary factors influencing heat conduction in cryogenic tanks. By developing a simplified mathematical model to elucidate the physical phenomena of evaporation and autopressurization, it becomes feasible to predict the rate of evaporation and pressure fluctuations over time, contingent upon storage conditions and tank design.

By identifying the parameters with the greatest impact on the evaporation phenomenon, an optimal configuration satisfying the need to increase filling percentage while adhering to pressure rise limits was determined. Consequently, calculations were performed to assess the savings in cryogenic product, reduced delivery costs, and lower CO_2 emissions associated with the optimal configuration compared to the standard configuration used currently.

Keywords: LN_2, cryogenic tanks, heat losses, evaporation, autopressurization.

Abstract in lingua italiana

L'azoto liquido (LN_2) è ampiamente utilizzato in diversi settori industriali, tra cui quello alimentare, farmaceutico e elettronico. Mentre il mercato globale dell'azoto liquido è in espansione, i costi di produzione e distribuzione rappresentano sfide significative. I serbatoi criogenici sono appositamente progettati per mantenere il liquido a basse temperature, ma incontrano problemi legati al calore e all'autopressurizzazione. Queste sfide sono particolarmente pronunciate nei serbatoi ad alta pressione, che, per motivi di sicurezza, vengono di solito riempiti solo al 50-60% della capacità, lasciando spazio vuoto per accomodare l'evaporazione e le variazioni di volume. Tali decisioni progettuali comportano svantaggi economici, tra cui consistenti costi aggiuntivi di logistica dovuti ai maggiori viaggi di rifornimento.
Questo studio mira a comprendere i principali fattori che influenzano la conduzione del calore nei serbatoi criogenici. Sviluppando un modello matematico semplificato che descrive i fenomeni fisici di evaporazione e autopressurizzazione, diventa possibile prevedere il tasso di evaporazione e le fluttuazioni di pressione nel tempo, a seconda delle condizioni di stoccaggio e di design del serbatoio.
Identificando i parametri di maggior impatto sul fenomeno di evaporazione, è stata determinata una configurazione ottimale che soddisfa la necessità di incrementare la percentuale di riempimento rispettando i limiti di aumento di pressione. Di conseguenza, sono stati eseguiti calcoli per valutare i risparmi di prodotto criogenico, i costi ridotti di consegna e le minori emissioni di CO_2, associate alla configurazione ottimale rispetto alla configurazione standard attualmente in uso.

Parole chiave: LN_2, serbatoi criogenici, rientri termici, evaporazione, autopressurizzazione.

Contents

List of Figures

List of Tables

List of Symbols

Variable	Description	Unit
$\boldsymbol{a}$	Attractiveness parameter	Pa $m^3/mol^2/Pa$
$\boldsymbol{a_c}$	Critical attractiveness parameter	Pa $m^3/mol^2/Pa$
$\boldsymbol{A}_{\mathrm{e}}$	Area of the external vessel	m^2
$\boldsymbol{A}_{\mathrm{i}}$	Area of the inner vessel	m^2
$\boldsymbol{A}_{\mathrm{mean}}$	Tank exchange area	m^2
$\boldsymbol{b}$	Repulsion parameter	$m^3/mol/Pa$
$\boldsymbol{C_{PC}}$	Superheated liquid heat capacity at constant pressure	kJ/(kg·K)
$\boldsymbol{C_P}$	Supercritic heat capacity at constant pressure	kJ/(kg·K)
$\boldsymbol{d}$	Derivative	-
$\boldsymbol{d_V}$	Vapour molar density at instant i	mol/m^3
$\boldsymbol{D}_{\mathrm{e}}$	Diameter of the external vessel	m
$\boldsymbol{D}_{\mathrm{i}}$	Diameter of the inner vessel	m
$\boldsymbol{exp}$	Exponential function	-
$\boldsymbol{h}$	Thickness of the insulation layer	m
$\boldsymbol{H}$	Enthalpy	kJ/kg
$\boldsymbol{H_{F,i}}$	Subcooled liquid enthalpy at instant i	kJ/kg
$\boldsymbol{H_{C,i}}$	Superheated liquid enthalpy at instant i	kJ/kg
$\boldsymbol{H_o}$	Subcooled liquid enthalpy at instant $t = 0$	kJ/kg
$\boldsymbol{H_V}$	Vapor enthalpy	kJ/kg
$\boldsymbol{i}$	Instant of time	s
$\boldsymbol{ln}$	Natural logarithm	-
$\boldsymbol{k}$	Peng-Robinson parameter	-
$\boldsymbol{k_e}$	Global thermal conductivity of insulation layer	mW/(m K)
$\boldsymbol{k_g^0}$	Gas thermal conductivity in the continuum limit.	mW/(m K)
$\boldsymbol{k_g}$	Thermal conductivity of interstitial gas	mW/(m K)
$\boldsymbol{k_{s.e}}$	Conductivity and thermal radiation of Perlite	mW/(m K)
$\boldsymbol{K_T}$	Isothermal compressibility	1/Pa
$\boldsymbol{L}_{\mathrm{c,e}}$	Length of the cylindrical section of the external vessel	m
$\boldsymbol{L}_{\mathrm{c,i}}$	Length of the cylindrical section of the inner vessel	m

Variable	Description	Unit
$\boldsymbol{m_{C,0}}$	Superheated liquid mass at instant 0	kg
$\boldsymbol{m_{C,i}}$	Superheated liquid mass at instant i	kg
$\boldsymbol{m_{F,i}}$	Subcooled liquid mass at instant i	kg
$\boldsymbol{m_o}$	Subcooled liquid mass at instant $t = 0$	kg
$\boldsymbol{m_e}$	Evaporated mass	kg
$\boldsymbol{m_{tot}}$	Supercritic mass	kg
$\boldsymbol{m_V}$	Vapor mass	kg
$\boldsymbol{P}$	Pressure	Pa
$\boldsymbol{P}_{\text{critic}}$	Critical Pressure	Bar
$\boldsymbol{P}_{\text{vac}}$	Pressure vacuum insulation	Bar
$\boldsymbol{PM}$	Molecular weight	kg/mol
$\boldsymbol{Q}$	Heat flux	kW
$\boldsymbol{R}$	Gas constant	$\text{m}^3/\text{mol} \cdot \text{K}$
$\boldsymbol{T}$	Absolute temperature	K
$\boldsymbol{T_c}$	Critical temperature	K
$\boldsymbol{T}_{\text{in}}$	Temperature inside the inner vessel	K
$\boldsymbol{T}_{\text{out}}$	Outside temperature	K
$\boldsymbol{T_{C,0}}$	Temperature of saturated liquid at instant 0	K
$\boldsymbol{T_{C,i}}$	Temperature of saturated liquid at instant i	K
$\boldsymbol{T_r}$	Reduced temperature	K
$\boldsymbol{V}$	Volume	m^3
$\boldsymbol{V_C}$	Saturated liquid volume	m^3
$\boldsymbol{V_F}$	Subcooled liquid volume	m^3
$\boldsymbol{V_V}$	Vapor liquid volume	m^3
$\boldsymbol{w}$	Acentric factor of nitrogen	-
$\boldsymbol{\alpha}$	Interaction parameter	-
$\boldsymbol{\Delta H}_{\text{vap}}$	Enthalpy of vaporization	kJ/kg
$\boldsymbol{\Delta t}$	Time step	s
$\boldsymbol{\epsilon_L}$	Saturated liquid mass fraction	-
$\boldsymbol{\epsilon_v}$	Evaporated mass fraction	-
$\boldsymbol{\pi}$	3.1415	-
$\boldsymbol{\rho_C}$	Saturated liquid density	kg/m^3
$\boldsymbol{\rho_F}$	Subcooled liquid density	kg/m^3
$\boldsymbol{\rho_V}$	Vapor liquid density	kg/m^3

Introduction

In industrial sector, nitrogen is extracted from the atmosphere by fractional distillation of air subjected to purification processes and subsequently cooled to a liquid state. Following this, it is stored in tanks of various sizes, adapted to the needs of production. The high level of interest in industry stems from the many fields of use. In fact, liquid nitrogen is in extensive demand as a refrigerant in the food, beverage and pharmaceutical industries, and this is the main impact of the global liquid nitrogen market. Also important is the use of the product for the production of flat panel displays, light-emitting diodes and semiconductors, which confirms the arrival of liquid nitrogen in the electronics field, which will increase the various growth opportunities in the market. In addition, liquid nitrogen has gained considerable importance in aerospace engineering, where it is used as a propellant for rocket engines, and the rise of cryopreservation cryotherapy and cryosurgery for moles, skin care, elimination of skin plaque, and treatment of skin neoplasms, is providing new marketing opportunities. In particular, studies predict fast market growth over the next decade, with an expected compound annual growth rate yearly growth rate of about 5%, which would lead to a market size of 25.65 trillion by 2029. The projected market growth holds significant impact, especially considering the baseline of USD 16.4 billion in 2020 [1, 29].

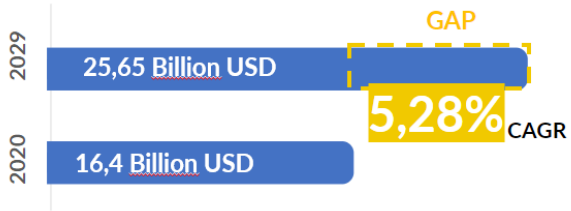

Figure 1: Nitrogen market growth forecast from 2020 to 2029

The substantial expenses associated with the production and distribution of liquid nitrogen pose a significant barrier for small businesses and industries, especially in terms of the high costs related to cryogenic systems and tanks. Currently, the major global players dominating the production and sale of liquid nitrogen include Air Liquide, The Linde

Group, Nex Air, Gulf Cryo, Messer, and Nippo Nanson [1].

Cryogenic nitrogen tanks are typically constructed from highly heat-resistant materials, such as stainless steel or aluminium. These tanks are engineered to maintain nitrogen at extremely low temperatures, approximately -196 °C, ensuring its existence in a liquid state.
Cryogenic liquids present several engineering challenges in processing, transport, and storage due to their extremely low normal boiling point. These challenges arise from the need to address issues related to heat management. Cryogenic tanks are extensively insulated, and ongoing research and advanced technology focus on minimizing heat reentry. Nevertheless, they are susceptible to heat ingress from their surroundings, driven by the temperature gradient between the ambient air and the cryogen. This heat input causes the stored cryogen to heat up and evaporate, leading to a continuous increase in tank pressure through a autopressurization process. As the pressure reaches the Maximum Allowable Working Pressure (MAWP), the cryogen is released from the tank as evaporative gas (BOG). The generation of BOG can result in economic losses, pose safety risks, due to the exceeding of structural integrity limits, and have adverse environmental effects, thereby limiting the widespread industrial application of cryogenic liquids.

Due to the aforementioned considerations, cryogenic tanks are not filled to 100%, primarily for safety reasons and to address the challenges associated with volume variations resulting from temperature fluctuations. As a standard practice, high-pressure tanks with an operative pressure greater than 30 barg are typically filled to 50-60%. This design choice is motivated by several factors.
Firstly, cryogenic fluids like liquid nitrogen can naturally evaporate even at low temperatures. When this evaporation occurs, the resulting gas occupies significantly more space than the liquid. If a tank were filled to its maximum capacity, there would be no room for the gas head, leading to a potential buildup of excessive pressure inside the tank. This pressure could pose a threat, potentially damaging the tank or causing an explosion. By maintaining a space, referred to as a 'gas head' or 'gas cushion', room is provided for the gas produced through evaporation.
Additionally, at low temperatures, the material of the tank contracts due to thermal effects. Filling the reservoir to its maximum capacity could subject the structure to excessive stress during temperature variations, risking potential damage. Therefore, maintaining a percentage of space within the tank serves as a safety measure to accommodate these temperature-induced changes. By preserving this space, the structure gains flexibility to accommodate temperature fluctuations. The gas head serves as a means to regulate the pressure inside the tank. In the event of an increase in internal pressure due to tempera-

ture changes or other factors, the gas in the head can be released or recycled to maintain pressure within safe limits.
It is crucial to recognize that completely filling the tank to its limit would make transportation and handling challenging, as any shock or vibration could result in the spillage of cryogenic liquid.

In summary, the common practice of maintaining an empty space at the top of the tank, known as a gas head, is integral to ensuring the safe utilization of cryogenic tanks. This space offers adaptability to address issues such as evaporation, temperature variations, and internal pressure, contributing significantly to the safety and operational efficiency of cryogenic tanks. Nevertheless, it's essential to acknowledge that partial filling incurs economic losses, necessitating larger cryogenic tank capacities and increased transportation costs. This, in turn, leads to an inevitable rise in capital expenditures (CAPEX).

The interest in heat return, autopressurization, and evaporation phenomena in cryogenic reservoirs dates back to the latter half of the 20th century. Furthermore, the widespread industrial application of cryogenic technologies has spurred increased research efforts in subsequent decades. Notably, the utilization of cryogenic systems in the space sector has garnered heightened attention from researchers examining leak-free storage and transport characteristics of liquid nitrogen tanks.
In the aerospace engineering field, where safety and efficacy are of paramount importance, the study of cryogenic propellant behavior has become a focal point. This critical context has stimulated a growing emphasis on research in this domain. The thermal insulation of cryogenic systems and components holds significant economic importance, as a heat loss of one Watt at low temperatures necessitates compensation by many Watts at room temperature [29][15].

The influx of heat from the surrounding environment initiates a series of intricate transport phenomena within the storage tank, including evaporation, thermal stratification, buoyancy-driven flow, thermal expansion of the liquid, and pressure build-up. Consequently, comprehending the physical phenomena associated with heat reentry is crucial for optimizing the design and operation of cryogenic systems. This understanding is vital to strike the optimal balance in terms of the invested capital expenditure (CAPEX), safety considerations, and the limitation of evaporated product.
Efficiency and meeting customer needs serve as the common denominator for these three factors. Customers seek high performance and the ability to fully utilize the purchased product while adhering to safety parameters. Therefore, a thorough understanding of the physical phenomena driving the evaporation of cryogens during storage is paramount in optimizing the design and operation of cryogenic systems.

For the in-depth study of these issues, this work was carried out with one of the world's leading manufacturers of cryogenic nitrogen: Air Liquide. In developing this work, there was collaboration with engineers specialising in the cryogenic sector and a better understanding of the issues surrounding cryogenic re-entry that are reflected in industrial problems. Fundamental to the detailed understanding of cryogenic tank operation and design were visits to the Chieve plant, during which much information was gathered for the modelling of this work.

1 State of the art

1.1. Cryogenic vessels

For the storage of cryogenic substances like nitrogen, oxygen, helium, argon, and hydrogen, typically at temperatures below -150°C, specialized tanks are employed. These tanks are designed to handle substances with boiling points below room temperature, ensuring efficient storage and transport. They enable space savings through gas liquefaction and contribute to safety during handling.

Various types of cryogenic tanks exist, tailored to the material stored, operating conditions, required capacities, and their intended function (transport or storage). Tanks can be categorized based on their geometry, commonly cylindrical or spherical, and the materials employed, which may include stainless steel, aluminum, austenitic alloys, and others.

Aimed at minimizing heat exchange with the external environment, each design choice is closely related to the specific environmental characteristics it encounters, including location, climate, and type of terrain, while satisfying the required capacity and type of liquid stored. One of the most critical parameters in the design choice is insulation. The economy is linked to the evaporation rate, which is determined by the effectiveness of the insulation.
A common configuration involves cylindrical double-walled tanks, characterised by a stainless steel inner tank and carbon steel outer tank, filled with insulation material in the cavity under vacuum conditions. For the insulation material, there are also several possibilities, including powder fillings such as perlite and silica aerogel, foam fillings such as polyurethane, polystyrene and polyamide, or fibre insulation. The choice between different materials is always relative to the material stored and the environmental conditions[15][29].

The invention of the first vacuum-insulated vessel for liquefied gases dates back to 1892, dictating a breakthrough in the field of thermal insulation that has yet to be matched by further developments. This invention consisted of a double-walled vessel with a high

vacuum condition in the cavity. Subsequent research and improvements in this field were merely modifications of Dewar's initial concept, in terms of reducing conduction and radiation transfer by using special external aluminised materials, reflective paints or by interposing screens that reflect or intercept radiant heat. The importance of this discovery was the presence of vacuum insulation, which was fundamental in almost completely limiting the two main modes of heat reentry: gaseous conduction and convection. Dewar's proposed vacuum cavity model, combined with measures to minimise heat transfer by radiation and conduction from solid structural elements, is the most effective known [15].

1.2. Example of industrial cryogenic tanks: Air Liquide and the Chieve site

Air Liquide is one of the world's leading players in terms of supplying industrial technical gases such as nitrogen, oxygen, helium, and argon. It supplies a wide range of cryogenic tanks, through compact and flexible solutions equipped with an integrated cryogenic storage and supply system, atmospheric vaporiser and cold protection device. The site in Chieve, in the province of Cremona, is Air Liquide's national centre for revamping and storing cryogenic equipment in Italy, to offer customers an increasingly safe, rapid service, and results with high quality standards. During this thesis research and study, the opportunity arose to visit the Chieve plant, enabling direct observation of the design and operation of a double-shell cryogenic tank in the field. The following provides valuable information gathered from technicians on-site, offering a detailed description of a typical Air Liquide tank for storing liquid nitrogen.

1.2.1. Design of a typical Air Liquide tank

A typical cryogenic tank made by Air Liquide essentially consists of an outer carbon steel wall, (called the outershell), or jacket, a high vacuum intermediate space, and the stainless steel tank, which is characterised by high chemical and low-temperature resistance and a higher cost than the outer shell.The air between the void is drawn in with the assistance of an air separation unit and rendered inert to enhance insulation. The double-shell configuration with a cavity is utilized to minimize heat transfer by conduction and convection, effectively isolating the low-temperature fluid inside and thereby establishing a physical barrier to achieve the lowest possible thermal transmission. In the classic cryogenic tanks used by Air Liquide, and to which this is devoted, a cavity filled with vacuum perlite, a few centimeters thick, is used for insulation purposes [12]. The vacuum cannot conduct by conduction and convection, but only by radiation, which can be minimised by using

white tanks and applying a reflective coating to the outer wall [25] [13]. For practical applications, perlite, a bulk granulate material of volcanic origin that is inflated at high temperatures, is highly qualified among powdered materials[15].

Perlite is introduced from the top of the tank for smaller capacity storage, while for larger capacity tanks, multiple side plugs allow perlite to be filled horizontally. The filling process occurs through vibration to ensure the perlite is evenly distributed and compacted. It's important to note that in the tanks under consideration, the last accurate vacuum value available is established and detected by the devices at the time of pumping, typically 2.6 mBar for the standard vessel and 0.4 mBar for more advanced vessels. Once nitrogen at cryogenic temperature is introduced, it causes a restriction of the tank itself and a consequent increase in vacuum to 0.26 or 0.04 mmBar. The loss of vacuum during tank use is a condition to be avoided and monitored closely. Ice formation in the vacuum perlite indicates cooling of the outermost wall due to heat transfer with the internal fluid, which can lead to serious risks associated with embrittlement of the carbon steel, unsuitable for low operating temperatures. A common property of all cryogenic insulation systems is that they must be protected against water vapor penetration due to their low operating temperature; otherwise, their efficiency is greatly reduced. This necessitates preventing gas exchange with the atmosphere and often requires the construction of expensive vapor barriers[15].
The cavity is also equipped with a safety device, positioned on the top of the tank, capable of controlling the filling of perlite. The primary function of this device is to safeguard the tank from possible rupture of internal pipes and spillage of product into the cavity with consequent loss of vacuum. In the event of a leakage of product inside, and therefore an increase in pressure, the movable flange comes into operation, rising, to prevent air and moisture from entering the interior.

The external tank, made of carbon steel, consist of a several external rings, which increases as the size of the tank increases, with the function of supporting the casing itself against the vacuum pressure that could induce implosion. This choice is closely related to economic reasons, as the use of stronger external materials or the choice of a thicker shell would be reflected in higher costs. These two shells (tanks) are connected by support blocks, which act as reinforcements and help maintain the structural stability of the reservoir, absorb stresses and hold the shell firmly in place. The number of these 'struts' varies depending on the size of the tanks and are dimensioned at a certain angle, usually 17.5°. The function is to support the inner tank while minimising the conduction. The struts connected to the external tank using of two plates in the case of small tanks, while for capacities greater than 20 m^3 they have a drainage strip. The stainless steel tank,

moreover, considering that it undergoes a contraction of 3 millimetres per metre when nitrogen is loaded, is equipped with a centring ring that ensures the stability of the inner tank even under conditions of contraction and expansion of the steel, thus avoiding possible overturning [25] [13]. The structure is also supported by support legs and anchor plates at the tank pads. The tank rests on 3 legs with a bottom attachment, while 4 legs, with a top attachment, are required for use in seismic areas [25].

The stainless steel tank consists of a liquid phase storage product fraction and a gaseous product fraction. The gas phase usually constitutes 10%, (5% in the latest generation of tanks), for tanks at atmospheric or medium pressure, while this figure rises to 40/50% when it comes to high-pressure tanks (operative pressure>30 barg). Filling the tank takes place from the bottom and results in an increase in pressure in the tank. The operator opens the valve called 'overflow' in the design project and is able to monitor the filling progress from both the level gauge and the venting of the valve itself. Once the maximum permissible filling is reached, liquid nitrogen escapes from the valve and the operator has completed the filling phase and can proceed to close the valve. There is also a second method of backfilling, called sprinkling filling, from above, usually intended for a smaller percentage of the filling and in the final part. It involves a decrease in internal pressure coupled with the liquefaction of part of the bearing gas phase, saving part of the product for the customer. In small tanks, a filling stop valve is installed to prevent overfilling. In the case of larger tanks, however, this task is left to the operator's discretion. Furthermore, in the case of tanks with an independent outlet, filling is possible without interrupting tank operation. Otherwise, filling is only be possible during shutdown and interruption of the liquid supply from the bottom.

All pipes inside the tank, intended for transporting liquid nitrogen and nitrogen gas, are also be equipped with a double-shell configuration to ensure an optimal degree of insulation.

1.2.2. Monitoring of the cavity void and revamping

Vacuum insulation can significantly reduce heat transfer by minimising the contribution of interstitial gas. Depending on the vacuum level achieved, heat conduction through the gas can also be reduced. However, maintaining a high vacuum level for large-scale cryogenic tanks or moving tanks can pose economic and technical challenges. In addition, escaping gas or condensed fluid may be present on the wall or inside the insulation panel. Therefore, when comparing insulation systems with different internal materials, the impact of gas conduction at various pressure and temperature levels must be considered[29].

The presence and monitoring of vacuum are therefore essential to avoid the risk of refrigerant loss and product integrity. Vacuum restoration is a procedure always carried out by Air Liquide, not by the customer. Revamping is also conducted every five years, during which time the cavity typically loses one degree of vacuum, from 26.7 to 267 Pascal, or from 0.26 to 2.6 mmBar for standard tanks, and from 4 to 40 Pascal, or from 0.04 to 0.4 mBar for more innovative tanks. In the following sections, the implications of this vacuum loss in terms of heat flow will be shown.

At the bottom of the tank there is one valve used for revamping, while in more advanced tanks there are two, the second of which is used for vacuum measurement.To ensure an accurate and consistent vacuum measurement after revamping, it is necessary to wait a minimum of 4 days to ensure homogenisation of conditions within the cavity. In addition, a sintered filter is inserted for pumping to prevent perlite from escaping, so that the removal of moisture and coarse molecules can be carried out using a primary pump, followed by refining work using a secondary pump. On digital devices it is possible to read the vacuum value, which coincides with the efficiency of the pump. During vacuum re-establishment procedures, it is necessary to take into account the fact that, once nitrogen is introduced at low temperatures, this results in a restriction and decrease in the volume of the cryogenic stainless steel tank, which is correlated with a consequent increase in volume in the cavity and a decrease in pressure, which raises the degree of vacuum.

1.2.3. Valves, safety devices and economiser

The valves on a typical Air Liquide tank are organised in such a way as to have valves relating to the liquid phase on the right and valves relating to the gas phase on the left. In particular, there are on the right-hand side double valves relating to the filling of liquid nitrogen to avoid problems arising in the event of wear.

If a sufficient quantity of liquid is transformed into gas in a closed container, due to an increase in temperature, fire, external heat sources or heat reentry, this can lead to a rise in internal pressure that can lead to explosion and rupture of the tank itself, with high safety risks. For this reason, cryogenic liquid tanks are protected with various pressure relief devices, which operates if the maximum allowable working pressure, (MAWP) the maximum pressure at which the tank or equipment can work at a specific temperature, is reached[15]. It's also possible to find safety valves and rupture discs, which operate if MAWP is reached, preventing the tank itself from exploding. These two devices work if excessive pressures are reached. There is also the pressure vacuum breaker, PVB, a relief

valve for nitrogen gas, sets at a lower setpoint than that of the safety valves and rupture discs, so that it acts as the first safety device. It is a more convenient device, in terms of management and economy, than a valve or disc to be replaced after its intervention. However, it is always preferable to continuously monitor and control the pressure inside the tank without having to resort to the safety devices just described.

Under operating conditions, when cold fluid is drawn from the bottom of the tank, by opening the appropriate valve, the pressure of the gaseous upper part decreases. If the pressure decreases beyond the set point, a device called pressure booster takes more liquid from the bottom, which, passing through a circular evaporator with finned tubes located under the tank, allows evaporation and the addition of new gas to the top with a consequent increase in pressure and reestablishment the set point [13][29]. This usually occurs when the tank is in operation, due to the extraction of liquid, which is not sufficiently compensated for by the increase in pressure due to the heat returns.
The mechanism of pressure booster is illustrated in the figure 1.1:

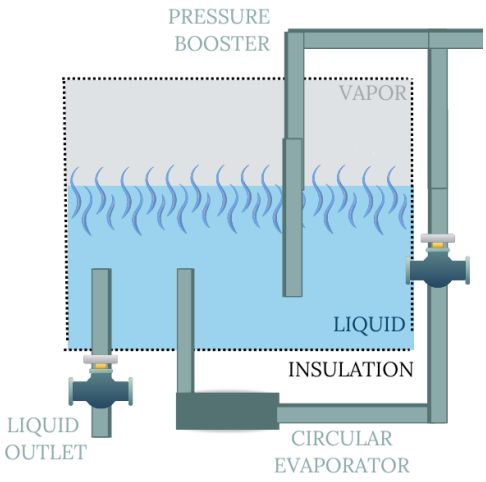

Figure 1.1: Mechanism of pressure booster. During tank operation, liquid is extracted from the left pipe. If the pressure falls below the set point, the mechanism of liquid vaporization and gas re-emission into the tank is activated to restore the pressure level.

The economiser, on the other hand, comes into operation when a pressure close to the overpressure setting is established at the top of the tank and the tank is in operation, with a demand for nitrogen in the gaseous phase, not liquid. It operates by directing gas from the vapor space to the gas utilization valve when it is open, thus minimizing gas loss due to overpressure. Any excess pressure at the top of the vapor phase is vented at the outlet of the gas utilization valve, maintaining normal operating pressure. In tanks intended for the use of nitrogen gas, the economiser prevents liquid extraction activity. This function

leverages pressure differences, allowing lower pressure gas to enter the pipe instead of liquid, which exits directly to the customer for use, contributing to a decrease in pressure. The economiser function is automatic and operates only during the operational phase of the tank. Consequently, the economiser cannot be used during stationary periods, such as plant shutdowns, resulting in venting and product loss.

In tanks for liquid nitrogen use, a safety device is also required for continuous use, correlated to a primary alarm with acoustic and visual signals following oxygen depletion, followed by a nitrogen inlet line lockout in the case of the most critical sub-oxygenated atmosphere zone. The liquid nitrogen service line for use consists of a double tube with a vacuum cavity and a stainless steel inner tube, correlated with a tube pressure gauge. Nitrogen in these pipes travels by pressure and temperature difference.

Non-return valves are present in the following sections: at the utiliser, to prevent the return of product, and at the economiser, to prevent the extracted liquid from reaching the economiser pipes; they are also present in multiple tank configurations in series.

1.2.4. Vapourisers

With the help of vaporisers, the liquid extracted at the outlet is converted to a gaseous state, as in the case of liquid nitrogen. A manifold controls the pressure at which the gas is fed to the process. For the conversion of liquid nitrogen into ready-to-use gas, finned tubes are used, where our liquid flows, in contact with air, in order to vaporise it. There are different types of gasifiers. The most common are room-air with natural circulation. There are also forced-circulation hot-air, water-operated or using electric heaters, in the case of more difficult ambient conditions for gasification [13][29].

It is clear that if the heating system had any problem performing its function correctly, there would be a danger of cold fluid passing through the pipes downstream of the evaporator and possible storage in containers made of 'non-resilient' material, with even fatal consequences for operators and users. In particular, after the accident in Caivano in 2003, where four workers lost their lives, the CSD, the cold safety device, was introduced more rigidly and regulated by law, to increase the safety of tank use. The accident occurred due to a failure of the evaporator that was responsible for transforming liquid nitrogen into gas. Due to the excessive inflow of liquid nitrogen into the vaporiser, a progressive icing of the evaporator and the 'T' valve occurred, which resulted in liquid nitrogen entering the next collector tank, at an estimated temperature of -160/-170°C. The tank, which had been designed to contain material at a temperature of no less than -10 degrees, suffered structural failure due to the liquid substance settling to the bottom at a temperature far

below what the structure could withstand [30].

The CSD safety system, a cold device with temperature probes on the output product, performs the function of monitoring the correct operation of the gasifier, acting on the output gas valve and closing it, in the event of reaching too low a temperature (approx. -10 C°), thus preventing the gas supply [13][29].

In Figure 1.2, a schematic of a cryogenic nitrogen utilization system can be pointed out, highlighting fundamental devices like the evaporator and the anoxia system discussed in earlier sections.

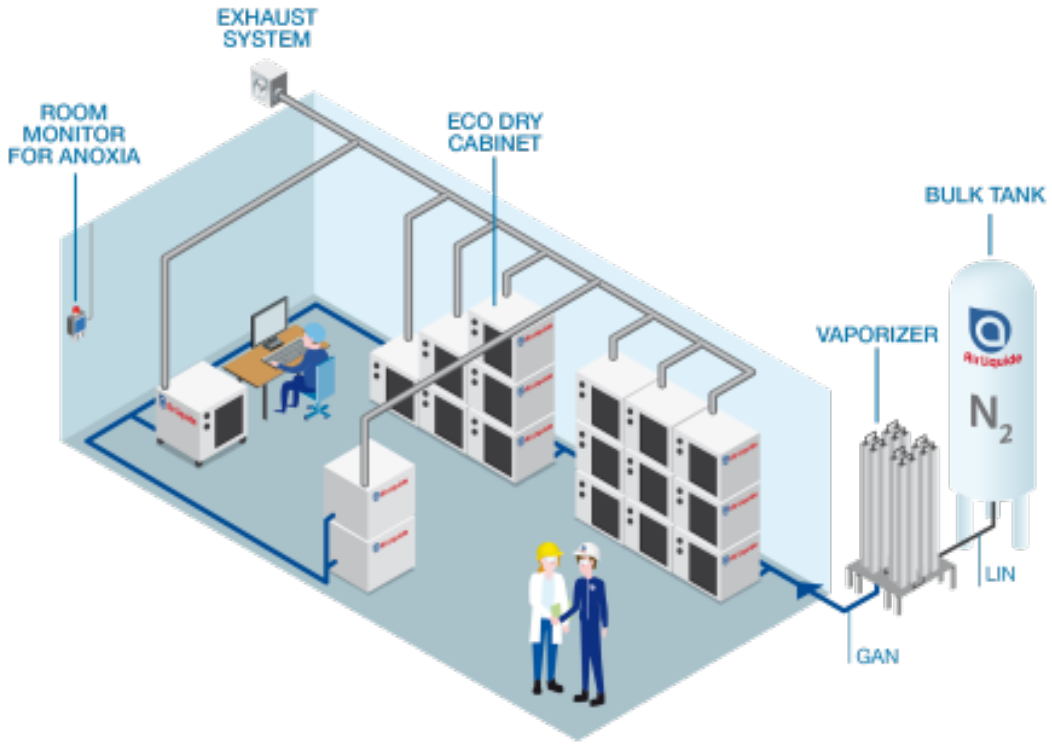

Figure 1.2: Installation and methods of using cryogenic nitrogen by the customer.

1.3. Heat recovery in cryogenic tanks: autopressurisation and liquid evaporation

As mentioned, among the issues attracting the most attention, within the subject of cryogenic tanks are the heat exchanges to which the tank is subjected both during service and during stationary periods of non-use.

Since liquefied nitrogen tanks cannot achieve absolute isolation, evaporation of a part of

the liquid is inevitable, due to the continuous thermal reentry which causes changes in the physical and thermodynamic characteristics of the stored nitrogen. This phenomenon threatens the safety of the system, as vaporisation can affect the very stability of the tank. Due to the heat penetrating the storage tank from the surroundings, part of the product vaporises, leading to an increase in the overall pressure of the tank. To avoid over-pressurisation of the tank, the evaporation gas is constantly removed through a vent valve, which opens once the MAWP, the set point for the maximum allowed tank pressure, has been reached. The evaporated nitrogen is referred to as Boil off Gas (BOG). Heat input, which can occur by conduction, convection and radiation, heats and evaporates the stored cryogen, continuously increasing the tank pressure in a process of self-pressurisation. If the heat returns are sufficient to vaporise the cryogenic liquid inside the tank, there will be a progressive increase in pressure due to the greater volume occupied by the gas phase compared to the liquid phase.

The liquid therefore needs space to expand in the tank. If the tank is 100% full, the lock-up pressure (or seal-off) exceeds the permissible values while the liquid phase is still present. It is therefore evident that the conversion of a cryogenic liquid to hot gas results in excessive pressures, catastrophic over-pressurisation and rupture of the storage tank [13]. Buoyancy space, a vapour-filled space above the liquid, is essential for safe cryogenic storage, its presence, however, requires tank oversizing, which correlates with an increase in CAPEX. The generation of BOG can produce economic losses, pose safety risks and have a detrimental environmental impact, thus limiting the industrial application of cryogenic liquids[28][13][10][34]. The extent of evaporation depends on the size of the tank and the mode of operation. In small-scale applications such as Liquid Natural Gas (LNG) vehicle fuel tanks and Liquid Hydrogen (LH_2) tanks in spacecraft, cryogens are stored under non-isobaric conditions and the tanks can withstand autopressurisation up to 1 MPa. In medium and large-scale industrial applications, where the tank volume varies from 20 to 200,000 m^3, the evaporated cryogen is removed as BOG to maintain constant tank pressure [10].

Figure 1.2 depicts a diagram of a cryogenic storage tank, showing the heat penetrating and the phenomena it causes inside, including the evaporation of the liquid and the creation of a liquid-vapour interface, a region characterised by thermal stratification.

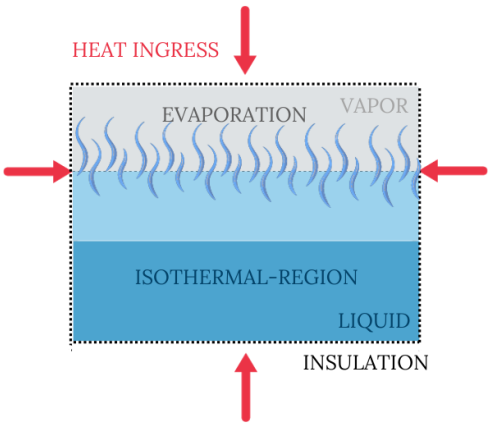

Figure 1.3: Heat rejection in a cryogenic tank.

It was already pointed out that the phenomenon of heat reentry generally causes an increase in the temperature of the fluid inside the reservoirs. In reality, this temperature change presents a phenomenon of thermal stratification characterised by a non-homogeneous state that is considered irregular. Since the density of a liquid depends on the temperature, different parts of the cryogenic liquid may have a slightly different densities due to temperature changes within the tank. Furthermore, as the tank is exposed to the surrounding environment, this can lead to an uneven distribution of temperatures within the cryogenic liquid. Due to the differences in density and temperature, the colder and denser parts of the cryogenic liquid tend to settle at the bottom of the tank, while the warmer and less dense parts accumulate at the top. This separation creates distinct layers within the tank. The density of the cryogenic working medium therefore changes due to the change in temperature and composition, resulting in stratification of the cryogenic working medium during storage. The density of the cryogenic liquid typically decreases with increasing temperature and this can lead to the phenomenon of local convection. This causes the surface temperature to increase as the heated liquid increases. Therefore, in large storage tanks, in the upper region, at the interface between liquid and vapour, a central jet of liquid forms and thermal stratification is observed, while the lower region of the liquid is not affected by convection, forming an isothermal region, where the temperature is constant with time. This phenomenon presents very different results from those predicted by homogeneous models, which assume that the fluid temperature is constant over time. After stratification has occurred, independent cycles of natural convection occur in the relatively stable stratification of the fluid. Thus, due to heat loss at the wall, a complicated heat transfer is formed in each layer and thermal instability is caused by density changes. In severe cases, the layer interface is disturbed to form a rollover. Figure

1.4 illustrates the rollover phenomenon schematically.

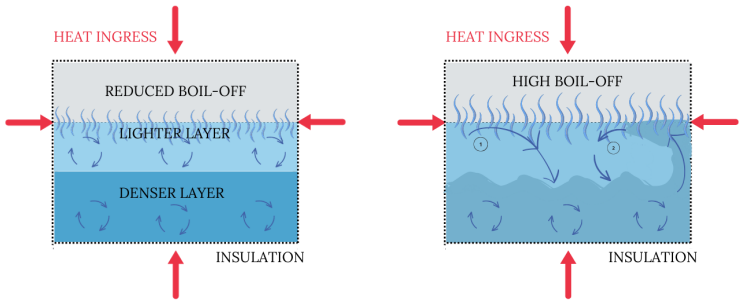

(a) Roll over: reduced boil-off (b) Roll over: high boil-off.

Figure 1.4: Illustration roll over phenomenon in cryogenic tanks.

This is an event in which the cryogenic liquid inside the tank undergoes violent mixing or agitation, often due to poor control of stratification and temperature variations. Rollover occurs when the liquefied product inside the tank is initially stratified, with the gas at the top and the liquid at the bottom. Over time, due to heat absorption from the surroundings or other external influences, the temperature of the liquid in the upper part of the tank may rise, causing it to vaporise. This released gas accumulates in the upper part of the tank, above the remaining cold liquid. When a significant amount of gas accumulates in the upper part of the tank, an unstable situation can occur. If there is sudden agitation or mixing of gas and liquid inside the tank, a rapid release of gas from the tank can occur, causing a sudden increase in internal pressure and a potential danger of explosion or uncontrolled gas release. Due to heat ingress through the walls, closed convection cells begin to develop in both layers, limiting heat and mass transfers between the two layers. In detail, while the upper layer can release the extra energy through the preferential evaporation of the more volatile components the lower layer cannot and becomes superheated, reducing the evaporation rate. As a result, overheating of the bottom layer, evaporation and mass transfer between layers contribute to reducing the density of the bottom layer and increasing that of the top layer. After a certain period, when the densities in the two layers begin to equalise, a sudden mixing called 'rollover' occurs with the release of energy previously trapped in the lower layer in the form of vapour. The latter could be dangerous if not carefully managed through controlled release to prevent overpressure inside the reservoir. To prevent rollover, it is crucial to carefully monitor the temperature, pressure and stratification within the reservoir. Rollover is a critical aspect to consider in tank management requiring careful supervision and adequate safety measures to prevent dangerous situations. Stratification is important to consider

in cryogenic reservoirs because it can affect the efficiency of the storage process and the management of the cryogenic liquid, leading to instability, and causing significant economic losses [4, 6, 18, 34].

1.4. Literature review: starting point for our model

Liquid nitrogen (LN_2) is the first cryogenic liquid used in industrial production. Therefore, the leak-free storage and transport characteristics of LN_2 tanks were the first to attract the interest of researchers. Studies on heat reentry in cryogenic tanks are of great importance in various fields, including astronautics, the energy industry and scientific research. Cryogenic tanks are used to store gases or liquids at extremely low temperatures, and the control of heat re-entry is crucial to maintain the stability and efficiency of such tanks.
The literature review is divided into two categories, to lay the foundations of the proposed models.
The first focuses on detailed theoretical and experimental studies on thermal conductivity analysis. The various contributions related to thermal returns are examined, along with how they are modeled to quantify the amount of heat entering, based on the various materials and conditions used in the reservoirs. In particular, attention is given to radiation and conductivity studies inherent to the materials used.
The second category involves literature relating to phenomena such as self-pressurization, thermal stratification, and boil-off gas, to better understand how to describe the types of cryogenic tanks under examination.

1.4.1. Review of analytical and empirical studies of thermal return modes: conduction and radiations

Studies of thermal exchanges in cryogenic tanks have often encountered difficulties in defining the thermal conductivity of the insulating materials used. Although the theory behind thermal conductivity measurements is simple, the actual implementation under cryogenic conditions presents several technical and non-technical challenges. In addition, the accuracy of stated values is sometimes questionable due to incomplete information about the materials and apparatus. Typically, the actual thermal conductivity reported in the literature depends on the density, structure, composition, and temperature gradient within the insulating material and the accuracy of the experimental system. Furthermore, for the thermal modelling of insulation materials, it is often possible to find thermal conductivity values in the data sheets of the materials used, but this information often

does not provide data based on the different degrees of vacuum used and is therefore not applicable in practice.

In general, there are two categories of approaches to measuring thermal conductivity: steady-state methods and transient methods. Typical steady-state methods include the protected hot plate method, the comparative method and the radial flow method. Conversely, transient state methods include the transient hot plate method, the hot-wire method, the laser flash method and similar ones [29].

In particular, for powder materials often used in cryogenic applications that include perlite, powder or aerogel spheres, and glass microspheres, the geometric description of the conductivity of these powder materials is complex due to variations in particle size distribution and their packing structure. The first approaches, dating back to the 1970s, for such a calculation considered powder particles as smooth-surfaced elastically deformed spheres to improve the accuracy in describing their physical and behavioural properties, and presented an analytical study to predict the apparent thermal conductivity of beds of glass microspheres of uniform diameter. The theory is valid for gas pressures ranging from vacuum to atmospheric conditions, with a good to excellent match between the coupled model and available experimental data. Subsequently, this theory was updated by considering surface roughness. The model visibly improved the accuracy of total strength prediction when compared to experimental results in basic macrosphere cells. Subsequently, on this basis, the first equations were derived by differentiating the conductivity of spherical insulating materials according to the different coatings used [8][27][29].

In 2017, based on experimental results, a theoretical model of thermal conductivity under vacuum conditions has been developed. The model makes it possible to predict thermal conductivity using a set of physical parameters, including particle diameter, porosity, temperature, compressive stress, and surface energy. In addition, many associations, such as the Perlite Institute or suppliers of these insulation materials themselves, make available and release thermal conductivity data for expanded perlite at average temperatures from 0°F (-18°C) to -160°F (-107°C) and under different degrees of vacuum, material-specific densities derived from experimental tests. It is common, however, that such retrievable data often do not reflect the characteristics of the materials under study, and that the validity ranges of conductivity n do not match those are investigated, in terms of density, vacuum, etc, providing an idea about the measure, but not in detail[16, 21, 26].

Furthermore, the degree of complexity in calculating the effective conductivity of these insulation layers has often been related to the consideration of interstitial gas and conductivity due to this contribution. Due to the complex impact of void space geometries

in the transition and temperature jump regimes, a rigorous theoretical expression of gas conductivity is not available in the literature. Several theories have been highlighted to model this. A semi-empirical technique for estimating conductivity has been proposed that takes into account molecule-molecule and molecule-wall collisions. Similarly, the literature has provided several alternative formulations for estimating the effective thermal conductivity of an insulating material that involve the use of accommodation coefficients and/or coupling terms between the gas and the solid, expressing the conductivity itself as a function of the temperature and average pressure of the insulating layer. In this way, for gas mixtures, the thermal conductivity can be estimated through a molar average of the thermal conductivity of the individual components [29]:

$$k_g(T) = \frac{k_g^0(T)}{(1 + \frac{P^{1/2}(T)}{P})} \tag{1.1}$$

where $P_{\frac{1}{2}}$ is a characteristic half-value pressure that is material-specific and depends on various factors such as the effective pore diameter, degrees of freedom, cross-section of intermolecular collisions, and thermal accommodation coefficient, and $k_g^0(T)$ is the gas thermal conductivity in the continuum limit.

Regarding the radiative contribution, multiple studies have been carried out in the literature for state-of-the-art technologies, such as cryogenic tanks for space use, with multilayer insulation (MLI), constructed with layers of metallised substrate films, or foils, that act as shields against low-emissivity radiation. Multiple tests, such as calorimeter tests, combined transmission and reflection tests, and laser tests, have determined transmission values of $10^{-4}/10^{-5}$, thus affirming the possibility of considering the radiation factor in heat reentry as negligible. For industrial configurations, however, this contribution becomes more relevant in nature. Heat transfer by radiation from the atmosphere is controlled by wrapping a radiating film on the inner wall of the container.
It is also possible find theoretical methods in the literature: the 'Rosseland' method, also known as the diffusion approximation for optically thick media, a method used in physics to estimate the transmission and absorption of radiation within a material when the optical density of the material is high. Essentially, the Rosseland approximation simplifies the problem of radiation transmission in dense media by introducing a weighted average of the thermal scattering within the material [29][32].

Among the most up-to-date models, a model based on the physics of insulation properties has been developed to extend the available correlations and predict the effective thermal conductivities of multiple insulation systems consisting of powders, foams, fibrous ma-

terials and multilayer systems. The predictions of the model have been compared with available experimental data, and it has been found that the accuracy of the model is sufficient for practical purposes. The model proposes a principled correlation that can be used to estimate the dependence of effective thermal conductivity as a function of temperature, interstitial gas composition, pressure and structural properties of the material. This model expresses both the contribution of conductivity (solid and interstitial) and radiation through a temperature and pressure dependence relationship, and is a useful tool, based on empirical data and physical models, to characterise the conductivity of a particular insulation material under certain operating conditions [29]:

$$k_e = k_{s.e} + k_g = 0.00252T + 7.98 \times 10^{-8} T^3 + \frac{1.243 T^{0.587} P}{0.895T + P} \tag{1.2}$$

With this relation the thermal conductivity of an insulating material can be estimated by summing three main contributions: solid contribution represented as a linear or power law in temperature, radiative contribution represented as a cubic power of temperature, and the interstitial gas contribution which is represented as a rational polynomial function in pressure and temperature.

1.4.2. Review of thermal reentry in cryogenic tanks: self-pressurisation, boil of gas and thermal stratification

Thermal stratification

Interest in the phenomena of self-pressurisation, thermal stratification and the phenomenon of boil-off gas has increased in parallel with the development of aerospace technologies and the increase in the industrial use of nitrogen, oxygen and LNG.

As early as the 1950s, some researchers introduced the phenomenon of LN_2 tank stratification. The study was prompted by the importance of cryogenics in fuels used for missiles, which underwent heating due to dynamic friction. The existence of the phenomenon of temperature stratification at the vapor-liquid interface was verified experimentally, calculating the value of the pressure in the reservoir based on the internal temperature of. Thus, it was found that the actual pressure in the reservoir obtained from the experiment was higher than the theoretical pressure calculated based on the average temperature of the liquid [22, 34].
Next, the flow pattern and thermal stratification of a cylindrical cryogenic tank has been studied numerically. A numerical study of buoyancy-induced convection in a cylindrical reservoir has been proposed, assuming that the liquid-vapor interface is flat, shear-free,

and at a constant saturation temperature and that the bottom of the reservoir is maintained at a constant temperature below that of the interface. The effects of Prandtl number, reservoir proportions, wall heat flux parameter and wall heat flux distribution on the velocity and temperature ranges of the liquid were investigated. In addition, the effects on the rate of heat transfer across the interface and bottom of the reservoir were examined. Note that for uniform thermal flow, the flow pattern contains a counterclockwise vortex carrying the superheated fluid, while a weak clockwise vortex also forms in the bottom region of the reservoir near the centerline. In the lower region, heat conduction is generally dominant because the fluid velocity is very low and the maximum liquid temperature occurs on the upper side walls of the reservoir [7].

More recent studies also focused on developing numerical models on natural convection and thermal stratification inside LOX and LN_2 storage tanks due to heat transfer from the surrounding environment. The mathematical model includes two non-equilibrium domains for the liquid domain in two cases, while a simplified thermodynamic model is used for the vapor domain. It is emphasized in this study, that the thermal stratification is closely related to the natural circulation within the reservoirs. The temperature of the circulation currents is influenced by the temperature of the reservoir walls. Evaporation of the liquid also contributes to the pressure increase in the vapor zone and influences the saturation temperature at the liquid-vapor interface. In addition, validated numerical simulations have been conducted by some researchers against existing experimental data with different heat flow conditions, where circulating flows develop at different times. At higher heat flow conditions, it appears that circulating flows develop more rapidly. For different liquid fill conditions, a relatively longer time was required for vaporization at higher fill levels, and relatively higher values of the flow function were observed at lower fill conditions. The pressure rise and rate of rise are strongly influenced by the liquid fill level and different heat flux levels. Pressure rise and velocity increase with increasing heat flux and decreasing fill level. Therefore, higher heat flux and lower fill rate lead to faster evaporation, stronger heat transfer and higher pressure [31][33].

1.4.3. Evaporation and boil-off gas

As far as cryogenic evaporation and BOG are concerned, the largest studies present concern LNG tanks, due to the high costs related to the loss of product and transport itself.

Again, the first simplified LNG alteration model was developed in the 1960s and was able to calculate the maximum BOG rate and wall temperature profiles. In subsequent decades, numerical calculations were used to provide the relationship curve between the

daily evaporation rate of the storage tank and the effective thermal conductivity of the insulating material under different insulation material conditions. Substituting the cylindrical wall thermal conductivity formula for these studies with the plate thermal conductivity formula for an approximate calculation of thermal conductivity with high accuracy. This led to the conclusion that evaporation in the cryogenic tank is due to heat loss, and it is the premise to study evaporation to explore the mode of heat loss and the accuracy of heat loss [34][11].

At the beginning of the 21st century, studies showed the evaporation rate of LN_2 storage tanks at three different locations through experiments. It was revealed that the fluctuation of ambient temperature is the internal cause of the fluctuation of evaporation in the reservoir. However the fluctuation of apparent evaporation is more influenced by the variation of atmospheric pressure. Further studies focused on the development of an equivalent thermal conductivity model to study the effect of the tank filling ratio on the boiling rate, concluding that heat transfer due to conduction dominates the BOG generation process[34].

Contemporary models are based on heat input flow, where heat input determines the behavior of the mass and energy balance. Current BOG estimation methods for large-scale storage reservoirs are entirely empirical, without the availability of accurate predictive models. Heat transfer models can be used to simulate both small- and large-scale storage tanks and can account for cryogenic liquids of different compositions. However, most models assume thermal equilibrium between the liquid and vapor phases. Non-equilibrium weathering models that distinguish heat input between the different phases have been developed recently, taking into account the different effect of heating on the liquid or the vapor phase. However, these models have not been validated against comprehensive experimental data.
In many studies discussed in the previous paragraphs, it was assumed that the liquid zone is in thermal equilibrium with the vapor zone. However, experimental studies have argued that the vapor typically reaches the superheated state with a temperature higher than the liquid temperature. This is taken into account in nonequilibrium models, which show superior performance in predicting changes in liquid and vapor zone parameters [11].
Among the earliest studies that considered different liquid and vapour temperatures, treating the heat input to each subsystem separately, while estimating the heat transferred from the hottest vapour to the coldest liquid, allowed comparison with industrial tests that supported this assumption of heat transfer between vapour and liquid by conduction; the inclusion of which provided more realistic results than the overestimation of the BOG rate, which occurs in the case of equilibrium models [5][20].

2 | Materials and methods

The development of a model for the prediction of various variables relating to the return of heat to cryogenic tanks proceeded through a series of well-defined steps. This process was crucial to understand and effectively managing the thermal behaviour of these tanks, which are essential for storing and transporting liquefied gases at extremely low temperatures, such as nitrogen,oxygen, or hydrogen.
During the study, the focus was first on analyzing the thermal return modes. This involved closely to examinate the thermal conductivity of the tank material and the heat flows occurring within the system. Understanding how heat was transferred within the tank was crucial for accurately predicting the amount of product that could evaporate. This assessment allows the identification of the parameters dominated heat input, thus to identify weak points to work on in terms of insulation as well.

Next, the variation of variables involved in the process using mass and energy balances was described. This allows to develop a mathematical model that takes into account crucial factors such as the temperature of the cryogenic liquid, the pressure inside the tank, and the rate of product evaporation. This model is designed to adapt to a wide range of environmental conditions and types of cryogenic tanks, providing an accurate estimate of the system's behavior in different operational scenarios.
This model is based on assumptions and hypotheses that implement a simple description on the physical level, but are close to reality.

During the implementation of the model, the specific characteristics of cryogenic tanks were considered, such as the presence of insulation materials to minimize the external heat transmission and the design of the venting system to safely manage evaporated gas. The main objective was to develop a model that not only faithfully reflected the available experimental data but also provided a solid foundation for optimizing the management and maintenance operations of cryogenic tanks.

The model of heat loss in cryogenic tanks aimed to find an optimized configuration by combining various design factors. This approach addressed the industrial issue by balancing evaporation, autopressurization, and economic losses. It focused on finding a compromise

to minimize product loss and reduce the need for frequent refills due to lower tank filling. The delivery of cryogenic nitrogen to a customer can involve various costs, which depend on various factors such as the quantity required, the delivery distance, the specifications of the transport vehicle, and other logistical factors.
The compromise and evaluation of various factors is primarily focused on high-pressure tanks. Unlike low-pressure tanks, which require a smaller gas cushion for liquid expansion and evaporation and can achieve 90-92% fills, high-pressure tanks are closer to the maximum permissible pressure. Thus, they are more sensitive to the evaporation and self-pressurization process, requiring a larger tank top space for gaseous cryogenics and reaching 50-60% fills.

The search of an optimal configuration to increase this level presents a challenge but could potentially offer an attractive economic solution in an industrial setting.

2.1. Evaluation of thermal conductivity and incoming heat flow

The importance and technological interest of insulation materials used in the design of cryogenic tanks have been emphasized. Despite the use of sophisticated materials, insulation, with minimal heat exchanges, cannot completely prevent heat exchange with the outside. Thermal insulation of cryogenic systems and components holds significant economic importance, as even a small heat loss at low temperatures requires compensation by a much higher amount of heat at room temperature. The starting point for this evaluation is the assessment of the heat coefficient between the insulating shell and the outside [15] [29].

To predict the amount of heat entering into the stored cryogenic product and furthermore to solve the energy balance, a thermal analysis is required. The well-defined geometry of an above-ground tank and the accurate availability of thermal properties of the insulation and the wall section materials allow a rigorous estimation of the heat in-leak rate. For a partially filled tank, the problem of predicting the heat in-leak rate and wall temperature as a function of liquid level depend on the relative contributions of the different modes of the heat transfer to the liquid, such as convection, radiation and wall conduction. Within this approach, the fundamental heat transfer relations to calculate the heat leakage, are reviewed in the following sections.

Starting from the cylindrical structure of a cryogenic tank, the parts most involved in the heat loss is first assessed, followed by the modes, with the aim of quantifying the heat

flow transferred to the cryogenic liquid.
The heat lost through safety valves and support struts is considered negligible, as they are designed to minimize heat exchange. Additionally, no contribution is related to the cryogenic liquid extraction pipe. This pipe is characterized by a curved geometry on the outside of the tank, creating a gas plug at the first liquid withdrawal. This prevents further liquid from escaping outside and acts as an insulator.

Furthermore, the contribution of solid conduction, radiation, and conduction through the interstitial gas within the cavity is assessed, while the convection is assumed as negligible.

First as far as the radiative contribution is concerned,the radiation is a very important heat transfer mechanism for cryogenic insulation systems, especially under conditions of high vacuum and high temperatures. As already pointed out, it would have been possible to use the Rosseland approximation or the Stefan-Boltzmann equation, knowing in addition to the emissivity of the insulating materials, additional parameters from the geometric analysis. To semplify the model, the contribution of irradiation could be neglected, given the low emissivities relative to the perlite vacuum jacket, and the additional outer shells, the primer and final coat in epoxy zinc and polyurethane, and the choice of white colour for the paintwork, allow to minimise the effects of irradiation. Nevertheless, this is considered in the empirical model we used [13] [19][29].
Then, is evaluated the contribution due to both solid and interstitial gas conduction. The contribution due to conduction of the outer carbon steel vessel (outer wall of the tank) is neglected in the heat transfer calculations, because of the dominant effect of the tank's insulating layer.The insulation layer, with a thickness of between 192/240 mm, it consist of vacuum perlite (at 4/26 Pascal), a granular solid used in the cryogenic industry. In our case it is Italian Perlite, with a grain size of $0.1 \div 1$ mm nominal, compacted density of $60 \div 70$ kg/m$_3$ $\pm$ 15%, characterised by a conductivity of 0.032 W/mK at -82°C and atmospheric pressures. For cryogenic applications at-101°C and below requiring 'super' insulation, the evacuated perlite provides superior insulation with up to 40 times lower thermal conductivity than atmospheric pressure, depending on vacuum and temperature [16] [26].
The vacuum value inside the cavity for cryogenic nitrogen tanks, is usually a standard value close to 26 Pa. More recent tanks, on the other hand, both for nitrogen and for other substances such as oxygen, have more stringent vacuum conditions, around 4 Pascal, offering significantly different performance and conditions. It is therefore interesting to evaluate both conditions, highlighting the extent of variations in results as this parameter changes [16][26][29].

In this work, a physics-based model of insulation properties is utilized to expand the

existing correlations and forecast the effective thermal conductivities of these materials based on temperature, vacuum level, material structure, and the type of gas present in the interstitial space. These model predictions were compared with available experimental data, revealing that the model's accuracy is adequate for practical applications.

Therefore, the equation 2.1 is used to calculate thermal conductivity [29]:

$$k_e = k_{s.e} + k_g = 0.00252T + 7.98 \times 10^{-8}T^3 + \frac{1.243T^{0.587}P}{0.895T + P} \tag{2.1}$$

Where $k_{s.e}$ and k_g have the unit mW and T is the absolute temperature in K. The actual thermal conductivity of an insulating material can be estimated by summing three main contributions: solid contribution represented as a linear or power law in temperature, radiative contribution represented as a cubic power of temperature, and the interstitial gas contribution which is represented as a rational polynomial function in pressure and temperature[29].
The fit of our case to such an empirical model is mainly based on the assumption of a compact layer of the perlite layer. In addition, in the tanks considered, the gas in the cavity turns out to be nitrogen, and given the similarity in conductivity of the gases used in the model in the literature, it is valuated suitable for our study [29].

Analysing the contributions of formula 2.1 for a nitrogen tank stored at -185 °C, with a vacuum of 26 Pa, the interstitial gas conduction, related to the pressure and vacuum degree of the cavity, is emerged as the main driver of heat transfer. The interstitial gas conduction contributing 93.5 % of the constitution of the thermal conductivity value. Less impactful factor (6 %) is related to the solid contribution of perlite, while, as expected from the literature review, the radiative contribution is the least relevant factor (0.5 %) [29]. The vacuum loss over the years is a key parameter for thermal returns, which results in a strong variation in the value of the incoming heat flux and the consequences of boiling and self-pressurization. These considerations are discussed in more detail in the following sections.

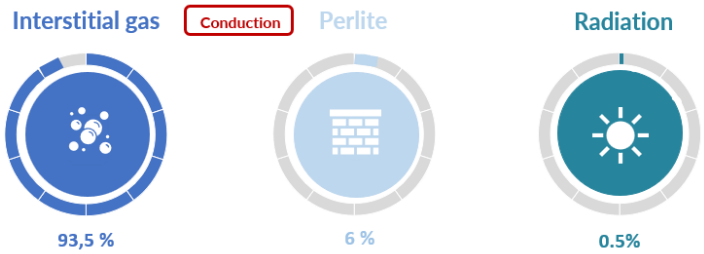

Figure 2.1: Percentage contribution of the various heat transfer mechanisms for a 192 mm perlite insulation layer. High-pressure liquid nitrogen tank.

For the heat flux calculation,the Fourirer equation, of one-dimensional conduction, is used [13]:

$$Q = \int_{T_{\text{in}}}^{T_{\text{out}}} \frac{k_e(T) \cdot A_{\text{mean}} \cdot dT}{h} \tag{2.2}$$

Where h is the thickness of the insulation layer, A_{mean} the exchange area, T_{in} the temperature inside the inner vessel, and T_{out} the outside temperature. A_{mean}, on the other hand, is the average area used to calculate the incoming heat flow exchange.

Regarding the heat input in the isothermal model approach, the system considers through all the walls of the cylinder. This includes the transfer of heat through the tank walls from the surroundings, the ones from external sources.
The exchange area, on the other hand, is calculated as the average area between the outer area of the carbon steel tank and the area of the inner stainless steel shell by the following equations [13]:

$$A_{\text{e}} = \left(\frac{D_{\text{e}}}{2}\right)^2 \cdot \pi + D_{\text{e}} \cdot \pi \cdot L_{\text{c,e}} \tag{2.3}$$

$$A_{\text{i}} = \left(\frac{D_{\text{i}}}{2}\right)^2 \cdot \pi + D_{\text{i}} \cdot \pi \cdot L_{\text{c,i}} \tag{2.4}$$

$$A_{\text{mean}} = \frac{A_{\text{externalvessel}} + A_{\text{internalvessel}}}{2} \tag{2.5}$$

Where A_{e} and A_{i} are the areas of the outer carbon steel vessel and the outer stainless steel vessel in m^2, calculated from the respective diameters (D_{e} and D_{e}) and lengths of the cylindrical section ($L_{\text{c,i}}$ and $L_{\text{c,e}}$) in m.

The conductivity of the insulating layer is not considered constant, given the large tem-

perature difference between the inside and the outside of the tank (of 185°C for -165°C nitrogen cryogenic storage placed in a 20°C environment). Thus, the integration of the conductivity coefficient is implemented, with respect to the temperature extremes so as to obtain an average value [13].

In this way, using a single relationship (2.2), depending on the environmental conditions, the stored substance used and on the size of the cryogenic tank, it is possible to immediately trace the amount of incoming flow, taking into account the degrees of tank vacuum, which may vary substantially during the various life cycles of the tank, offering quite different performances.

2.2. Model development

2.2.1. Assumptions and hypotheses: subcritical state

Before delving into the matter and energy balances, it is essential to devote a section to the assumptions and hypothesis that guide the entire development of the model.

First, the analysis is performed for a vessel in its most critical condition with respect to the heat reentry problem, thus in a steady-state and non-operational condition. During the operating phase, in fact, where the extraction of liquid from the bottom takes place, the heat reentries directly compensate for the pressure drop related to the lowering of the liquid level, avoiding the phenomenon of autopressurisation. In this circumstance, therefore, the heat reentries don't result in a risk in terms of darkening and product loss. For these reasons, the interest is focused on reservoir in idle condition, where the pressure rise due to the heat reentry is not counteracted by any other factor.
In addition, a situation of perfect vacuum conditions is evaluated. This decision-making aspect is very impactful, considering that at the time of tank revamping, which occurs every five years, one degree of vacuum is usually lost.
A homogeneous distribution condition of the perlite itself is also considered. Even though, over time, due to the continuous filling and emptying cycles of the tank, this distribution is no longer be homogeneous.

Second, since one of interest of this research lies in the study of pressure versus time trends and heat inputs, is considered a closed vessel, unable to exchange mass with the outside, under non-isobaric conditions. In this way, it is possible to show the pressure trend until the overflow valve setting is reached, after that the vapor fraction begins to leave the tank, promoting a decrease in pressure to ensure the safety and integrity of the tank itself.

Thus, the liquid and gas phases have already reached a state of equilibrium, which takes time after filling with cryogenic liquid from a high pressure cistern.

Fourth, the entering heat (Q) is considered constant, assuming that its contribution causes an enthalpy increase of the liquid product inside the cryogenic tank.

On the other hand the isothermal model descriibes the storage tank as a system in thermodynamic equilibrium, which leads to two key implications for the model.
Firstly, from an energy balance perspective, the model treats the storage tank as a system where all the heat entering is absorbed by the liquid. This implies that the incoming heat is entirely considered as latent heat to vaporize the liquefied product.
Secondly, in terms of vapor-liquid equilibrium, the system remains in thermal equilibrium throughout the process.

The situation at time zero is a liquid layer at the bottom of the vessel in a subcooled state and an upper gas pad, of a vessel filled according to design and placed in an external environment

Due to normal heat flows (from the external environment), a thermal expansion occurs on the subcooled liquid and the generated heat flows bring part of the liquid to saturation conditions at the reservoir pressure.

To simplify of calculation, it is assumed that, in addition to the vapour layer, the cryogenic liquid is stratified in two layers: at the top, the liquid is in saturated conditions, while at the bottom the liquid is subcooled and remains in the same condition under the new pressure as time progresses. Again for simplicity of calculation, the saturated liquid mass at equilibrium is not considered as stratified.
Considering that our tank is at ambient conditions, since it is placed outside a plant, it can state that there is not case of extremely high heat flows, as in the case of fires. For these reasons, the flows circulating and phenomen of local convenction inside the tank, resulting in a clockwise vortex in the superheated liquid zone and a weak vortex in the bottom zone, are considered to be negligible. The phenomenon of conduction from outside is considered as the driving factor [4, 6, 18, 31, 33, 34].

As time progresses, the subcooled liquid shrinks, as, due to thermal reentry, a part evolves into hot liquid under saturation conditions, while a part of the hot liquid in equilibrium evaporates, increasing the gas phase under saturation conditions.

Summarizing, the assumptions are as follows:

- Non-operational condition of the vessel;
- Perfect vacuum conditions,homogeneous distribution condition of the perlite;;
- Closed vessel, unable to exchange mass with the outside, non-isobaric conditions;
- Q = costant ;
- The incoming heat is entirely considered as latent heat to vaporize the liquid;
- Vapor-liquid phases in thermal equilibrium throughout the process;
- Stratification of phases: subcooled liquid at the bottom, saturated liquid above it and vapour at the top of the tank;
- Flows circulating, local convenction and vortexs negligible.

The evolution of the phases over time is illustrated in the pictures 2.2 and 2.3. At time zero, there are only the stored cryogenic liquid and the gas phase. Subsequently, thermal returns cause the formation of saturated liquid and the consequent evaporation process. As time progresses, the subcooled liquid phase decreases in favor of the saturated liquid and gas phases.

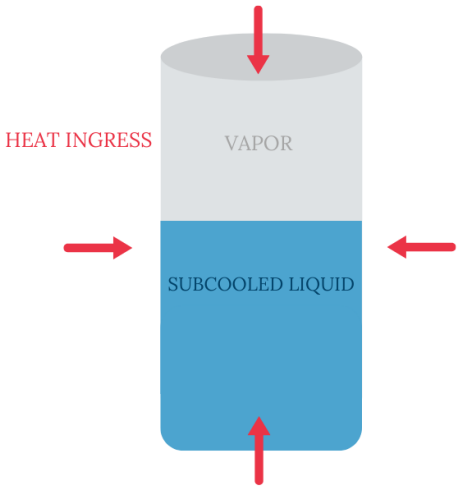

Figure 2.2: Cryogenic vessel at time zero.

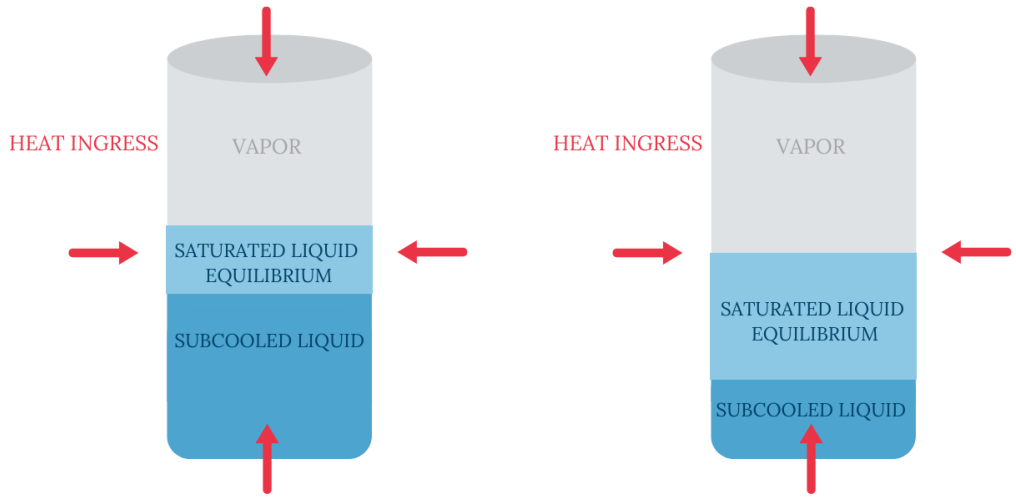

(a) Thermal stratification due to heating of the liquid phase

(b) Increase in saturated liquid and vapour phase due to evaporation.

Figure 2.3: Evolution of the subcooled, saturated liquid phase and vapour phase with respect to time, caused by heat reentry.

The phenomenon of thermal reentry therefore causes the evaporation of the liquid cryogenic product, progressively decreasing the liquid phase itself, in favour of the gaseous phase.
Considering a closed system, with no gas phase escaping, the tank undergoes a self-pressurisation process until the maximum allowable pressure (MAWP) is reached, after which the the safety devices intervene.
For cryogenic vessels characterised by a MAWP greater than the supercritical pressure of the fluid under test, the continuous exchange with the outside world leads to the formation of a supercritical phase, which is similar to a fog in the supercritical state. At this point what has been said so far is no longer valid, because there is no equilibrium phase and no subcooled phase, but there is only one state in which the fluid is supercritical.
The thermodynamic balances and assumptions, are therefore different from previous conditions,since the mass and energy balances for the supercritical stage.
An interesting example that can satisfy this condition is a high-pressure nitrogen storage tank, e.g. 31 barg. In this case, the critical nitrogen pressure being approximately 33.9 bar, very close to the initial operating pressure, it is essential to evaluate and investigate the pressure trend once the supercritical regime is reached.

Figure 3.4 graphically shows the vessel under supercritical conditions, subject to heat reentry, where where only one phase is detectable.

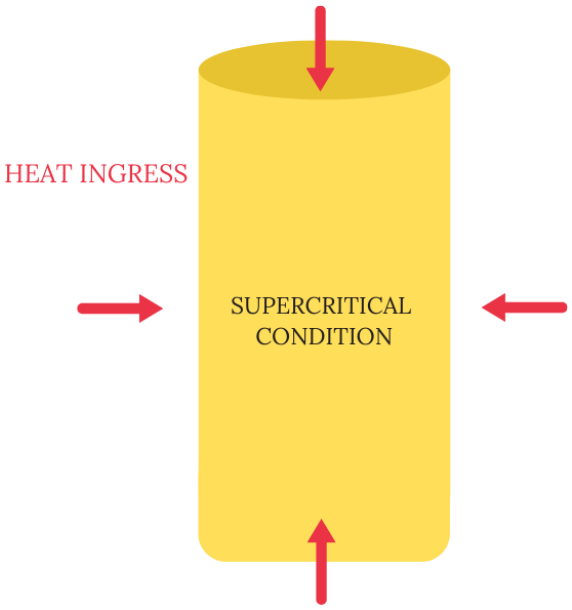

Figure 2.4: Cryogenic vessel at supercritical condition.

2.2.2. Mass and energy balances

Once explained the assumptions underlying the model, to create a simple and efficient model, it is possible to move to the mass and energy balances. These are essential for understanding the behavior of the thermodynamic properties of the phases involved.
In particular, mass and energy balances are developed by considering two different control volumes : the first concerning only the subcooled liquid phase, and the second concerning the saturated liquid mass in equilibrium.

The balances are the starting point for understanding and developing a mathematical model that can illustrate and help to understand how the system responds to heat exchange over time.

Mass and energy balances: subcooled liquid

As a first step, the phenomenon of heating the liquid product is studied, resulting in the formation of saturated liquid in equilibrium.
This balance is based on the assumption that all incoming heat is devoted to the enthalpic contribution of the liquid product.
Focusing primarily on the subcooled phase, the mass and energy balance have the following formulation:

$$m_{F,i} = m_o - m_{C,i} \tag{2.6}$$

$$Q \cdot \Delta t = m_{F,i} \cdot H_{F,i} + m_{C,i} \cdot H_{C,i} - m_o \cdot H_o \tag{2.7}$$

Where :

- Q = constant incoming heat flow (kW);
- Δt = time step considered (s);
- $m_{F,i}$= subcooled liquid mass at instant i (kg);
- $m_{C,i}$= superheated liquid mass/saturated condition at instant i (kg);
- m_o= subcooled liquid mass at instant t=0 (kg);
- $H_{F,i}$= subcooled liquid enthlpy at instant i (kJ/kg);
- H_o= subcooled liquid enthalpy at instant t=0 (kJ/kg);
- $H_{C,i}$= superheated liquid /saturated condition enthalpy (kJ/kg);

Figure 2.5 graphically depicts the evolution of the liquid and gas phase with respect to time, showing how the subcooled liquid phase at time zero due to thermal reentry evolves, stratifying into saturated liquid above and subcooled liquid below.

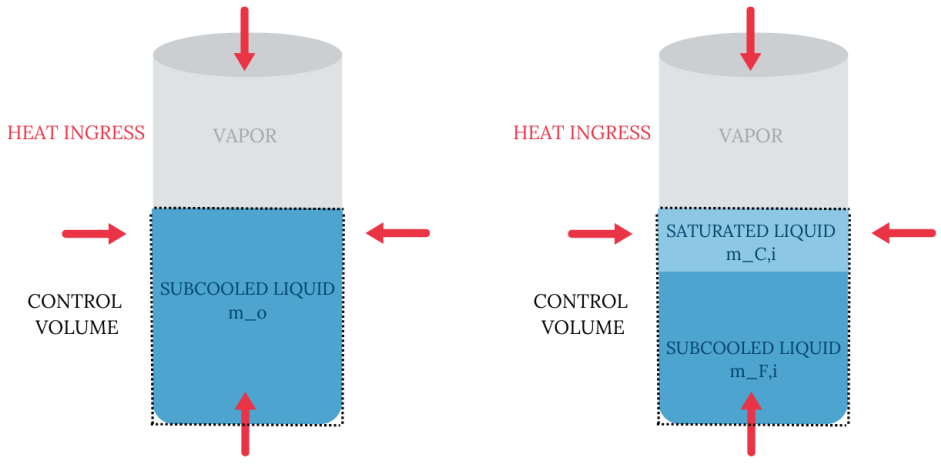

(a) cryogenic vessel at instant t=0 (b) cryogenic vessel at instant t=i.

Figure 2.5: Evolution of the subcooled liquid phase in response to thermal returns. Control volume: subcooled liquid

From a sensitivity analysis, the enthalpy of the subcooled liquid, especially considering nitrogen and oxygen in the cryogenic use ranges in industrial tanks, does not vary significantly. Therefore, the following approximation is introduced:

$$H_o = H_{F,i} \tag{2.8}$$

$$m_{C,i} = \frac{Q \cdot \Delta t}{H_{C,i} - H_{F,i}} \tag{2.9}$$

From this first balance, an initial relationship can be derived to define the formation of the superheated mass at each instant i, in correlation with the thermodynamic properties.

Mass and energy balances: saturated liquid mass in equilibrium

Since one of our goals is the definition ofthe rate of evaporation, we move now on to defining mass and energy balances by considering the saturated liquid phase in equilibrium at a generic instant i as the control volume. The change in mass and energy is driven by the phenomenon of evaporation and thus by the phase change.
The mass and energy balances have the following formulation:

$$\frac{d(m_C)}{dt} = -\dot{m}_e \tag{2.10}$$

$$\frac{d\,(m_C \cdot H_C)}{dt} = -\dot{m}_e \cdot \hat{H}_V \tag{2.11}$$

Where :

- t = time (s);
- m_C= superheated liquid mass/saturated condition (kg);
- m_e= evaporated mass (kg);
- H_V= vapor enthalpy (kJ/kg);
- H_C= superheated liquid /saturated condition enthalpy (kJ/kg);

These two equations show the evaporation process occurring at the saturated liquid-vapor interface. The combination of the two balance equations leads to:

$$\frac{d(m_C \cdot \hat{H}_C)}{dt} = \frac{d(m_C \cdot \hat{H}_V)}{dt} \tag{2.12}$$

By mathematically developing this relationship:

$$\frac{d(m_C \cdot \hat{H}_C)\hat{}}{dt} = \frac{d(m_C \cdot \hat{H}_V)\hat{}}{dt} = m_C \frac{d\hat{H}_C}{dt} + \hat{H}_C \frac{d(m_C)}{dt} \tag{2.13}$$

At this point, an approximation for the enthalpy of the saturated liquid is introduced:

$$dH_C \approx C_{PC}\, dT \tag{2.14}$$

And given that:

$$(\hat{H}_V - \hat{H}_C)\hat{} = \Delta H_{\text{vap}} \tag{2.15}$$

By separating the variables the equation leads to :

$$\frac{1}{\Delta H_{\text{vap}}} \frac{C_{PC}\, dT}{dt} = \frac{1}{m_C} \frac{d(m_C)}{dt} \tag{2.16}$$

Integration from initial state to the next instant :

$$\ln\left(\frac{m_{C,i}}{m_{C,0}}\right) \approx \left(\frac{C_{PC}}{\Delta H_{\text{vap}}}\right)(T_{C,i} - T_{C,0}) \tag{2.17}$$

Where $\mathrm{T}_{C,i}$ and $\mathrm{T}_{C,0}$ are respectively the extremes of integration, the temperature of the saturated liquid at time 0 and time i considered. Introducing now the following definitions :

$$\epsilon_v = \frac{m_{\mathrm{e},i}}{m_{C,i-1}} \tag{2.18}$$

$$\epsilon_L = \frac{m_{C,i}}{m_{C,i-1}} \tag{2.19}$$

It is posssible to obtain the evaporation rate :

$$\frac{m_{C,i}}{m_{C,0}} \approx \exp\left(\frac{C_{PC}}{\Delta H_{\text{vap}}}(T_{C,i} - T_{C,0})\right) = \epsilon_L = 1 - \epsilon_v \tag{2.20}$$

$$\epsilon_v = \exp\left(\frac{C_{PC}}{\Delta H_{\text{vap}}}(T_{C,0} - T_{C,i})\right) \approx \frac{C_{PC}}{\Delta H_{\text{vap}}}(T_{C,0} - T_{Ci}) \tag{2.21}$$

Specifications:

1. The equations used in the computational model, considering small Δt such that they result in small changes in pressure and temperature.
2. In the mathematical model, it is assumed the heat capacity at constant pressure and the enthalpy of vaporization to be independent of T. To improve the accuracy of the model, C_{PC} and ΔH_{vap} are determined based on the pressure for each Δt considered in the computational model.

Figure 2.6 highlights the phenomenon of evaporation in a cryogenic vessel, showing the transition of state from the saturated phase liquid to the gas phase.

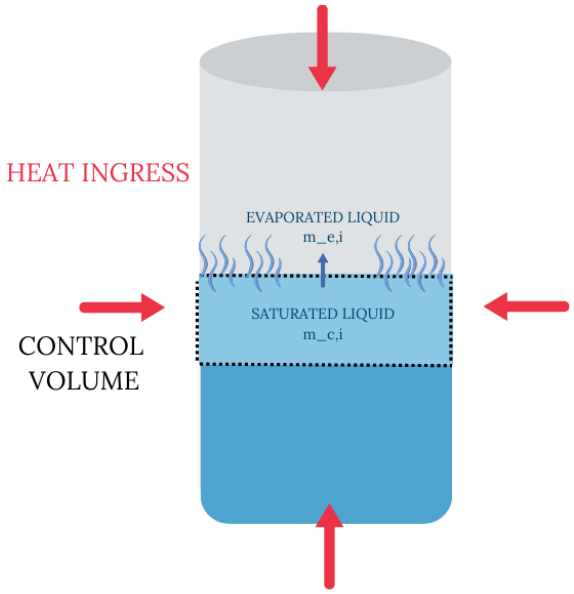

Figure 2.6: Evaporation phenomenon volume: ssaturated liquid mass in equilibrium

2.2.3. Evaluation of pressure trend

One of the most interesting parameters, is the pressure trend inside the cryogenic tank, which is mainly related to safety issues.

The tanks under consideration are cryogenic tanks for pure components, such as nitrogen. This characteristic enables significant simplification. Specifically, the study does not address variations in composition resulting from primary evaporation of lighter components, as these are single-component vessels.
A wide range of cryogenic products, including nitrogen, carbon dioxide, oxygen, etc., are utilized in their pure state, with purity percentages of 99.99%. This allows for the use of a simple relationship to evaluate pressure trends applicable across the entire range of industrially relevant products.

The phenomenon of autopressurisation, related to evaporation, is an assumption and simplification for our model: since the saturated vapour at the top of the tank can reach at the maximum permissible pressure in the range considered (so from the initial operating pressure to the critical or the maximum permissible one), the saturated vapour at the top of the tank is subjected to a variation of a few degrees. For this reason, the temperature is considered constant.

Using the Peng-Robinson Equation of State, which is more accurate due to a more complex temperature dependence, the relationship describing the pressure is:

$$P = \frac{RT}{1 - b\rho} - \frac{a\rho^2}{1 + 2b\rho - b^2\rho^2} \tag{2.22}$$

Where:

- $a = a_c\alpha$;
- $a_c = 0.45723553\frac{R^2T_c^2}{P_c}$;
- $\alpha = \left[1 + k(1 - T_r^{1/2})\right]^2$;
- $k = 0.37464 + 1.54266\omega + 1.54226\omega^2 - 0.26992\omega^3$;
- $\omega =$ acentric factor;
- $\rho =$ molar density $[\mathrm{mol/m^3}]$.

Given a constant temperature, this equation can be rewritten:

$$RT = \frac{P + \frac{a\rho^2}{1+2b\rho-b^2\rho^2}}{\frac{\rho}{1-b\rho}} = cost \tag{2.23}$$

The RT term therefore remains constant at each time interval considered, allowing to write the pressure at a given time i as a function of the pressure at the previous interval i-1:

$$T_i = T_{i-1} \tag{2.24}$$

$$RT_i = RT_{i-1} \tag{2.25}$$

$$\frac{P_1 + \frac{a\rho_1^2}{1+2b\rho_1-b^2\rho_1^2}}{P_2 + \frac{a\rho_2^2}{1+2b\rho_2-b^2\rho_2^2}} = \frac{\rho_1(1 - b\rho_2)}{\rho_2(1 - b\rho_1)} \tag{2.26}$$

$$P_2 = \frac{\rho_1(1 - b\rho_2)}{\rho_2(1 - b\rho_1)}\left(P_1 + \frac{a\rho_1^2}{1 + 2b\rho_1 - b^2\rho_1^2} - \frac{a\rho_2^2}{1 + 2b\rho_2 - b^2\rho_2^2}\right) \tag{2.27}$$

By means of the previous assumptions, it was possible to determine a relationship to derive at each step the pressure inside the tank, correlating it to the pressure of the previous step, the molar density of the vapour phase at time i and i-1 [17].
Knowing the value of the pressure inside the tank at each interval, it is possible to define the thermodynamic properties of each phase involved, in order to perform the calculations of the equations just derived.
Furthermore, despite the assumption of constant temperature for the vapour phase, knowing the pressure at each instant, it is possible to identify the expected temperature for

the saturated liquid and saturated vapour, keeping only the temperature of the subcooled liquid constant, at the new pressure coniditions.

2.2.4. Assumptions and hypotheses: supercritical state

When the pressure inside the tank reaches the supercritical pressure, the balance changes in parallel to the thermodynamic conditions that have been considered; what has been said up to now is no longer valid, because there is no an equilibrium phase and a subcooled phase, but there is only a single state in which the fluid is supercritical (similar to a gas with a density of the corresponding liquid).

The supercritical state of a substance occurs when it is subjected to a temperature and a pressure above the critical point. Every substance has a specific critical point representing the temperature and pressure above which there is no clear distinction between the liquid and gas phases. Under these conditions, the properties of liquid and gas mix, results in a supercritical state. In addition, the supercritical substance shows no clear distinction between the liquid and gaseous states. Instead, a continuous change in thermodynamic properties is observed.

Supercritical state of a substance is therefore characterized by :

- the disappearance of the difference between gas and liquid;
- the divergence of compressibility;
- the phenomenon of critical opalescence.

The phenomenon of divergence from compressibility is expressed by the conditions :

$$\frac{dP}{dT} = 0 \tag{2.28}$$

$$\frac{d^2P}{d^2T} = 0 \quad \text{at } T \text{ cost} \tag{2.29}$$

These two equations highlight the divergence of isothermal compressibility:

$$K_T = -\frac{1}{V}\frac{dV}{dP} \tag{2.30}$$

At the critical density and with a temperature around the critical one,, K_T is much higher than that of a perfect gas at the same density. Thus, near the critical point, large density fluctuations can be generated at low cost in terms of free energy. To understand the mechanical behaviour of supercritical fluids, the evolution of K_T is related to the pressure change (ΔP) induced by a 1% reduction in the volume of the system. The evolution of the pressure, apart from the proximity of the critical point, shows that a supercritical fluid is not very compressible.

When the fluid becomes supercritical, the thermodynamic properties undergo a discontinuity and are no longer specifically defined:

$$C_p = \frac{dH}{dT} \tag{2.31}$$

$$\lim_{dT \to 0} C_p = \infty \tag{2.32}$$

In fact, as can be seen in the following picture 2.7, there is a discontinuity closed to the critical point (around -150°C) , both for the enthalpy and for the C_p:

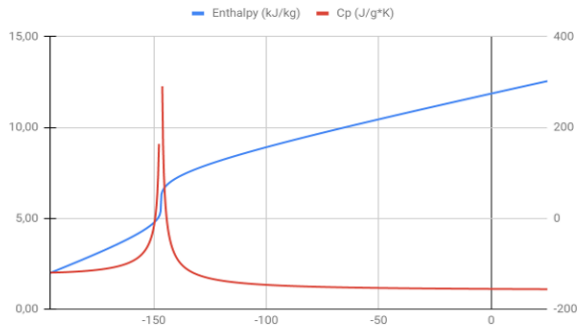

Figure 2.7: Cp [kJ/kg K] and Enthalpy [kJ/kg] vs Temperature [°C] at 34 Barg.

The above graph is calculated for a pressure of 34 barg, but also by varying the pressure the trend is the same. As it can be seen the value of Cp increases up to its maximum value around the critical point, thereafter this is approximately linear. The enthalpy, on the other hand, increases approximately linearly after the critical point.
Once the fluid becomes supercritical, it remains at constant volume, both because the mass of the fluid remains constant and because the volume of the reservoir remains constant. It can therefore be considered an isochoric transformation. The graph 2.8 describes the path of the entire transformation that the fluid undergoes by following the set point pressures [2, 9, 14, 17, 24].

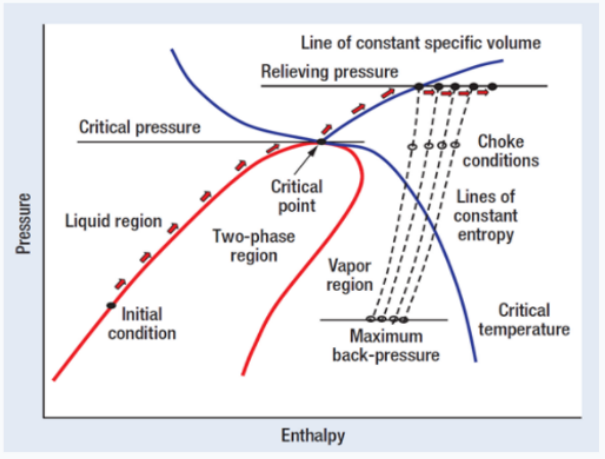

Figure 2.8: Pressure-enthalpy trends for a liquid under subcritical and supercritical conditions [14]

.

2.3. Mass and energy balances : supercritical state

Considering the assumption of isochoric transformation from the moment supercritical conditions arise in the tank, as explained in the previous section, it is now possible to show the energy balances, considering the entire vessel as the control volume. The incoming heat is traced back to the enthalpy increase of the supercritical phase.

$$Q \cdot \Delta t = m_{\text{tot}} \cdot H_{i-1} - m_{\text{tot}} \cdot H_i \tag{2.33}$$

Where :

- Q = constant incoming heat flow (kW);
- Δt = time step considered (s);
- m_{tot}= supercritical mass(kg);
- H_i= supercritical phase enthalpy at instant i (kJ/kg);
- H_{i-1}= supercritical enthalpy at instant i-1 (kJ/kg);

In this way, it is possible to derive a relation to calculate at each instant at the specific enthalpy of the supercritical state.

$$H_i = \frac{Q \cdot \Delta t - m_{\text{tot}} \cdot H_{i-1}}{m_{\text{tot}}} \tag{2.34}$$

Having the value of the specific enthalpy, H_i, available at each step, it is possible to trace the temperature and pressure conditions from the thermodynamic data by consulting any

database. given the assumption of constant mass and volume within our vessel [23].
Given two variables and utilizing isochoric transformations,it is possible to define the pressure corresponding to the physical state of the system. This assumption is considered applicable, given the restricted temperature and pressure range considered in this study. The focus lies in delineating the pressure evolution within the cryogenic tank undergoing heat exchange with the surroundings, as the substance approaches supercriticality at the relief valve's designated pressure setting. It's common for safety valves to be configured at pressures considerably lower than the supercritical pressure, as seen in cryogenic liquid oxygen tanks. However, in scenarios such as liquid nitrogen stored at high pressures, e.g., 31 barg, the supercritical regime emerges between 34 bar and a maximum pressure of 37 barg, aligning with the vent's initial pressure.
In the last mentioned case, the model is applied within a 3-bar range, for which the assumption of isobaric transformation is considered acceptable.

Figure 2.9 schematically illustrates the cryogenic tank under supercritical conditions, emphasizing the presence of a single phase.

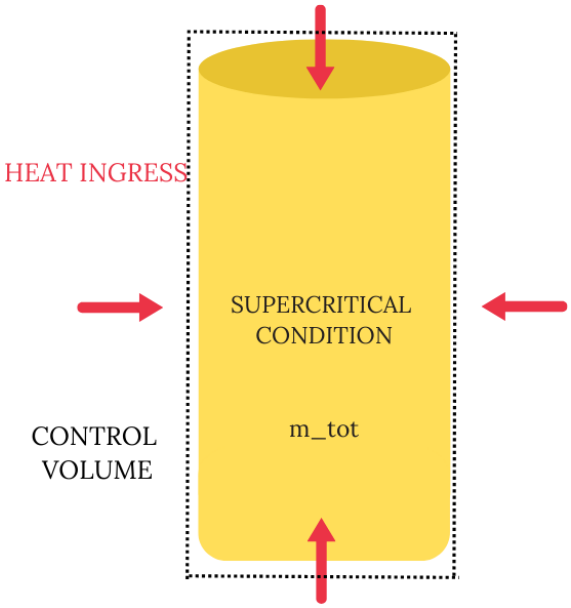

Figure 2.9: Cryogenic vessel under supercritical conditions. Control volume: entire volume of the tank.

2.4. Calculation model

Starting from the equations derived from the mass and energy balances, modelled according to the assumptions applied, the calculation model can be implemented.

In particular, the calculation model requires an iterative calculation mechanism, so that at each step, (time instant), the variables necessary for the next step is derived.
The thermodynamic informations relating to the saturated and subcooled liquid, saturated vapour and supercritical state are directly extrapolated from available databases,

in this case the NIST Chemistry WebBook ® [14].

2.4.1. Calculation model: subcritic-state

For the subcritical state, the reference equations for the calculation model are the evaporation rate and saturated mass:

$$\epsilon_v = \exp(\frac{C_{PC,i}(T_{C,0} - T_{C,i})}{\Delta H_{\text{vap,i}}} \tag{2.35}$$

$$m_{C,i} = \frac{Q \cdot \Delta t}{H_{C,i} - H_{F,i}} \tag{2.36}$$

Knowing the initial pressure and temperature conditions of the stored liquid and using the thermodynamic data available for the subcooled and saturated phase at the initial pressure, it is possible to determine the saturated mass at the desired instant, as well as the evaporation rate.
By combining these two values, it is to determine the evaporated mass at each step:

$$m_{\text{e,i}} = \epsilon_v \cdot m_{C,i} \tag{2.37}$$

Thus, knowing the evaporated mass, it is possible to know and update the masses of each phase involved, which can then be converted into volumetric terms.

$$m_{\text{V}_i} = m_{\text{V}_{i-1}} + m_{\text{e,i}} \tag{2.38}$$

$$m_{\text{F}_i} = m_{\text{F}_i} - m_{c_i} \tag{2.39}$$

By converting the mass terms just calculated into volumetric terms, the new value of molar density at instant i is determined. This is necessary to apply equation of state 2.27 to the new value of pressure increased by the evaporation phenomenon.
Once the new value of the pressure has been determined, the new thermodynamic properties of the subcooled and saturated liquid and saturated vapour at the new temperature are derived, so that the iterative cycle can be restarted.
This mechanism is operated until the critical pressure or maximum permissible pressure is reached.
To carry out our model, MATLAB® is utilized as the calculation tool, by constructing a suitable code adapted to these conditions.

Figures 2.10 and 2.11 summarize the equations derived from the balances used and the iterative logic of the calculation process.

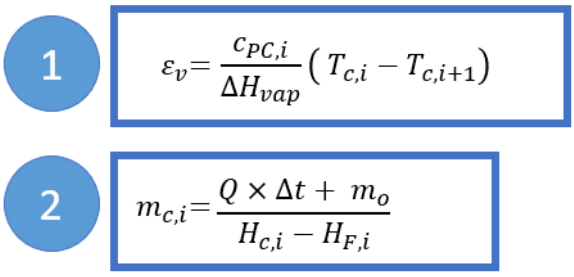

Figure 2.10: Subcritical state equations for iterative mathematical modelling,

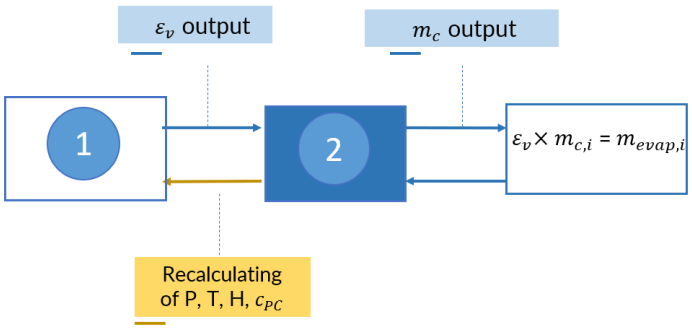

Figure 2.11: Iterative logic applied to the calculation model for subcritical state.

2.4.2. Calculation model: supercritical-state

Regarding the supercritical state, the reference equation for the enthalpy relative to the mass in the supercritical phase at each considered instant is:

$$H_i = \frac{Q \cdot \Delta t - m_{\text{tot}} \cdot H_{i-1}}{m_{\text{tot}}} \tag{2.40}$$

In this way, knowing the initial conditions of the supercritical mass and using the thermodynamic data banks relating to the isochoric transformations of the substance under investigation in the supercritical state, it is possible to trace back to the pressure and temperature at each instant, associated with the calculated enthalpy [23].
Once the maximum permissible tank pressure has been reached, the iterative cycle is stopped, as safety measures intervene to prevent a further pressure increase.

Once again, Matlab ® is used as calculation tool to carry out our model, by constructing a suitable code suited to these conditions.

Figures 2.12 and 2.13 summarize the equations derived from the balances used and the iterative logic of the calculation process.

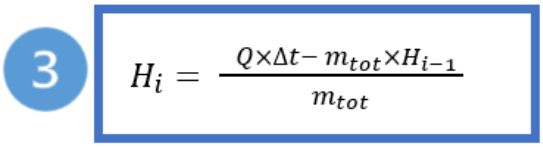

Figure 2.12: Subcritical state equations for iterative mathematical modelling.

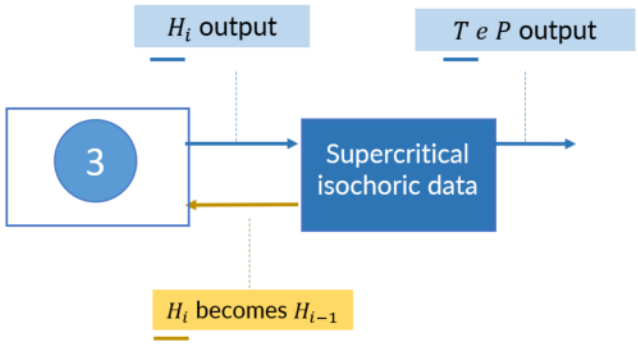

Figure 2.13: Iterative logic applied to the calculation model for supercritical state.

2.4.3. Iterative model

In this section, the iterative diagram underlying our model can be visualised, where both sections of the study are combined: sub-critical state and critical state.

The logic represented this diagram is implemented in Matlab ®. The latter can be used for any given environmental condition, type of substance and reservoir. By changing the input data related to the variables of the external temperature, conduction of the insulating material, tank volume, tank filling and substance, it is possible to obtain information regarding the variation of the volume of the stored product and the pressure conditions, as well as the times within which the tank reaches the supercritical condition or the safety valve is triggered.

Following the flowchart from "START," by inputting all the required information, including the tank's design characteristics and the thermodynamic data of the stored product at operating conditions, it is possible, using derived equations, to calculate the incoming heat flux, which remains constant throughout the simulation. Starting from time t=0, it is then possible to calculate, for each time interval, the rate of evaporation and the saturated liquid mass using equations derived from mass and energy balances. By combining the evaporation rate and the value of the saturated mass, the evaporated mass can be obtained.

In this way, knowing the liquid and vapor masses of the product at time t=0 and knowing the evaporated mass, it is possible to update the quantities of subcooled liquid, saturated liquid, and vapor masses at each time interval, which vary in correlation with the evaporation phenomenon.
The update of the involved phases is performed in terms of both mass and volume, utilizing the density at the given pressure and temperature conditions.
Through this procedure, the molar density of the vapor phase can also be updated after each time interval. This value, in correlation with the molar density of the previous interval, is used via the Peng-Robinson equation to calculate the pressure, which undergoes an increment due to evaporation.

This calculation model is iterative and undergoes variations based on the pressure value reached. If the pressure remains below the MAWP (Maximum Allowable Working Pressure) and the supercritical pressure, the thermodynamic properties are recalculated at the new pressure condition, and the iteration begins again. If the pressure reaches the MAWP, the cycle terminates. However, if the pressure reaches the supercritical pressure, the equation derived from the balances for the supercritical ise used. At each time interval, the enthalpy of the isochoric transformation is calculated, correlated with the new pressure value. Similarly, once the MAWP is reached, the iterative cycle will be terminated.

By implementing this calculation model, for each stored substance and type of tank, it's possible to obtain as output the variables describing the phenomena of autopressurization and evaporation. These outputs can include parameters such as:

- **Evaporation Rate**: The rate at which the stored substance evaporates over time.
- **Liquid Mass**: The mass of the substance remaining in liquid form inside the tank at each time interval.
- **Saturated Mass**: The mass of the substance at saturation point inside the tank at each time interval.
- **Vapor Mass**: The mass of the substance in vapor form inside the tank at each time interval.
- **Pressure**: The pressure inside the tank at each time interval.
- **Temperature**: The temperature inside the tank at each time interval.
- **Density**: The density of the substance inside the tank at each time interval.
- **Enthalpy**: The enthalpy of the substance inside the tank at each time interval.

These variables provide a comprehensive understanding of how the autopressurization and evaporation phenomena evolve over time for different storage conditions and substances.

Moreover, this calculation model is fundamental for estimating, depending on the conditions and external temperature, during periods of tank inactivity, the time required to reach the MAWP (Maximum Allowable Working Pressure), a parameter of great importance for decision-making and industrial safety. Furthermore, it is capable of describing the behavior of pressure in the supercritical region, where it is often difficult to predict

behaviors and understand the unpredictability of changes in thermodynamic characteristics.
This calculation scheme is the starting point for validating our model with experimental results, to verify its validity and implementation and to obtain consistent information for optimizing and improving the conditions of cryogenic tanks.

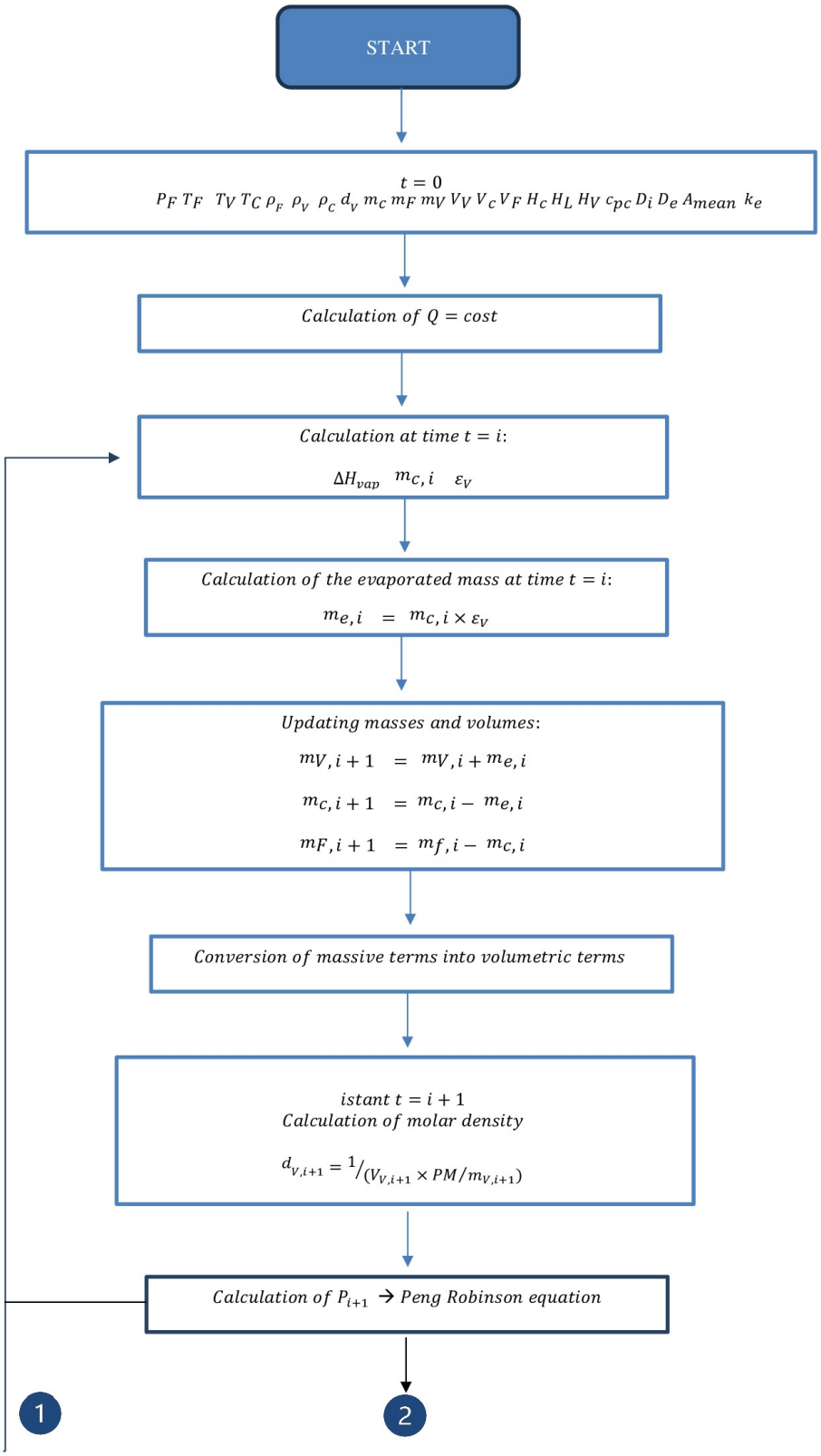
START
$t = 0$
$P_F\ T_F\ \ T_V\ T_C\ \rho_F\ \rho_V\ \rho_C\ d_V\ m_C\ m_F\ m_V\ V_V\ V_C\ V_F\ H_C\ H_L\ H_V\ c_{pc}\ D_i\ D_e\ A_{mean}\ k_e$
Calculation of $Q = cost$
Calculation at time $t = i$:
$\Delta H_{vap}\ \ m_{C,i}\ \ \varepsilon_V$
Calculation of the evaporated mass at time $t = i$:
$m_{e,i} = m_{c,i} \times \varepsilon_V$
Updating masses and volumes:
$m_{V,i+1} = m_{V,i} + m_{e,i}$
$m_{c,i+1} = m_{c,i} - m_{e,i}$
$m_{F,i+1} = m_{f,i} - m_{c,i}$
Conversion of massive terms into volumetric terms
istant $t = i + 1$
Calculation of molar density
$d_{V,i+1} = {}^{1}/_{(V_{V,i+1} \times PM/m_{V,i+1})}$
Calculation of P_{i+1} → Peng Robinson equation
1
2

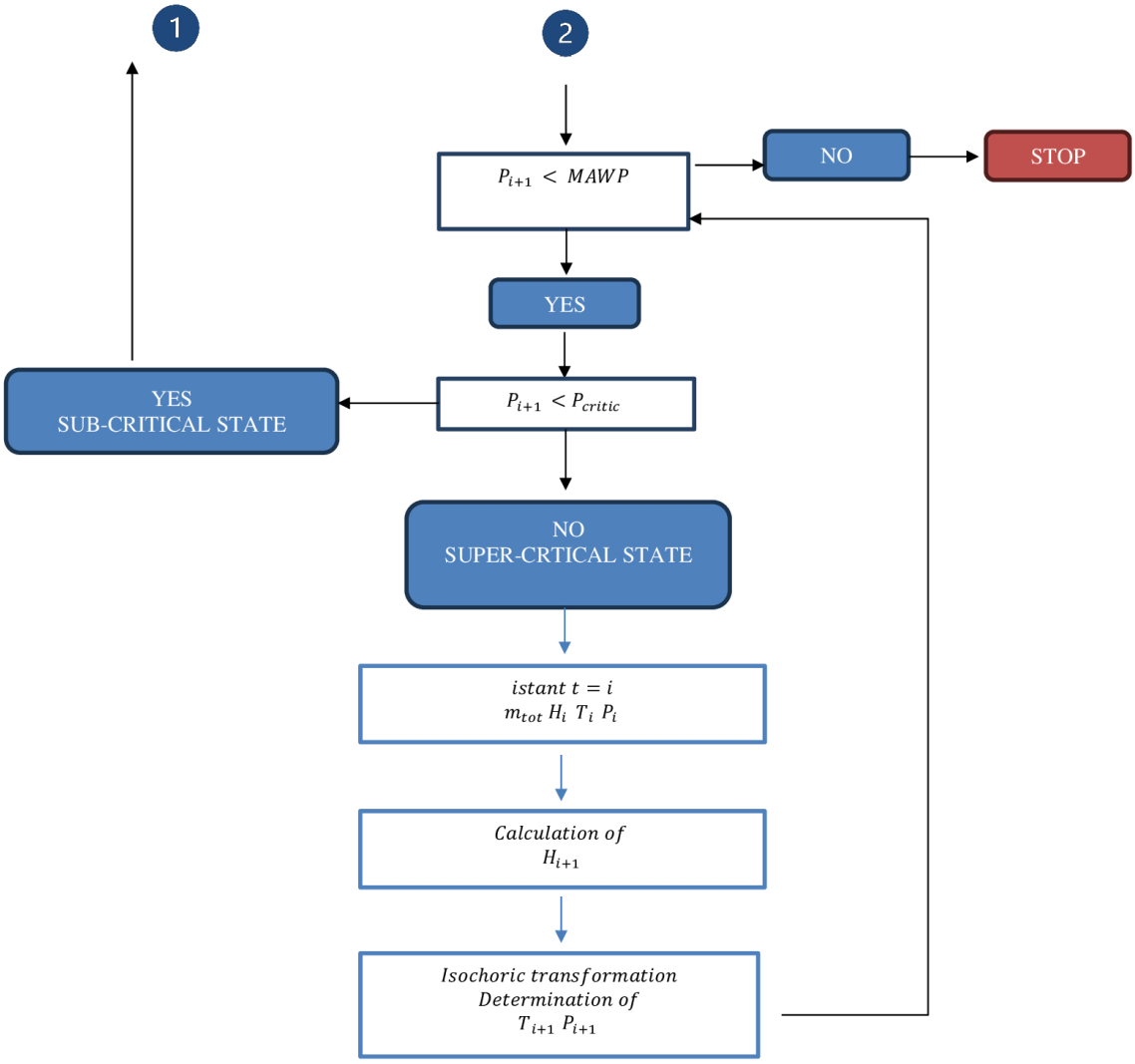
1
2
$P_{i+1} < MAWP$
NO
STOP
YES
$P_{i+1} < P_{critic}$
YES
SUB-CRITICAL STATE
NO
SUPER-CRTICAL STATE
$istant\ t = i$
$m_{tot}\ H_i\ T_i\ P_i$
$Calculation\ of$
H_{i+1}
$Isochoric\ transformation$
$Determination\ of$
$T_{i+1}\ P_{i+1}$

2.5. Economic and environmental impact evaluation

Low-pressure cryogenic tanks are filled to a certain percentage of their maximum capacity, which depends on tank specifications and safety regulations. This practice is implemented to optimize the reservoir's capacity and enhance the efficiency of gas transport and storage. Filling the tank to a percentage below its maximum capacity serves to provide a safety margin and prevent issues related to gas expansion during transport or storage.
Filling the tank to a percentage below the maximum capacity serves to provide a safety margin and avoid problems with gas expansion during transport or storage. In addition, leaving an empty space inside the tank makes it possible to compensate for temperature and pressure variations that may occur during cryogenic gas use.

By the way, there are many benefits derived from successfully filling the tanks to the highest possible level:

- Maximisation of space utilisation: filling the tank completely allows the best possible use of available space, maximising the amount of gas that can be transported or stored;
- Transport efficiency: in transport applications, such as the transport of liquefied gas, filling the tank completely allows more gas to be transported with fewer trips, thus reducing operating costs and environmental impact;
- Reduced risk of contamination: keeping the tank completely filled reduces the empty space inside the tank, thus reducing the possibility of contamination or oxidation of the gas;
- System stability: a fully filled tank offers greater stability during transport or storage, reducing the risk of unwanted movement or deformation of the tank;

If the tank is high-pressure, the filling typically takes place up to the maximum safe working pressure of the tank, rather than filling up to a specific percentage of the tank capacity as in cryogenic tanks.
In particular, different types of telemetry are used, capable of determining for a specific pressure at which the tank works the volume required to be left at the top of the tank and consequently the maximum level of cryogenic liquid. Such devices therefore mark the level at 100 % once the maximum permissible filling at a given calibration pressure has been reached. As mentioned earlier, for high-pressure tanks, they typically allow a filling of 50-60%.

Once a model capable of describing the behavior of the cryogenic tank in response to thermal reentry, considering various conditions, substances, and designs, has been developed, the objective is the identification of an optimal configuration. This involves assessing the feasibility of effectively increasing the filling level of the high-pressure tank and then correlating it with the economic benefits.
Our analysis will be developed as follows:

- data analysis of Air Liquide® cryogenic tanks in Italy with pressure greater than 25 Barg and identification of the most used capacity;

- the identification of the number of days required to reach the maximum pressure for different filling levels is achieved through the calculation model. This involves studying pressure trends for the selected reservoirs and considering the design MAWP;
- the identification of an optimal filling percentage ensuring that the maximum pressure is not reached within one week, the usual stopping time for customers.
- calculation, based on the average consumption and the customer's monthly or annual requested fills, of the number of fewer deliveries, related to both a lower evaporation rate and the gain in terms of less evaporated product lost.

It is important to emphasize that the reference for temperature fluctuation is linked to the duration of the company's closure days. Therefore, if the maximum pressure reached is studied within a 7-day period, it is correlated with the average duration of the company's maximum closure days. The most significant timeframe to study for this research is the days of plant closure, as it corresponds to the period of maximum pressure increase and loss of evaporated product. This is because during operational periods, customers using the product in gaseous form can utilize the evaporated product through the economizer, while customers using the product in liquid form, by extracting it, result in a decrease in pressure in the tank, reducing the percentage of product lost through the relief valve.

The downtime period for companies thus represents the most unfavorable moment and must be considered as a reference for determining an optimal tank configuration, thereby ensuring a safety margin.

$$Savings_{\text{manufacturer}} = \text{delivery costs variable } [€] \times \text{number deliveries saved} \tag{2.41}$$

$$Savings_{\text{costumer}} = \text{delivery costs fixed } [€] \times \text{number deliveries saved} \tag{2.42}$$

It is important to emphasize, again referring to Air Liquide's® policies, that while the delivery costs for the customer are fixed, amounting to €150 per delivery, for the producer, the calculation of the cost per delivery is subject to factors such as kilometers traveled, fuel consumption of the tanker truck, and motorway tolls. In order to obtain an economic estimation of the savings for the company based on the reduction of deliveries, a customer is used as an illustrative example for the calculation output of our computational model, considering the distance between supplier and customer.

The number of deliveries saved is counted consiering the kg of cryogenic consumed monthly and the kg that can be unloaded with reference to a 50/60% fill compared to the number of deliveries that can be made with the same kg consumed with the new fill level.
In addition, the kg saved due to reduced evaporation in the case of the optimal conifguration found is taken into account in this calculation.

In addition to the economic impact, considering that large industrial companies operate more than 2000 tanks, the reduction in the amount of product discharged at each delivery and the decrease in product lost through evaporation also have a strong correlation with environmental impact.

The average emission for the delivery of liquid nitrogen during the year 2021 is 372 kg/tonne of carbon dioxide, including transport. In order to reduce the carbon footprint of your application, Air Liquide® has designed a low carbon liquid gas supply solution which guarantees that cryogenic nitrogen is produced with 100% renewable energy, resulting in a 94% decrease in emissions, reaching a value of 22.32 kg of CO_2 per tonne of nitrogen produced and supplied.
It is therefore interesting to determine the annual emission reduction for each customer, given the total number of tanks, and then provide a preliminary estimation of the reduced emissions at a national level in this sector.

3 | Results

3.1. Experimental data for comparison

The results obtained from the model are directly compared with experimental data. The latter are related to the international standard ISO21014, concerning the insulation performance of cryogenic vessels [3].
These data pertain to the daily evaporation rate, calculated for vessels placed at room temperature (15°C) and atmospheric pressure (1 bar absolute). Tests were conducted with precautions to avoid agitation of the liquid, determining the gas discharge rate from the vessel using a flow meter. The gas flow rate is determined as the mass flow rate using a mass flow meter or volumetric flow meter.
In particular, the evaporation rate is specified according to the configuration (horizontal or vertical), the type of insulation, the capacity, and the substance.
For a storage tank for cryogenic oxygen, with a vertical configuration and vacuum perlite insulation, dedicated to storing cryogenic oxygen, with a capacity between 60 and 70 thousand liters, a volumetric loss of 0.13% of the initially stored product is expected [3].
In contrast to the analysis condition, the ISO211014 measurement method only considers product loss once the vaporized phase leaves the vent/bleed valve. However, in this study, product loss is considered once it has vaporized inside the tank. This leads to an overestimation of the product vaporized in the calculation model, compared to the comparison data [3].

An initial validation of the model, in comparison with experimental data, is essential to understand the reliability and predictability of the model.

Once the usability of the method has been confirmed, it becomes possible to extrapolate information that is not readily available or difficult to determine experimentally. This includes the ability to vary multiple variables. Consequently, it enables the exploitation of the code's repeatability by computationally and promptly extracting data without the need for mimicry in the field.
Finally, the analysis of the results obtained can be used to optimize the design of the current cryogenic tanks used in the company, in order to meet economic and safety terms in response to the problem of thermal losses.

The table 3.1 shows how the daily evaporation rate varies according to capacity. Even from a first analysis, it is expected from the results an increase in liquid loss as the tank size decreases.

Net evaporation rate

Net capacity in litres x 1000	insulation type	NER (% per day in LO2)
3	Perlite	0,45
3	Super insulation	0,45
6	Perlite	0,32
6	Super insulation	0,23
10	Perlite	0,26
10	Super insulation	0,18
20	Perlite	0,22
20	Super insulation	0,15
35	Perlite	0,15
35	Super insulation	0,18
40	Perlite	0,16
40	Super insulation	0,1
50	Perlite	0,15
50	Super insulation	0,15
60	Perlite	0,13
60	Super insulation	0,1
80	Perlite	0,13
80	Super insulation	0,1
110	Perlite	0,1
160	Perlite	0,1
200	Perlite	0,1
300	Perlite	0,1

Table 3.1: Net vaporation rate for different net capacity and insulation type.
Substance : cryogenic liquid oxygen.

3.2. Case Study 1: $L0_2$ tank- medium pressure

The first example of the application of the model is a medium-pressure tank for the storage of liquid oxygen.

The table 3.2 summarises the characteristics of the tank under consideration:

LO_2 tank- medium pressure

Vessel design characteristics		
T	-196	[°C]
P	17	[Barg]
Capacity	77 000	[L]
% fill	94	%
$\mathbf{V}_L$	72380	[L]
$\mathbf{V}_V$	4620	[L]
$\mathbf{D}_e$	5000	[mm]
$\mathbf{D}_i$	4611	[mm]
h	240	[mm]
$\mathbf{L}_{c,e}$	5400	[mm]
$\mathbf{L}_{c,i}$	4611	[mm]
$\mathbf{A}_{mean}$	124	[m^2]
$\mathbf{P}_{vac}$	0,04	[mBar]
$\mathbf{P}_{set}$	28	[Bar]
$\mathbf{P}_{crit}$	49,7	[Bar]

Table 3.2: Specification about design and operative condition of the cryogenic vessel.

Considering an outdoor temperature of 15C, the value of the incoming heat flux as: Q= 0.19 kW is obteined.

The first data extrapolated from the model are the trends of the liquid and vapor phases in response to thermal losses.
Graphs 3.1, 3.2, 3.3, 3.4, and 3.5 show the variation in both mass and volume of liquid and gaseous oxygen over a 24-hour period. From these results, it is easy to calculate the daily evaporation rate and compare it with available data.
Pressure trend graphs are then presented, allowing determination of the time required to reach the maximum permissible pressure before the safety valve is triggered and an accident occurs.
In this case, the critical pressure is not reached and only the first part of the calculation model is utilized.

Figure 3.1: Trend of LOX volume [L] versus time [h].

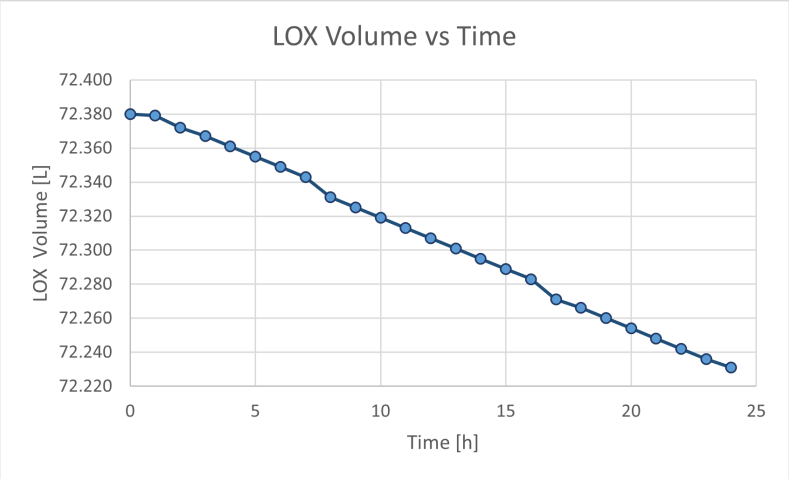

Figure 3.2: Trend of LOX mass [Kg] versus time [h].

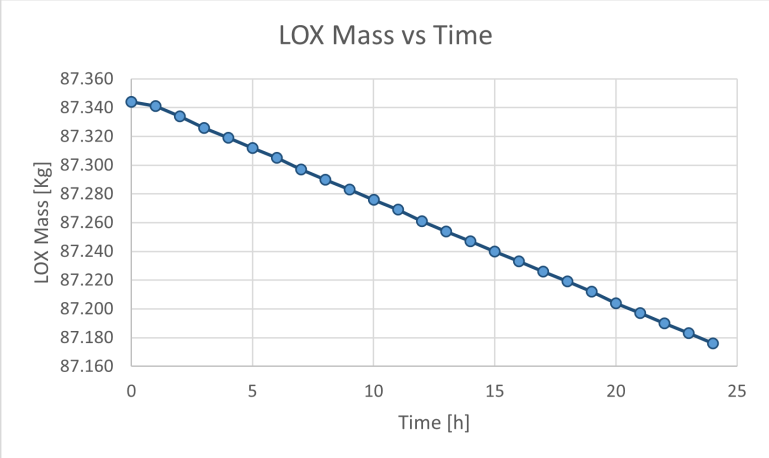

Figure 3.3: Trend of vapor volume [L] versus time [h].

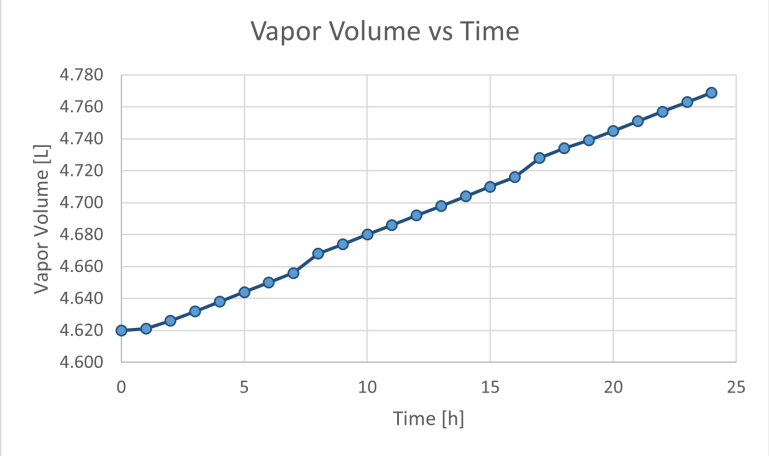

Figure 3.4: Trend of vapor mass [Kg] versus time [h].

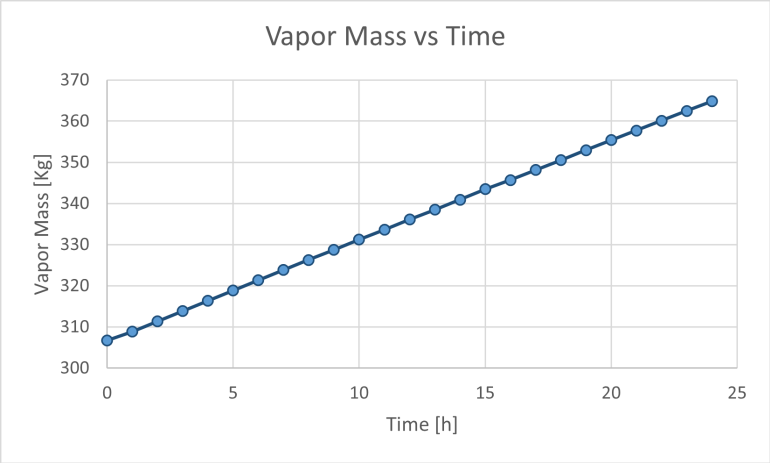

Figure 3.5: Trend of vessel Pressure [Barg] versus time [h].

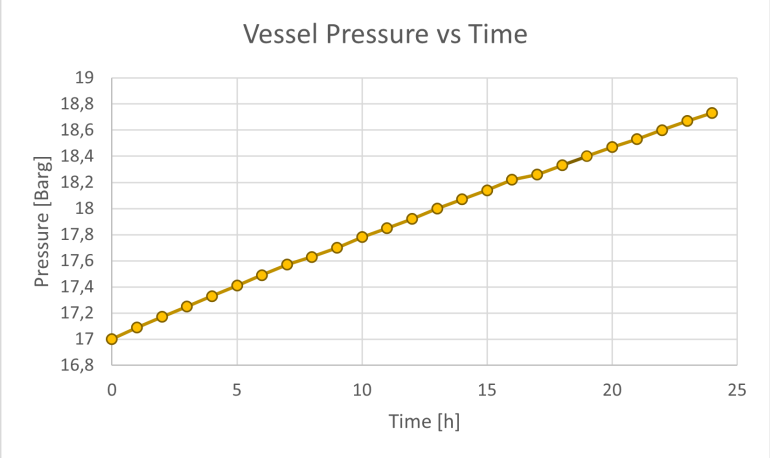

From analysis of the graphs, it becomes immediately evident that, as expected, the cryogenic liquid product tends to decrease over time, while the vapor phase exhibits the opposite trend.
From graph 3.1, it is possible to determine the net daily evaporation value in L/day, which is $0,21\%$. These results are consistent, as shown in the previous sections, with the experimental data in Table 3.1. For a tank with perfect perlite insulation, intended for the storage of cryogenic oxygen with a capacity of 80 thousand liters, the evaporation rate is less than $0,13\%$ [3].

Considering the phenomenon of evaporation of the subcooled liquid and the related process of autopressurization of the vessel, the daily pressure inside the tank is characterized by a progressive increase, starting from 17 Barg up to a value of 18.6 Barg, which constitutes an increase of 1.6 Bar per day.
In addition, as the daily pressure rise is shown, it is possible to predict after how many days the tank reaches MAWP, leading to the opening of the overflow valve and safety

valve. In this case, the maximum permissible pressure (P_{set}) being 28 bar, the tank in an idle state and exposed to heat loss, it takes 7 days before the safety devices intervene to counteract the pressure rise.

Sensitivity analysis

In order to validate the trend of the mathematical calculation model it is interesting to perform a sensitivity analysis by analyzing the model's results using different parameters and comparing them to the experimental data (as expressed in Table 3.1 [3]). The same tank just studied is used as an example, varying only the geometrical parameters relating to the design and the total capacity of the tank. In particular, three additional tanks with lower capacities, respectively 50,000, 30,000, and 20,000 L, are considered.
The expected results, with reference to Table 3.1, predict an increase in the evaporation rate as the tank capacity decreases.
It is important to emphasize that as the net capacity of the tank varies, the quantities involved in the liquid and gaseous phases, as well as the geometrical specifications such as diameter, length of the cylindrical section, and thickness of the insulating layer, also vary. These parameters are related to the calculation of the exchange area and the incoming heat flow.

The tables 3.3 and 3.4 summarize the results obtained for the daily evaporation rate and the pressure trend as a function of capacity for a cryogenic tank LO_X:

Net evaporation rate-different capacity

Net capacity in litres x 1000	NER (exper data)	NER (calc model)
77	0,13	0,21
50	0,15	0,23
30	0,22	0,39
20	0,26	0,43

Table 3.3: Net vaporation rate for different net capacity.

Substance : cryogenic liquid oxygen.

Auto-pressurisation trend- different capacity

Net capacity in litres x 1000	Daily pressure variation[Bar]
77	1,6
50	1,96
30	2,84
20	3,1

Table 3.4: Auto-pressurisation for different net capacity.
Substance: cryogenic liquid oxygen.

The trends between the net evaporation rate relative to the experimental data and the model calculation model show the same increasing trend as the capacity of the cryogenic tank decreases.
In the case of the results obtained using the iterative method, however, there is a more acute overstimulation of the percentage of product lost per day. In particular, the deviation is more pronounced for smaller capacity tanks.
This phenomenon is certainly related to the calculation assumptions, which, as already emphasized, tend to overstate the results. Furthermore, the discrepancy tends to be more pronounced for smaller capacities, as the initial liquid volumes involved are smaller.

Another relevant parameter to evaluate is the response in terms of evaporation and auto-pressurization to varying tank filling levels. As we have already mentioned several times, this is a crucial issue in the industrial field, especially for high-pressure cryogenic tanks, for which filling is limited to ensure the integrity and safety of the tank.
The same tank described in Table 3.2 is placed under different filling conditions to demonstrate how it is affected by heat exchange as it varies.

Evaporation rate - different % fill

% fill	NER
94	0,21
80	0,22
60	0,3
50	0,35

Table 3.5: Net evaporation rate for different % fill.
Substance: cryogenic liquid oxygen.

Figure 3.6: Trend of vessel Pressure versus time- different % fill.

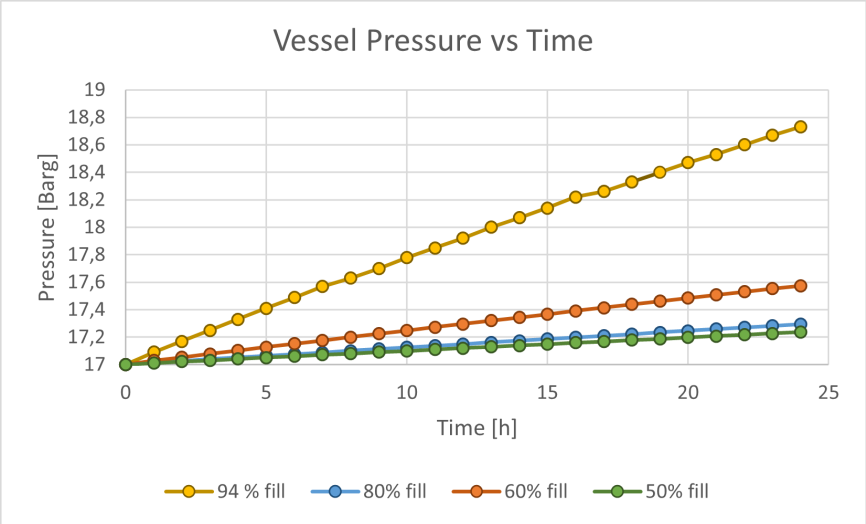

As the filling level of the cryogenic liquid inside the tank decreases, the evaporation rate increases. This condition is mainly influenced by the lower initial liquid quantity, which, under the same design conditions and exposure to heat exchange with the outside, impacts this parameter.
Regarding autopressurization, filled tanks are expected to be more exposed to this phenomenon, as per industrial precautions and procedures.
From graph 3.6, it is evident that the daily pressure trend exhibits different slopes depending on the filling level: the much steeper slope for tanks filled to 94% compared to 50% confirms the greater safety found in the latter case. Here, a more modest variation (0.24 compared to 1.6 bar/day) of the pressure is observed.
Lower filling levels not only enhance safety but also reduce product loss. Although the evaporation rate is higher, tanks with significant pressure increases often require frequent bleeding of product via the relief valve to restore operating conditions and lower the pressure. This results in the complete loss of product without the possibility of using cryogenic gas, particularly in cases where the economizer is present for customers using the product in the gas phase.
Improving this condition involves finding an optimal fill level in terms of the expected pressure rise. This allows for a compromise between safety, product waste due to purging to restore pressure, and savings related to filling trips. High-pressure tanks filled in smaller quantities typically require more time-consuming and frequent filling trips.

Among the parameters to be investigated that may influence our model is the conductivity used for the insulation layer, perlite in this case.
In the illustrated model, a constant value of perlite conductivity is not used; instead, the variation of the coefficient with respect to the internal and external temperature is evaluated. Additionally, a relationship is employed to determine the conductivity correlated to the degree of vacuum inside the cavity.
The same calculation model is simulated, but using an average conductivity of perlite $k_{\text{mean}} = 0.04$ kW/mK, extracted directly from the Perlite Italiana supplier's datasheet

[29] [26][16].

The first variable on which the different conductivity values are reflected is the calculation of the heat input, which consequently leads to significantly different results. A comparison of these two cases can be seen in the table 3.6 and graph 3.7.

Perlite conductivity	Heat flux	NER
k_e[29]	0,19	0,21
k_{mean}[16]	0,31	0,34

Table 3.6: Heat flux and net evaporation rate-different perlite conductivity
Net vaporation rate Substance: cryogenic liquid oxygen.

Figure 3.7: Trend of vessel Pressure versus time- different perlite conductivity.

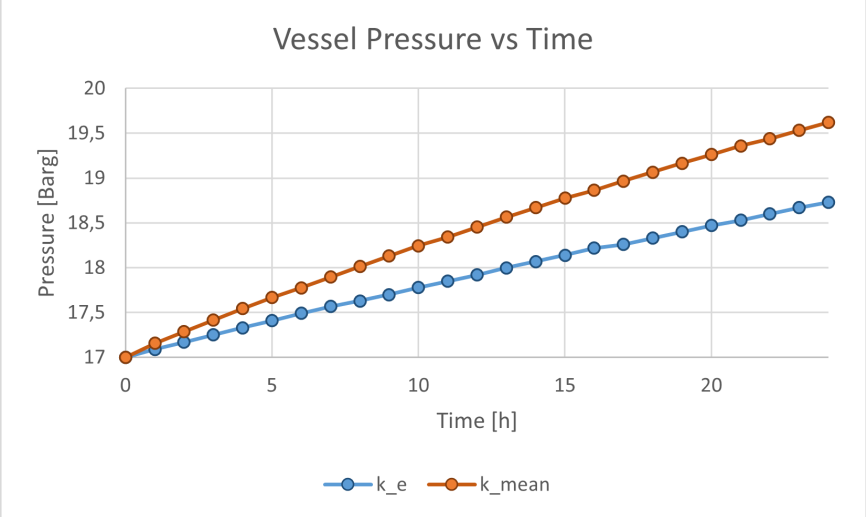

The different evaluation of the conductivity coefficient leads to very different results, both in terms of the evaporation rate and with respect to the trend of the autopressurization phenomenon. It is therefore advisable to pay particular attention to the evaluation of this parameter using the reports and data available that are closest to the description of one's own case study, as neglecting some particularity may lead to the determination of a conductivity coefficient and the obtaining of results very different from reality.
In this case, the value k_e is considered more suitable, discarding the values available from the supplier's data sheets. The main reason is related to the latter's inability to account for a gradient and specification with respect to the degree of vacuum present in the cavity where the insulation material is distributed. In fact, the results obtained using k_{mean} reflect a phenomenon of greater evaporation and a more significant increase in pressure, correlated with the greater incoming heat flux, which may be related to the high vacuum characteristics of the tank under consideration, which are not taken into account.

Considering now that the tanks in the plant are subjected to multiple climatic conditions over the course of the year, the sensitivity of the results to the average seasonal temperatures in the province of Cremona is evaluated. In Table 3.7, the specifications with respect to the seasonal temperatures considered, and the trends in evaporation rate and daily pressure in all the cases mentioned are shown. In particular, average temperatures of 6°C in winter, 15°C in autumn and spring, and 26°C in summer are used.

Evaporation rate - different outdoor temperatures

Outdoor temperature [°C]	NER
6	0,19
15	0,21
26	0,23

Table 3.7: Evaporation daily rate for different seasonal average temperatures. Substance: cryogenic liquid oxygen.

Figure 3.8: Trend of vessel Pressure versus time- different outdoor temperatures

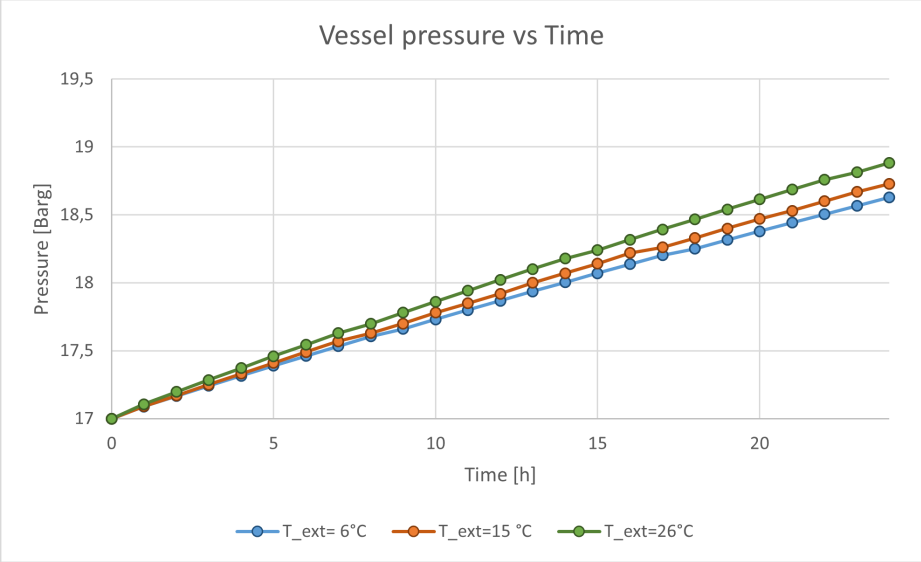

As the outside temperature increases, especially during the summer season, the evaporation rate is higher, as the tank is exposed to greater heat exchange with the environment. The same trend occurs for the autopressurization phenomenon, as shown in graph 3.8, with a steeper slope of the daily variation for the tank exposed to 26°C compared to 15°C and 6°C.
Despite the differences shown, the variations observed do not have a pronounced impact. Although the outside temperature is a very important factor, in areas where the thermal

excursions are not so pronounced during the different seasons, the variation of the daily evaporation rate trend during the year is not so significant.

A final interesting parameter to investigate is the variation of the vacuum degree within the cavity of the insulation layer.
The latest generation of tanks is characterized, when delivered to the customer, by a perfect vacuum degree and distribution of perlite, guaranteeing an estimated vacuum degree of approximately 0.04 mBar (30 microns). This condition has allowed for many changes and advances compared to the tanks used until a few years ago, still on the market, which were characterized by a vacuum of about 0.26 mBar (200 microns).
In particular, it is interesting to assess the difference in performance of the most recent tanks compared to their predecessors.
Furthermore, it is crucial to obtain a comparison between the results obtained under optimal vacuum conditions and after about 5 years, before the planned maintenance and revamping operations, in which a vacuum loss of one degree is expected, reaching about 0.4 mmBar in today's tanks.
In Table 3.8 and graphs 3.9 and 3.10, the daily evaporation rate of the cryogenic tank for these three different conditions is shown.

Evaporation rate - different insulation vacuum condition

Vacuum condition [mBar]	NER
0,26	0,38
0,04	0,21
0,4	0,73

Table 3.8: Evaporation daily rate for different insulation vacuum condition .
Substance: cryogenic liquid oxygen.

From the analysis in the table 3.8, it is already evident how the degree of vacuum significantly impacts the efficiency of the tank's insulation layer. There is a significant difference in performance and difference in evaporated product in the latest produced tanks compared to standard tanks at 0.26 mBar.
The most significant difference, however, can be seen in the variation in the evaporation rate of the tank under inception conditions, compared to the situation before revamping. In the latter case, in fact, the daily evaporation rate is more than three times that estimated at perfect vacuum, resulting in a clear difference in terms of L/day lost to the costumer.

Graph 3.9 shows the trend in the volume of cryogenic liquid over a 24-hour interval. From it, it is easy to see that in one day, an estimated evaporation of 150 liters of cryogenic oxygen occurs for a tank under ideal conditions, as opposed to 530 liters in the case of a tank after 5 years of operation.
These daily differences in product quantities are reflected monthly and yearly in large

quantities of lost product and consequent transport costs related to increased supplies. This issue highlights how the degree of vacuum is one of the key parameters in the heat exchange of cryogenic tanks.

Figure 3.9: Trend of LO_x versus time- different insulation vaacum condition.

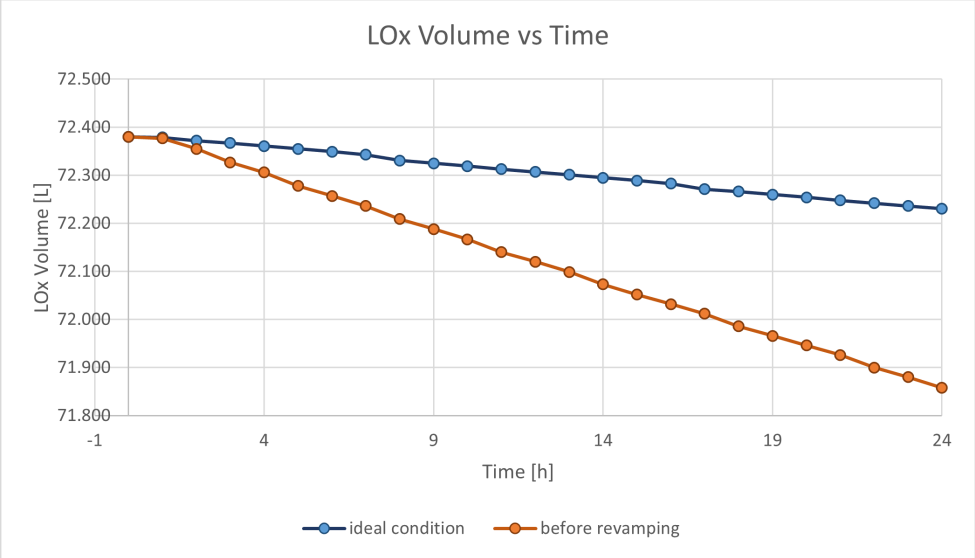

It is also interesting, in the graph 3.10, to highlight the trend of the autopressurisation phenomenon for the same conditions:

Figure 3.10: Trend of pressure versus time- different insulation vaacum condition.

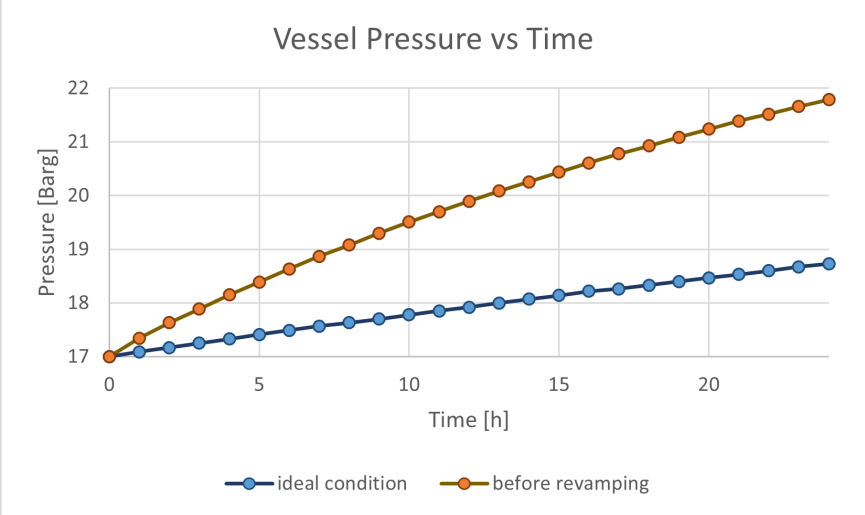

In terms of pressure, the variation is also very significant, with a rate of 1.7 bar per day in the case of higher vacuum compared to 4.7 bar per day after the tank has been in operation. This difference is reflected in the time required for the purge valve to open to restore operating pressure, for the customer to disperse gaseous product directly into the

environment, and for the maximum allowable pressure to be reached and for the safety valve to activate.
In numerical terms, while a tank in optimal vacuum conditions takes seven days to reach the maximum allowable pressure; before revamping, the same tank at medium pressure reaches maximum pressure after not even two days.

The trends shown in Figures 3.9 and 3.10, show a clear difference in the results depending on the tank condition considered.
The degree of vacuum therefore, from the analysis of the results just made, appears to be one of the most influential variables and one of the main players in the phenomenon of thermal shrinkage.
For this reason, it is fundamental to carefully consider this aspect for the optimization and minimization of this issue, especially for high-pressure tanks, which are dealt with in the second case study. They represent a key example in the industrial field regarding the issue of thermal losses in cryogenic tanks.

3.3. Case study 2: LN_2 tank- high pressure

Having validated the mathematical calculation model with the available experimental data, it is possible to apply it to the tanks of our greatest interest: tanks for the storage of high-pressure nitrogen.

Table 3.9 summarizes the characteristics of the tank:

LN_2 tank- high pressure

Vessel design characteristics		
T	-185.2	[°C]
P	31	[Barg]
Capacity	20 000	[L]
% fill	60	%
$\mathbf{V}_L$	12 000	[L]
$\mathbf{V}_V$	8000	[Lt]
$\mathbf{D}_e$	2550	[mm]
$\mathbf{D}_i$	2150	[mm]
h	192	[mm]
$\mathbf{L}_{c,e}$	6300	[mm]
$\mathbf{L}_{c,i}$	5500	[mm]
$\mathbf{A}_{mean}$	52.55	[m^2]
$\mathbf{P}_{vac}$	0,04	[mmBar]
$\mathbf{P}_{set}$	37	[Bar]
$\mathbf{P}_{crit}$	33.9	[Bar]

Table 3.9: Specification about design and operative condition of the cryogenic vessel.

Considering an outdoor temperature of 15°C, the value of the incoming heat flux obtained is: Q= 0.10 kW.

Different graphs are presented here, differentiating the subcritical region from the supercritical region.
The first data extrapolated from the model are the liquid and vapor phase trends in response to thermal reentry in the subcritical regime. Graphs 3.11, 3.12, 3.13, and 3.14 show the change in both mass and volume of nitrogen liquid and gas over a 24-hour period. From these results, it is therefore immediate to calculate the daily evaporation rate. Graph 3.15 presents the pressure trend, allowing to determine the time required to reach supercritical pressure.

Figure 3.11: Trend of LN_2 volume [L] versus time [h].

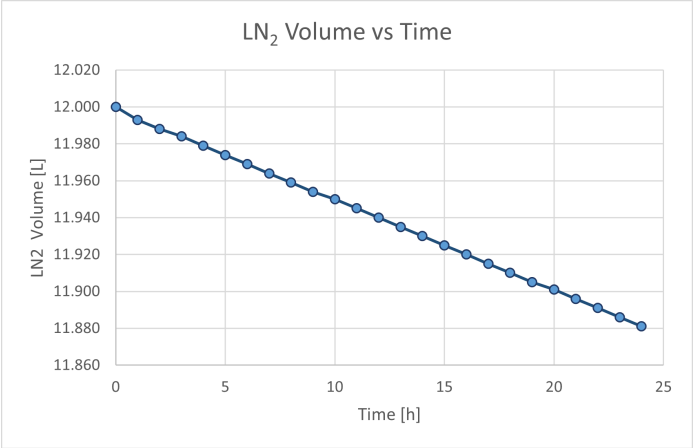

Figure 3.12: Trend of LN_2 mass [Kg] versus time [h].

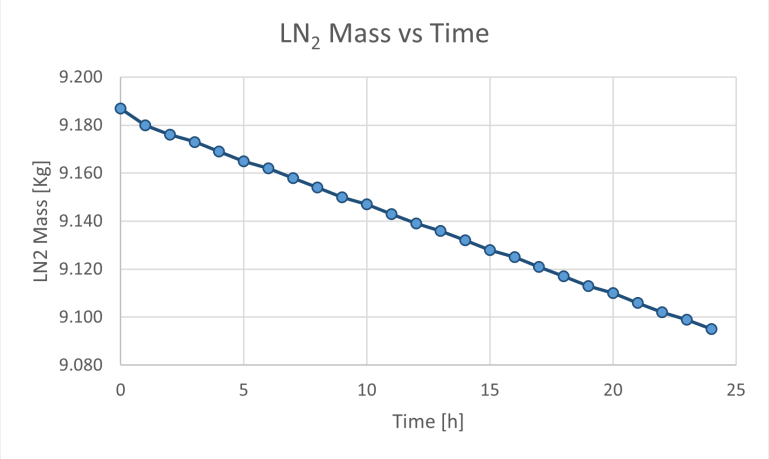

Figure 3.13: Trend of vapor volume [L] versus time [h].

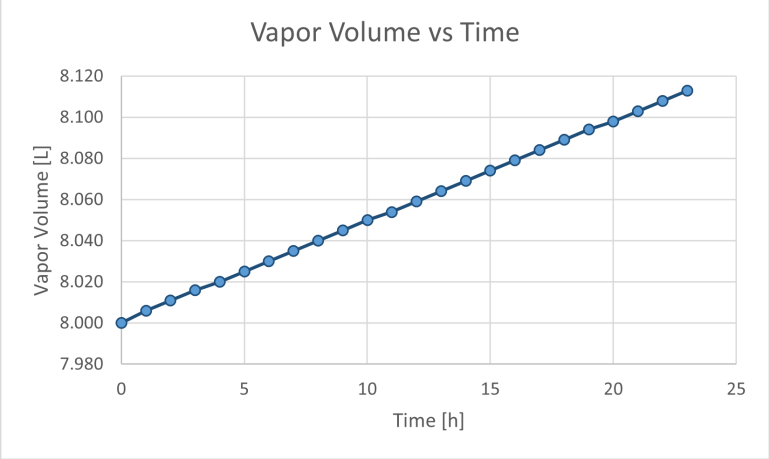

Figure 3.14: Trend of vapor mass [Kg] versus time [h].

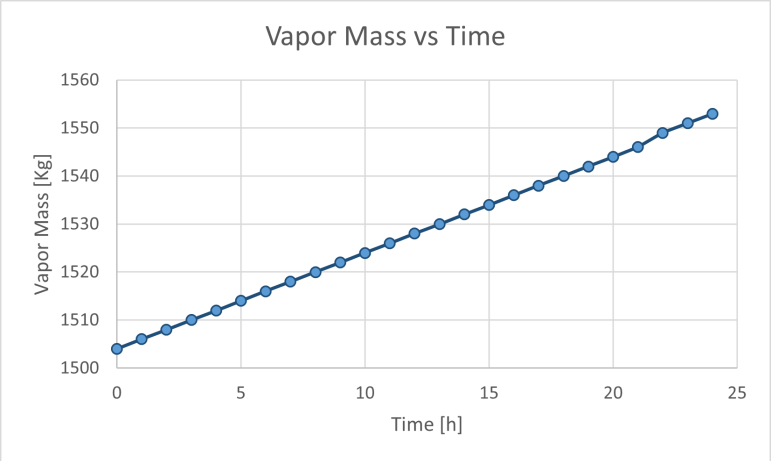

Figure 3.15: Trend of vessel Pressure [Barg] versus time [h].

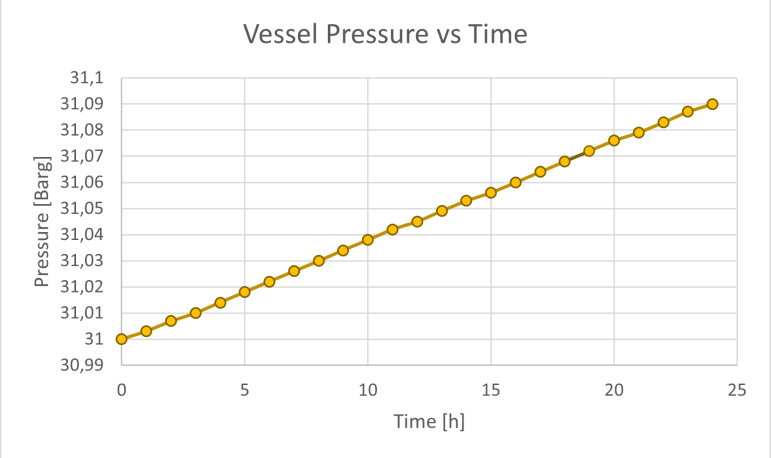

From analysis of the graphs, it is immediately clear that, as expected, the cryogenic liquid product tends to decrease with respect to time, in favour of the vapour phase, which has the opposite trend.
From graph 3.6 it is thus possible to determine the daily evaporation rate, which is 0.99% of the net evaporation value in L/day, with a quantitative loss of 119 kg per day.
Considering the phenomenon of evaporation of the subcooled liquid and the related process of atupressurisation of the tank, the daily pressure inside the tank is characterised by a progressive increase, starting from 31 Barg up to a value of 31.1 Barg, which constitutes an increase of 0.1 Bar per day.
It is therefore simple to determine after how many days of inactivity the tank reaches a supercritical state. Considering the critical nitrogen pressure of 33.9 bar for the stationary tank subject to thermal loss, the cryogenic fluid inside the tank will be identified by a single supercritical phase after 29 days.

The pressure increase is much lower than the results obtained in case study 1, that was

of 1,6 Bar/day. This conidtion is related both to the different cryogenic substance, but above all to the filling level, which in the case of high-pressure tanks is kept low, to ensure, given the high operating pressures, less oscillation and greater control of this parameter. In addition, the evaporation rate, on the other hand, is significantly high, (0,99 % vs 0,21 %), due to the combination of the tank capacity and the initial level of the cryogenic liquid.
These aspects are advantageous in terms of safety but disadvantageous in terms of economic loss.

The conditions after reaching the supercritical state are entirely different from those in the subcritical state. The parameter of greatest interest is the estimation of the pressure trend, as it becomes much more complex to monitor and control high-pressure increases once the supercritical phase is reached.
It is advisable to ensure that the tank is always operating below the critical state.

The graph 3.17 shows the trend of the enthalpy increase for the supercritical phase, starting from 33.9 Barg, the pressure at the beginning of the supercritical state, where the isobaric storage assumption is applied, up to 37 Barg, the maximum allowable operating pressure.

Figure 3.16: Trend of Enthalpy versus time- Supercritical state.

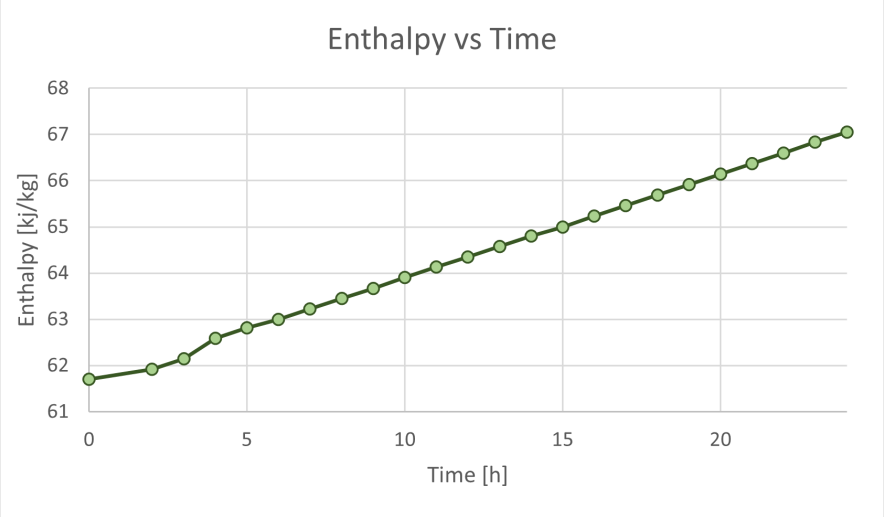

The increase in enthalpy corresponds to an increase in pressure inside the vessel. This trend is illustrated in the graph 3.17.

Figure 3.17: Trend of Pressure versus time- Supercritical state.

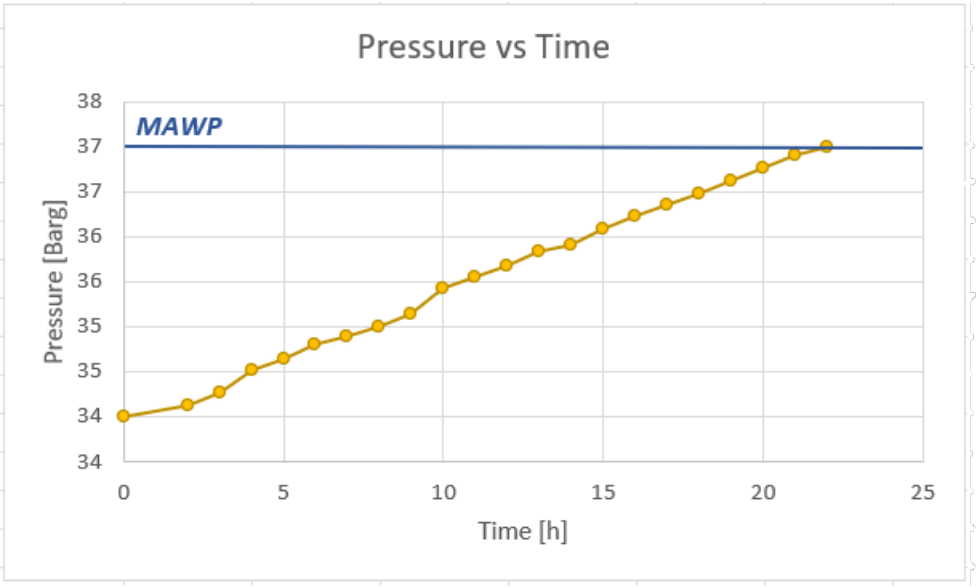

After reaching the supercritical state, the autopressurisation phenomenon takes on a different magnitude compared to the subcritical zone. The increase in pressure inside the tank is much more pronounced, reaching from 34 to 37 bar, the maximum pressure allowed, in just 22 hours, before the safety devices opens.

An essential parameter to investigate, given the results obtained in case study 1, is the variation of the results according to the different void conditions in the cavity where the insulation material is distributed.
This parameter was found to be the main factor relating to the fluctuation of the evaporation rate and the autopressurization condition of the tank in the case of medium-pressure cryogenic oxygen.

In graphs 3.18 and 3.19 the trends of the liquid product volume and tank pressure in relation to the daily time interval are shown.
The trends are markedly different, with a decrease in the case of liquid volume and a much more pronounced increase in tank pressure under less severe vacuum conditions.
In quantitative terms, for vacuum grades of 0.4 mBar, the daily pressure increase is 0.45 Bar, resulting in supercritical conditions being reached after only 6.4 days and a loss of 749 L each day.
These results are highly relevant, demonstrating how certain technical characteristics over the lifetime of a tank lead to completely different behaviors, necessitating equally different interventions and management of these types of vessels.

Considering a company that closes for approximately a week during the Christmas holidays, the results indicate that during this time, the customer loses half of the usable volume of the stored material, with the risk of approaching the maximum permissible tank pressure and activating safety systems.

Figure 3.18: Trend of LN_2 versus time- different insulation vacuum condition.

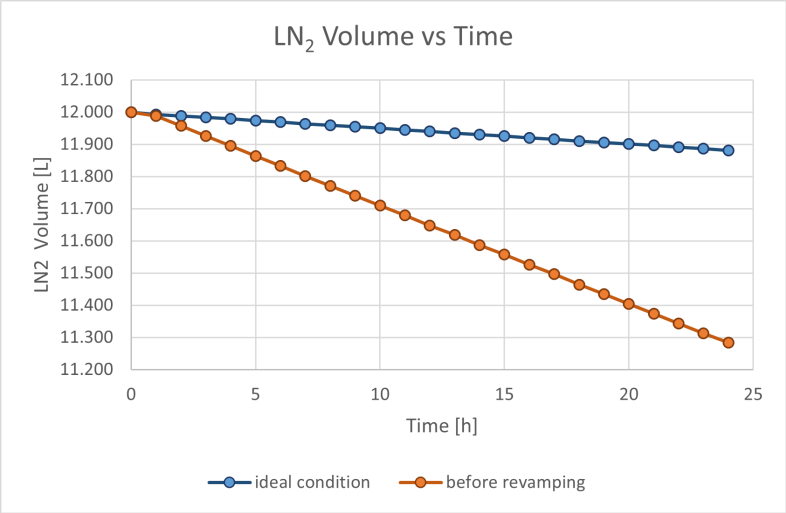

Figure 3.19: Trend of LN_2 pressure versus time- different insulation vacuum condition.

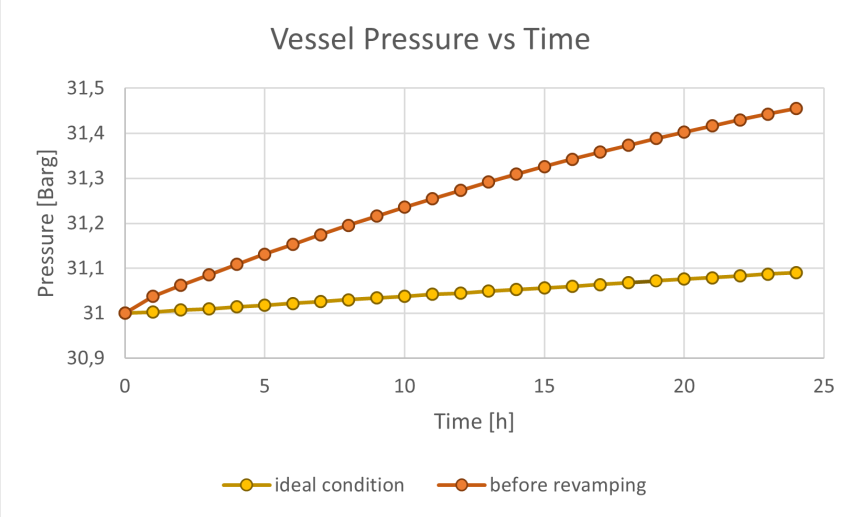

Similarly, considering that the primary motivation for this research was the inability to fill high-pressure tanks to high percentages, maintaining a level of around 50/60%. Indeed, the level, regulated by telemetry, is controlled at the time of filling by specifying the calibration pressure, determining the space to be left at the top of the tank for thermal expansion due to thermal shrinkage and consequent pressure increase. Specifically, increasing the operating pressure of the tank increases the space required for the expansion and evaporation process.
At this point, it is interesting to evaluate the performance of the most significant variables concerning different tank fill levels. Here again, fillings of 60, 80, and 94% are considered in the table 3.10.

Evaporation rate - different % fill

% fill	NER
94	0,64
80	0,75
60	0,99

Table 3.10: Net evaporation rate % fill.
Substance: cryogenic liquid nitrogen. Capacity: 20 000 L.

Table 3.10 shows the development of the evaporation rate according to the varying degree of filling, with higher values being found for lower fills.

As far as pressure trends are concerned, they are illustrated in Figure 3.20:

Figure 3.20: Trend of vessel Pressure versus time- different % fill.

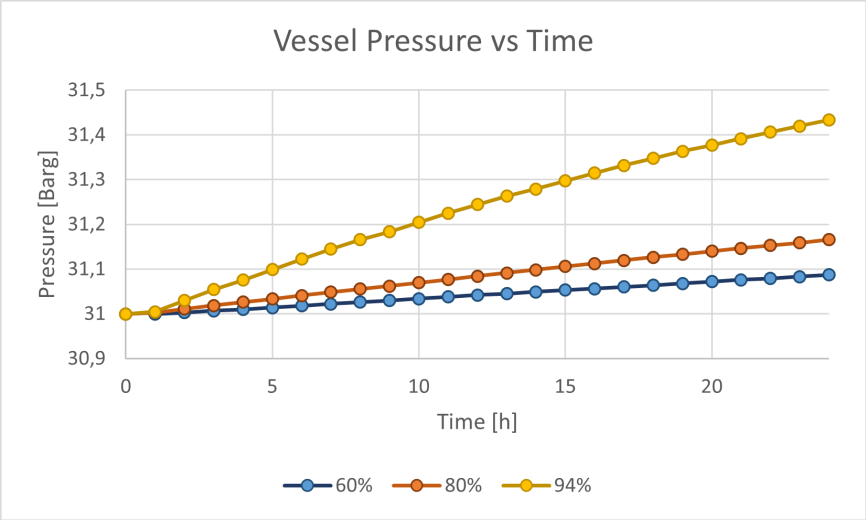

The trends, as expected, follow different patterns and slopes, showing a more pronounced increase for larger fills.
Taking the extremes of our analysis, 60% and 94%, we have an estimated autopressurization of 0.9 bar per day in the former case, versus 0.43 in the latter.
These results are reflected in a time interval for reaching supercritical conditions of 32 days vs. 6.7 compared to tanks with a smaller initial gas buffer.

The significant phenomenon of autopressurization, with a 94% filling in high-pressure tanks, nearing supercritical conditions and the maximum permissible pressure, renders it impossible to operate under such conditions in an industrial environment, given the small margin with the initial operating pressure of the tank.
For these reasons, confirmed by our mathematical model, the filling level for tanks with

pressures greater than 25 Barg is maintained at 50/60%, ensuring smaller pressure variations.

3.4. Case study 3 : Optimization high pressure LN_2 tank

Having reached this point, it is interesting to see if an optimal configuration can be found for high-pressure tanks in order to find a compromise between pressure variation, given the high operating pressures, evaporation rate and filling level.
In fact, being able to increase the level of liquid allowed in high-pressure tanks means a higher delivery, in terms of kg per order to the customer, while decreasing the number of expected deliveries for the same amount of product consumed.

In particular, the most commonly used capacity for high-pressure storage, 3 000 L, is taken as a reference at 31 Barg, the most commonly used operating pressure.
The table 3.11 summarises the characteristics of the tank:

LN_2 tank- high pressure

Vessel design characteristics		
T	-185.2	[°C]
P	31	[Barg]
Capacity	3000	[L]
$\mathbf{D}_e$	1590	[mm]
$\mathbf{D}_i$	1331	[mm]
h	180	[mm]
$\mathbf{L}_{c,e}$	2650	[mm]
$\mathbf{L}_{c.i}$	2090	[mm]
$\mathbf{A}_{mean}$	14,36	[m^2]
$\mathbf{P}_{vac}$	0,04	[mBar]
$\mathbf{P}_{set}$	36	[Bar]
$\mathbf{P}_{crit}$	33.9	[Bar]

Table 3.11: Specification about design and operative condition of the cryogenic vessel.

The next step is the study of the evolution of the evaporation rate and the autopressurisation phenomenon according to the different filling of the tank.
Specifically, considering that the tank is very close to supercritical conditions, and that there is a risk of reaching maximum pressure within a few hours after reaching it, it decided to set a limit of not reaching supercritical conditions, and therefore having a maximum variation within 7 days of 2,5 bar.
This decision is made to ensure that in the optimal configuration, there is no risk of

product emission into the atmosphere due to the intervention of safety devices, under normal operating conditions and not extraordinary conditions such as fires or sudden heat sources.

The graph 3.21 and the table 3.12 allow to highlight evaporation rate, and the kg of lost product.

Evaporation rate - different % fill

% fill	NER
50	2,4
60	2
65	1,9
70	1,8
75	1,64
80	1,6
85	1,45

Table 3.12: Net evaporation rate % fill.
Substance: cryogenic liquid nitrogen. Capacity: 3 000 L.

Figure 3.21: Trend of cryogenic liquid mass versus time- different % fill.

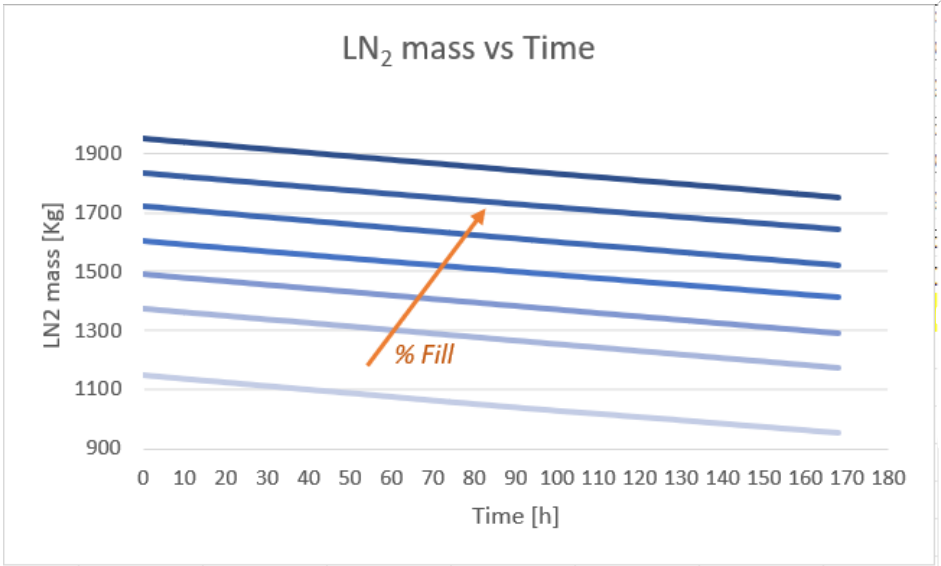

The daily evaporation rate increases for tanks filled to a lesser extent due to the fact that the starting liquid is less and the evaporated quantity has a greater impact on this value.

The amount of kilograms lost per filling is approximately the same, reaching 200 kg lost for 7 days.
The evaluation of non-evaporated product is not related to the filling level but to other factors identified as more impactful, such as the degree of vacuum in the cavity.

At this point, it is interesting to highlight the pressure trend in the tank, again over a 7-day period, in order to understand to what extent it is possible to fill the tank at high pressure, considering the maximum variation of 2.5 bar. This avoids the opening of the relief valve and the purging of ingenuous amounts of product and getting too close to the supercritical pressure of nitrogen. After which, it has been observed that there is a sudden rise in pressure, which could reach the maximum permissible pressure in a few hours.

Figure 3.22: Trend of vessel Pressure versus time- 50,60,65,70,75,80,85 % fill. Substance : Nitrogen. Capacity : 3000 L.

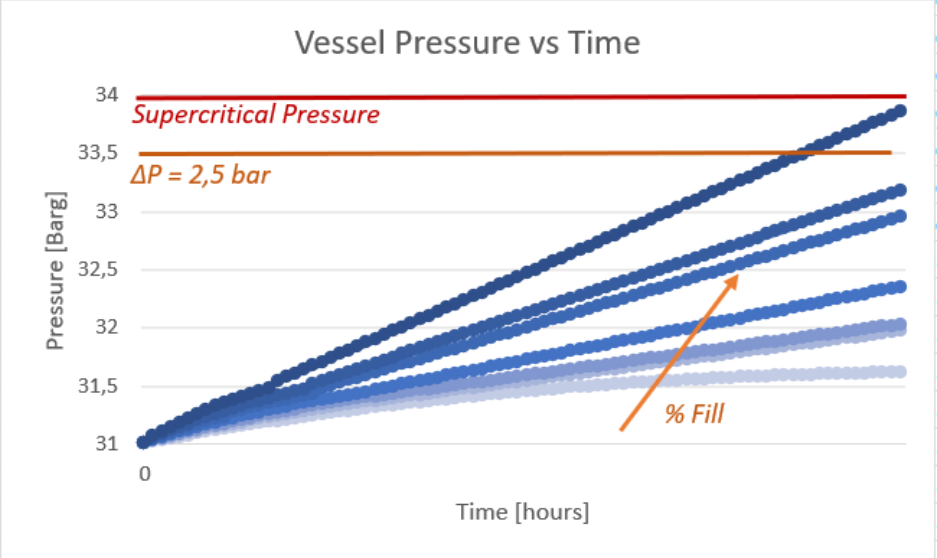

The approach employed aims to conserve as much product as possible, thereby avoiding direct purges into the atmosphere to lower the tank pressure. This strategy prioritizes efficiency.
Consequently, the tank is not pushed to the maximum allowable pressure conditions. Instead, staying below the supercritical conditions and the setting of the relief valve is recommended, with a limit of 2.5 bar over the course of a week.

Figure 3.22 illustrates the pressure trends for the 3000 L capacity tank under various filling conditions, highlighting both the super-critical pressure limit and the pressure limit set to prevent the overflow valve from opening, considering a variation of 2.5 bar. As expected from previous analyses, the self-pressurisation phenomenon is most significant for higher tank fills. Specifically, the graph depicts fills at 50, 60, 65, 70, 75, 80, and 85 %.
According to considerations and depending on the tank design and operating conditions, it is impossible to fill to 85% or more, as indicated by the steepest slope in the graph, with a potential limit of 80% instead.

Since tanks are typically filled to 50 /60%, adopting the new level of our calculation model at 80% would result in a significant difference in the kilograms of cryogenic nitrogen delivered.

At this stage, the final parameter to investigate before the economic and environmental assessment is the kilograms of cryogenic nitrogen not used for evaporation, comparing the higher vacuum of the new tanks to the standard vacuum of the tanks still on the market. This comparison aims to highlight the performance difference between the new and old generations of tanks.
Table 3.13 presents the annual loss in kilograms due to evaporation for a 3000 L tank filled to 80 percent, based on different degrees of cavity vacuum.
In particular, a customer using gaseous nitrogen instead of liquid nitrogen, equipped with an economizer for the reuse of vaporized nitrogen. Therefore, the hours involved in product losses during holidays, with a one-week closure for both winter and summer seasons, are considered. For working days, it is assumed that 10 hours per day when nitrogen is not used, and thus the evaporated product is considered lost.

Nitrogen lost - different vaacum condition

Vaacum conidition [mBar]	Nitrogen lost [Kg]
0,26	16 065
0,04	6 318

Table 3.13: Nitrogen lost [Kg]- different vacuum condition

Substance: cryogenic liquid nitrogen. Capacity: 3 000 L.

At this stage, it is possible to proceed with the economic and environmental evaluation. For the calculations, a customer located 50 km from the site is considered, characterized by 2 monthly deliveries with 50 percent tank filling. Each delivery consists of 1 148 kg. Annually, a total of 24 deliveries are made, resulting in a discharge of 27 552 kg. However, due to having an outdated tank, 16 065 kg of this will be wasted, leaving only 11 487 kg available annually.
Assuming the tank is replaced with an identical design but with a larger vacuum space, the customer has an additional 9 747 kg of cryogenic nitrogen available for use.

With the new optimized configuration, verified using the pressure oscillation calculation model, since the tank reaches 80 percent capacity at each delivery, it's possible to unload 1836 kg. Taking into account the client's net annual consumption, the saved kilograms in terms of evaporation with the new tank configuration, and the increased filling level, it's possible to reduce the annual deliveries from 24 to 6.
Using relations 2.41 and 2.42, it's possible to determine the annual cost savings both for the company and the consumer related to the number of deliveries and transportation costs.

$$Savings_{\text{manufacturer}} = \ 106\ [€] \times 18 = \ 1\ 908\ [€] \tag{3.1}$$

$$Savings_{\text{costumer}} = 150\ [€] \times 18 = 2\ 700\ [€] \tag{3.2}$$

In addition to the delivery costs for the customer, the costs related to the purchase of nitrogen must also be added. These costs depend on the manufacturer's price and are related to the kilograms of product not evaporated with the new configuration, which the customer previously purchased despite the inability to effectively use them.
For a company with a large number of high-pressure tanks, the result obtained in equation 3.1 can translate into significant savings, as well as fewer man-hours for technicians who have to deliver and fill the tank.

The reasoning done can now be applied in terms of reduced carbon dioxide emissions resulting from the new tank technologies and increased filling capacity.

First, there are fewer emissions associated with the seven fewer annual deliveries.
Second, it's possible, starting from the data illustrated in section 2.5, to determine and calculate the difference in terms of kg/CO2 emitted in the case of the initial tank configuration and the optimized configuration, using a multiplicative factor that considers emissions associated with both transportation and production.

$$Emissions_{\text{standard}} = 372\ [\text{kg/tonne}] \times \ \text{LN}_2\ [\text{tonne}] \tag{3.3}$$

$$Emissions_{\text{renewable}} = 22.32\ [\text{kg/tonne}] \times \text{LN}_2\ [\text{tonne}] \tag{3.4}$$

The table 3.14 highlights the emissions based on the scenarios considered:

CO_2 Emission in one year- different tank condition

	CO_2 emission [tonne]
Standard cryogenic vessel	10 249
Optimized cryogenic vessel	4 097

Table 3.14: CO_2 Emission considering different tank condition in one year.

Table 3.4 shows the environmental impact of the improvements in cryogenic tank performance, with a clear difference in tonnes. Furthermore, if only renewable energy were used for nitrogen production, only 246 tonnes would be emitted per year for this tank.

Considering that the emission of a thousand tonnes of carbon dioxide coincides with the use of electricity in a small town for several days, the heating of an entire city with natural gas for several months, the manufacture of millions of plastic bottles, and that in Italy

there are about 170 cryogenic tanks for high-pressure nitrogen, the impact of improving and optimising these tanks is high, and even more so if it is applied to all substances produced and stored in cryogenic tanks.
Applying this methodology to all high-pressure tanks, one could estimate an annual reduction in emissions of millions of tonnes of carbon dioxide, which is an extremely significant amount, especially given the current climate conditions.

4 | Conclusions and future developments

Liquid nitrogen is extensively utilized across various industrial sectors, with the global market projected to expand significantly in the coming years, reaching a staggering market size of 25.65 trillion by 2029, driven by a compound annual growth rate of approximately 5%. The continued demand for this product spans across well-established sectors such as food, beverages, pharmaceuticals, and aerospace, while also garnering increasing interest in electronics and cryotherapy.

However, production and distribution costs pose a significant obstacle for small businesses and industries. Cryogenic nitrogen tanks, typically constructed from stainless steel or aluminum, are designed to maintain nitrogen in a liquid state at extremely low temperatures. These tanks face engineering challenges related to heat management and pressure regulation due to heat ingress from the surrounding environment, leading to evaporation and pressure increase.

Despite continuous progress in engineering and materials design for cryogenic tanks, optimizing the minimization of heat exchange with the surroundings, thermal reentries remain a significant issue in liquid nitrogen storage. The economic losses associated with this phenomenon include:

- Product loss due to evaporation
- Inability to fully fill high-pressure cryogenic tanks, resulting in limits on the quantity delivered to the customer, leading to increased deliveries and transportation costs. High-pressure tanks are typically filled to about 50/60% of their capacity due to the autopressurization and liquid expansion phenomena.

These two significant limitations in cryogenic storage emphasize the importance of further investigation and deeper understanding of thermal reentries to identify the parameters that most influence this phenomenon and find relationships that allow us to predict the pressure and evaporation rate trends based on the conditions. This understanding is crucial for optimizing the design and operation of cryogenic systems to mitigate economic losses and ensure safety.

The study was divided into two main areas. The first involved identifying heat exchange mechanisms to quantify the incoming heat flux based on environmental conditions and tank design. The second aspect involved the development of a mathematical model capable of realistically describing the evolution of phases within the tank. The physical

model, based on assumptions and hypotheses drawn from literature review, particularly centered around the concept of the tank initially comprising subcooled liquid and continually evolving gas phase due to external heat absorption. As the liquid stratifies into subcooled and saturated liquid, a portion of the saturated liquid, due to evaporation, continues to migrate into the vapor phase, leading to a decrease in the liquid phase in favor of the gas phase until reaching supercritical conditions.

Through simplifications of the physical model, relationships concerning the evaporation rate and pressure evolution within the tank over time in response to heat exchange with the external environment were derived from mass and energy balances. An iterative calculation tool was thus constructed to predict the evolution of mass and volume of present phases and oscillation over time. For tanks operating near supercritical conditions, relationships pertaining to the subcritical and supercritical regions were described to highlight the different pressure trends in the two regions.

From the computational model used and the comparison with experimental data, coherence with the obtained results emerged, allowing us to apply it to various case studies. Sensitivity analysis, by varying input variables such as external temperature and insulation layer conductivity, revealed that the most impactful parameter in tank design is the vacuum degree of the interspace. The autopressurization phenomenon appeared more pronounced as the cryogenic substance reached the supercritical state, resulting in the maximum allowable tank pressure being reached in a few hours. This result highlights the importance of keeping the tank below supercritical conditions to ensure tank safety and avoid sudden uncontrolled pressure increases. Furthermore, thanks to the reproducibility of the model, it was possible to use it for various tank capacities and fillings, showing the higher sensitivity of smaller capacity tanks to heat ingress and the self-pressurization phenomenon for more filled tanks.

In this way, it was possible for a high-pressure nitrogen tank, based on the obtained results, to identify an optimal tank configuration according to customer needs and safety factors. This allowed for increasing the filling level while monitoring pressure increase to avoid the risk of product losses due to safety device intervention. Specifically, by considering the most impactful design choice,the vacuum conidtion of the insulation layer, it was possible to estimate the kilograms of cryogenic nitrogen not wasted through evaporation compared to standard tank configurations. Combining this aspect with the newly found filling level, for a generic customer's consumption, it was possible to calculate the economic savings in terms of deliveries and transportation for both the customer and the nitrogen producer over the course of a year. Consequently, an estimate of reduced carbon dioxide emissions was also obtained. The differences, both in economic and environmental terms, are significant when comparing the standard starting configuration with the configuration proposed by the mathematical model results. These differences are even more impactful when considering the total number of tanks managed by the producing companies.

The proposed study offers a description of the complex process of cryogenic evaporation and autopressurization through a simple realistic mathematical model. Its strength lies in the model's reproducibility, allowing for variations in operational conditions, tank design characteristics, and stored substances, while outputting the pressure and phase behavior. This model serves as a valuable starting point for studying heat exchange minimization,

enabling the evaluation of numerous variables and adapting the model to specific research needs. Consequently, it provides a quick estimate without resorting to slower and more costly experimental procedures. Given the growing interest and market demand for a wide range of cryogenic substances, the potential for future reuse of this study for other industrial purposes is compelling, warranting further detailed investigation to accurately emulate reality through computational modeling.

Bibliography

[1] Liquid nitrogen market for storage , technology , end use and region, global trends and forecasts from 2022 to 2029. Technical report, Exactitude consultancy, 5 2023.

[2] Pressure-relieving and depressuring system. *American Petroleum Institute, API Standard 521*, January 2014.

[3] *Cryogenic vessels-Cryogenic insulation performance*. International ISO Standard , 21014, Second edition, 2019.

[4] P. D. J. W. Antoine Hubert, Siaka Dembele. Predicting liquefied natural gas (lng) rollovers using computational fluid dynamics. *Journal of Loss Prevention in the Process Industries*, 62:103922, 2019.

[5] V. V. Calogero Migliore, Cristina Tubilleja. Weathering prediction model for stored liquefied natural gas (lng). *Journal of natural gas science and engineering*, 2015.

[6] M. K. J. K. H. Y. D. Chang. Experimental investigation of thermal stratification in cryogenic tanks. *Experimental Thermal and Fluid Science*, 96:371–382, 2018.

[7] M. H. Chin-Shun Lin Mohammad. Numerical investigation of the thermal stratification in cryogenic tanks subjected to wall heat flux. *NASA*, 1990.

[8] C. T. C.K. Chen. Conductance of packed spheres in vacuum. *ASME J. Heat Transfer*, pages pp. 302–308, 1973.

[9] R. Done. Hydrocarbon processing. pages 63–67, 2010.

[10] V. V. Felipe Huerta. Cfd modelling of the isobaric evaporation of cryogenic liquids in storage tanks. *International Journal of Heat and Mass Transfer*, 2021.

[11] L. G. A. S. Y. R. S. K. S. G. K. M. L. J. E. F. M. Fernando Perez, Saif Z.S. Measurements of boil-off gas and stratification in cryogenic liquid nitrogen with implications for the storage and transport of liquefied natural gas. *Energy*, 222, 2021.

[12] A. Ferraioli. *Manuale dei sistemi di gas medicali e del vuoto*. Dario Flaccovio Editore, 2023.

[13] T. M. Flynn. *Cryogenic Engineering*. Marcel Dekker, USA, 2005.

[14] A. Hajipour. Sizing of pressure safety valves in the supercritical region. 2021.

[15] A. Hofmann. The thermal conductivity of cryogenic insulation materials and its temperature dependence. *Cryogenics*, pages 815–824, 2006.

[16] P. Italiana. Scheda tecnica perodic, 2019. URL `https://www.perlite.it/wp-content/uploads/2019/06/Scheda_tecnica_Perodic.pdf`.

[17] C. L. J. Elliott. *Introductory Chemical Engineering Thermodynamics*. Pearson, 2018.

[18] D. A. W. Maksym Kulitsa. Lng rollover challenges and their mitigation on floating storage and regasification units: New perspectives in assessing rollover consequences. *Journal of Loss Prevention in the Process Industries*, 54:352–372, 2018.

[19] S. M. Michael F. Modest. *Radiative Heat Transfer*. Academic Pr, 2021.

[20] A. C. P. S. S. Y. W. Miltiadis Kalikatzarakis, Gerasimos Theotokatos. Model based analysis of the boil-off gas management and control for lng fuelled vessels. *Energy*, 251:123872, 2022.

[21] Y. I. M. A. R. H. S. T. N. Sakatani, K. Ogawa. Thermal conductivity model for powdered materials under vacuum based on experimental studies. *AIP Adv*, 2017.

[22] R. Neff. A survey of stratification in a cryogenic liquid. *Springer US*, 1960.

[23] U. D. ofcommerce. Nist chemistry webbook,srd 69, 2023. URL `https://doi.org/10.18434/T4D303`.

[24] R. Ouderkirk. Chemical engineering progress magazine. 2002.

[25] V. S. Pasala. Designing and analysis of cryogenic storage vessels. *Cryogenics*, 7:11, 2016.

[26] I. Perlite Institute. "super" insulating perlite for evacuated cryogenic service, 2018. URL `https://www.perlite.org/wp-content/uploads/2018/03/super-insulating-perlite-evacuated-cryogenic-service.pdf`.

[27] M. Y. P.J. Turyk. Modified effective conductivity models for basic cells of simple cubic packed beds. *Proc. 23rd national heat transfer Conference*, pages 2–4, 1985.

[28] V. P. Q.S. Chen, J. Wegrzyn. Analysis of temperature and pressure changes in liquefied natural gas (lng) cryogenic tanks. *Cryogenics*, pages 701–709, 2004.

[29] V. B. Ram R. Ratnakar, Zhe Sun. Effective thermal conductivity of insulation materials for cryogenic lh2 storage tanks: A review. *International Journal of Hydrogen Energy*, pages 7770–7793, 2023.

[30] B. M. Rosaria. Cassazione penale, sez. 4, 30 agosto 2018, n. 39283 - scoppio nella fabbrica di vernici e morte di quattro operai. valutazione dei rischi e obbligo di periodico aggiornamento del dvr. *Olympus*, 2018.

[31] E. M. H. K. Seyed Ali Jazayeri. Numerical comparison of thermal stratification due natural convection in densified lox and ln2 tanks. *American Journal of Applied Sciences*, pages 1773–1779, 2008.

[32] D. C. J. D. W.L. Johnson, N.T. Van Dresar. Transmissivity testing of multilayer insulation at cryogenic temperatures. *Cryogenics*, pages 70–79, 2017.

[33] H. M. C. S. W. V. S. Y. S. Choi, M. N. Barrios. Thermal conductivity of powder insulations for cryogenic storage vessels. *Transactions of the Cryogenic Engineering Conference - CEC*, 2005.

[34] S. Y. X. Yang. Research progress of lossless and safe storage technology for cryogenic liquid tanks. *International Journal of Green Energy*, pages 1230–1251, 2022.

A | Appendix A

Algorithm A.1 Heat flow calculation

1: $T\_in =$; % T sostanza criogenica Kelvin
2: $T\_out =$; % T esterna Kelvin
3: $A\_mean =$; % Area scambio termico m^2
4: $h =$; % spessore strato isolante m
5: $N = 1000$; % Numero di intervalli
6: $step = (T\_out - T\_in)/N$; % Passo tra i punti
7: $k\_e = 0$; % Inizializzazione
8: % Funzione per calcolare il coefficiente di conducibilità termica in mW/(m K)
9: $k\_formula = @(T)0.0025 \times T + 7.98 \times 10^{-8} \times T^3 + (1.243 \times T^{0.587} \times 26)/(0.895 \times T + 26)$;

10: % Calcola il coefficiente di conducibilità medio utilizzando il metodo dei trapezi
11: **for** $i = 1 : N$ **do**
12: $T\_start = T\_in + (i - 1) \times step$;
13: $T\_end = T\_in + i \times step$;
14: $k\_e = k\_e + (k\_formula(T\_start) + k\_formula(T\_end)) \times (T\_end - T\_start)/2$;
15: **end for**
16: $Q = (k\_e \times A\_mean/h)/1000000$; % Calore entrante in kW
17: % Visualizza il risultato
18: `disp(['integrazione coefficiente conducibilità rispetto alla temperatura ', num2str(k_e), ' mW/m'])`
19: `disp(['Calore entrante in watt ', num2str(Q), ' kW'])`

B | Appendix B

Algorithm B.1 Calculation model - Cryogenic Vessel - Subcritical state - Nitrogen

Input data

T_{in} =; % Temperatura iniziale dell'azoto (°C)
T_{out} =; % Temperatura ambiente(°C)
P =; % Pressione iniziale dell'azoto (bar)
Q =; % Flusso di calore entrante (kW)

Azoto
$R = 8.314$; % Costante dei gas (m^3/mol/°C)
$w = 0.04$; % Fattore acentrico azoto
$P_{\text{critic}} = 33.9$; % Pressione critica dell'azoto (bar)
$T_{\text{critic}} = -146$; % Temperatura critica dell'azoto (°C)
$Tr = (124.3/(T_{\text{critic}} + 273.15))$; % Temperatura ridotta (K)
$PM = 0.028$; % Peso molcecolare azoto (kg/mol)
$k = 0.37464 + 1.54226 * w - 0.26992 * (w^2)$;
$ac = 0.45724 * (R * (T_{\text{critic}} + 273.15))^2/(P_{\text{critic}} * 10^5)$;
$\alpha = (1 + k * (1 - \sqrt{Tr}))^2$; % K
$a = \alpha * ac$;
$b = 0.07780 * R * (T_{\text{critic}} + 273.15)/(P_{\text{critic}} * 10^5)$;

Condizioni iniziali
$CapacitaTank$ =; % Capacità del tank (m^3)
$Filling$ =; % Tasso di riempimento del tank con azoto liquido in percentuale (%)
VF_i =; % Volume liquido sottoraffreddato (m^3)
VV_i =; % Volume gas (m^3)

% Condizioni iniziali liquido sottoraffreddato e vapore
H_{in} =; % Entalpia iniziale liquido sottoraffreddato (kJ/kg)
$\rho_{F_{\text{in}}}$ =; % Densità del liquido iniziale (kg/m^3)
$\rho_{V_{\text{in}}}$ =; % Densità del vapore iniziale (kg/m^3)

Masse e volumi
$mV_i = \rho_{V_{\text{in}}} \times (VV_i)$; % massa della fase gas iniziale (kg)
$mF_i = \rho_{F_{\text{in}}} \times (VF_i)$; % Massa iniziale liquido sottoraffreddato (kg)
$mCnet_i = 0$; % massa calda netta istante = 0, non ho massa calda nelle condizioni iniziali (kg)

Calculation model - Cryogenic Vessel - Subcritical state - Nitrogen

$mC_i = 0$; % massa calda istante = 0, non ho massa calda nelle condizioni iniziali
$me_i = 0$; % massa evaporata istante =0, non ho massa evaporata nelle condizioni iniziali
$mtot_i = mF_i + mV_i + mCnet_i$; % massa totale iniziale (kg)
$dmgas_i = 1/(VV_i/(mV_i/PM))$; % densità molare della fase gas (mol/m^3)
$VC_i = 0$; % Volume massa calda/condizioni saturazione nelle condizioni iniziali
$Vtot_i = VF_i + VC_i$; % Volume totale azoto liquido = liquido sottoraffreddato + liquido caldo (m^3)

Dati termodinamici

Dati relativi al Liquido saturo

% Temperature (°C), Pressure (bar), Density (kg/m^3), Volume (m^3/kg), Internal Energy (kJ/kg), Enthalpy (kJ/kg), Entropy (kJ/kg*K),
% Cv (lJ/kg*K), Cp (kJ/kg*K), Sound Spd. (m/s), Joule-Thomson (K/bar),
% Viscosity (uPa*s), Therm. Cond. (W/m*K), Surf. Tension (N/m)

$datiLiquidoSaturo = []$;

% Dati relativi al liquido sottoraffreddato

% Temperature (°C), Pressure (bar), Density (kg/m^3), Volume (m^3/kg), Internal Energy (kJ/kg), Enthalpy (kJ/kg), Entropy (kJ/kg*K),
% Cv (kJ/kg*K), Cp (kJ/kg*K), Sound Spd. (m/s), Joule-Thomson (K/bar),
% Viscosity (uPa*s), Therm. Cond. (W/m*K), Surf. Tension (N/m)

$datiLiquidoSottoraffreddato = []$;

% Dati relativi al vapore

% Temperature (°C), Pressure (bar), Density (kg/m^3), Volume (m^3/kg), Internal Energy (kJ/kg), Enthalpy (kJ/kg), Entropy (kJ/kg*K),
% Cv (kJ/kg*K), Cp (kJ/kg*K), Sound Spd. (m/s), Joule-Thomson (K/bar),
% Viscosity (uPa*s), Therm. Cond. (W/m*K), Surf. Tension (N/m)

$datiVaporeSaturo = []$;

Inizializzazione delle variabili per i risultati

$TF = []$;
$HF = []$;
$HV = []$;
$HC = []$;
$\rho C = []$;
$\rho F = []$;
$Tsat = []$;
$mC = []$;

Calculation model - Cryogenic Vessel - Subcritical state - Nitrogen

$mF = [];$
$mV = [];$
$me = [];$
$mtot = [];$
$mCnet = [];$
$VF = [];$
$VC = [];$
$VV = [];$
$Vtot = [];$
$Tc = [];$
$cPC = [];$
$ER = [];$
$deltaHvap = [];$
$dmgas = [];$
$P = [];$

Ciclo iterativo

% Numero di ore da simulare
$oreTotali =;$
$numeroDiIterazioni = oreTotali + 1; \%i = 1istante0$

Preallocazione
% Inizializzazione dei vettori per i risultati

$TF = \text{zeros}(1, numeroDiIterazioni);$
$Tc = \text{zeros}(1, numeroDiIterazioni);$
$HF = \text{zeros}(1, numeroDiIterazioni);$
$HC = \text{zeros}(1, numeroDiIterazioni);$
$HV = \text{zeros}(1, numeroDiIterazioni);$
$\rho F = \text{zeros}(1, numeroDiIterazioni);$
$\rho C = \text{zeros}(1, numeroDiIterazioni);$
$Tsat = \text{zeros}(1, numeroDiIterazioni);$
$mC = \text{zeros}(1, numeroDiIterazioni);$
$mF = \text{zeros}(1, numeroDiIterazioni);$
$mV = \text{zeros}(1, numeroDiIterazioni);$
$me = \text{zeros}(1, numeroDiIterazioni);$
$mCnet = \text{zeros}(1, numeroDiIterazioni);$
$mtot = \text{zeros}(1, numeroDiIterazioni);$
$VF = \text{zeros}(1, numeroDiIterazioni);$
$VC = \text{zeros}(1, numeroDiIterazioni);$
$VV = \text{zeros}(1, numeroDiIterazioni);$
$Vtot = \text{zeros}(1, numeroDiIterazioni);$
$cPC = \text{zeros}(1, numeroDiIterazioni);$
$ER = \text{zeros}(1, numeroDiIterazioni);$
$deltaHvap = \text{zeros}(1, numeroDiIterazioni);$
$dmgas = \text{zeros}(1, numeroDiIterazioni);$
$P = \text{zeros}(1, numeroDiIterazioni);$

Calculation model - Cryogenic Vessel - Subcritical state - Nitrogen

Modello iterativo

$dmgas(1) = dmgas_i;$
$P_i = P; \%bar$
$P(1) = P_i; \%bar$
for $i = 1$ **to** $numeroDiIterazioni$ **do**

Ricerca nei dati termodinamici

Trova l'indice del valore più vicino nei datiLiiquidoSottoraffreddato
$[valoresimile, indiceLiquidoSottoraffreddato] = \min(\text{abs}(datiLiquidoSottoraffreddato(:, 2) - P_i));$
$HF_i = datiLiquidoSottoraffreddato(indiceLiquidoSottoraffreddato, 6);$
$rhoF_i = datiLiquidoSottoraffreddato(indiceLiquidoSottoraffreddato, 3);$
Trova l'indice del valore più vicino nei datiLiquidoSaturo
$[valoresimileLiquidoSaturo, indiceLiquidoSaturo] = \min(\text{abs}(datiLiquidoSaturo(:, 2) - P_i));$
$HC_i = datiLiquidoSaturo(indiceLiquidoSaturo, 6);$
$rhoC_i = datiLiquidoSaturo(indiceLiquidoSaturo, 3);$
$c_PC_i = datiLiquidoSaturo(indiceLiquidoSaturo, 9);$
$Tc_i = datiLiquidoSaturo(indiceLiquidoSaturo, 1);$
Trova l'indice del valore più vicino nei datiVaporeSaturo
$[valoresimileVaporeSaturo, indiceVaporeSaturo] = \min(\text{abs}(datiVaporeSaturo(:, 2) - P_i));$
$HV_i = datiVaporeSaturo(indiceVaporeSaturo, 6);$

Calcoli

Calcolo deltaH$_v$*apall'istante*i$\text{deltaHvap}_i = HV_i - HC_i; \%(kj/kg)$

Calcolo del tasso di evaporazione all'istante i
$ER_i = \text{abs}((cPC_i/deltaHvap_i) \times (Tc_i - Tcritic)); \%(-)$

Calcolo della massa calda all'istante i (kg)
$mC_i = (Q \times 3600)/(HC_i - (HF_i));$

Aggiornamento della variabile massaCalda e tasso di evaporazione
$mC(i) = mC_i; \%$ Correzione dell'assegnazione
$ER(i) = ER_i; \%$ correzione dell'assegnazioe

Calcolo delle masse
$me_i = mC_i \times ER_i; \%(kg)$
$mV_i = mV_i + me_i; \%(kg)$
$mF_i = mF_i - mC_i; \%(kg)$
$mCnet_i = mC_i - me_i; \%(kg)$
$mtot_i = mV_i + mF_i + mC_i; \%(kg)$

Calculation model - Cryogenic Vessel - Subcritical state - Nitrogen

$VF_i = mF_i/rhoF_i; \%(m^3)$
$VC_i = mCnet_i/rhoC_i; \%(m^3)$
$Vtot_i = VF_i + VC_i; \%(m^3)$
$VV_i = CapacitaTank - Vtot_i; \%(m^3)$
$dmgas_i = 1/(VV_i/(mV_i/PM)); \%$ Volume molare del gas in (mol/m3)
$dmgas(i+1) = dmgas_i;$

Aggiornamento delle masse e dei volumi
$me(i) = me_i;$
$mV(i) = mV_i;$
$mF(i) = mF_i;$
$mCnet(i) = mCnet_i;$
$mtot(i) = mtot_i;$
$VF(i) = VF_i;$
$VC(i) = VC_i;$
$Vtot(i) = Vtot_i;$
$VV(i) = VV_i;$

Calcolo della Pressione-Peng Robinson
$y_i = a \times (dmgas(i+1)^2/(1 + 2 \times b \times dmgas(i+1) - (b \times dmgas(i+1))^2));$
$z_i = a \times (dmgas(i))^2/(1 + 2 \times b \times dmgas(i) - (b \times dmgas(i))^2);$
$w_i = (dmgas(i) \times (1 - b \times dmgas(i+1)))/(dmgas(i+1) \times (1 - b \times dmgas(i)));$
$P_i = ((((P_i \times 10^5) + z_i)/w_i) - y_i)/10^5; \%$ Bar
$P(i+1) = P_i;$

Aggiornamento variabilii
$c_PC(i) = c_PC_i;$
$\rho F(i) =_i;$
$\rho C(i) =_i;$
$HF(i) = HF_i;$
$HC(i) = HC_i;$
$HV(i) = HV_i;$
$deltaHvap(i) = deltaHvap_i;$
$VF(i) = VF_i;$
$VC(i) = VC_i;$
$VV(i) = VV_i;$
$Vtot(i) = Vtot_i;$
$Tc(i) = Tc_i;$
$z(i) = z_i;$
$y(i) = y_i;$
$w(i) = w_i;$
end for

C | Appendix C

Algorithm C.1 Calculation model - Cryogenic Vessel - Supercriticall state - Nitrogen

Input data

P_{critic} =; % Pressione Supercritica dell'azoto (bar)
P =; % Pressione iniziale dell'azoto Supercritico (bar)
Q =; % Flusso di calore entrante (kW)
H =; % Entalpia iniziale stato Supercritico (kJ/kg)
$mtot$ =; % Massa totale stato supercritico (kg)

Dati termodinamici

Dati relativi allo stato Supercritico

% Temperature (°C), Pressure (bar), Density (kg/m^3), Volume (m^3/kg), Internal Energy (kJ/kg), Enthalpy (kJ/kg), Entropy (kJ/kg*K),
% Cv (lJ/kg*K), Cp (kJ/kg*K), Sound Spd. (m/s), Joule-Thomson (K/bar),
% Viscosity (uPa*s), Therm. Cond. (W/m*K), Surf. Tension (N/m)

$datiSupercritico = []$;
Inizializzazione delle variabili per i risultati

$P = []$;
$H = []$;
Ciclo iterativo

% Numero di ore da simulare
$oreTotali$ =;
$numeroDiIterazioni = oreTotali + 1; \%i = 1istante0$

Preallocazione
% Inizializzazione dei vettori per i risultati

$P = \text{zeros}(1, numeroDiIterazioni)$;
$H = \text{zeros}(1, numeroDiIterazioni)$;

Calculation model - Cryogenic Vessel - Supercritical state - Nitrogen

Modello iterativo

$P_i = P; \%bar$
$P(1) = P_i; \%bar$
$H_i = H; \%bar$
$H(1) = H_i; \%bar$
for $i = 1$ **to** $numeroDiIterazioni$ **do**

  Ricerca nei dati termodinamici

  Trova l'indice del valore più vicino nei datiSupercritico
  $[valoresimile, indiceSupercritico] = \min(\text{abs}(datiSupercritico(:, 6) - H_i));$
  $HF_i = datiSupercritico(indiceSupercritico, 2);$

  Calcolo entalpia- Trasformazione isocora
  $H_i = ((Q \times 3600) - (mtot_i \times (H_i)))/(mtot_i);$
  $H(i+1) = H_i;$

  Aggiornamento variabili
  $P(i) = P_i;$
end for